



**Nansen Environmental and Remote Sensing Center**

**Bergen, Norway**

**Technical University Berlin**
**Fachbereich 6**
**Institut für technischen Umweltschutz**

**Berlin, Germany**

# Comparison between chlorophyll data derived from space-borne ocean colour sensors and biomass fields of a 3-dimensional physical-biogeochemical model and the implications for primary production estimates of the North Atlantic Ocean

Diplomarbeit

Markus Weber
Matr.-Nr.: 150788

Bergen, October 1998

## Acknowledgement

Data used in this study include data provided by the Earth Observing System Data and Information System (EOSDIS) , Distributed Active Archive Center at Goddard Space Flight Center which archives, manages and distributes this data set through funding from Earth Observing System of NASA's Mission to Planet Earth.
NASDA's Earth Observation Research Center contributed satellite images within the framework of the ADEOS program.
*In situ* data was collected with funding under the Bermuda Atlantic Time-series Station (BATS) and Hydrostation S programs from grants from the National Science Foundation to the Bermuda Biological Station for Research, Inc.
The help of all of the individual scientists, technicians, ship crews or whoever helped in assembling the ocean time series or satellite data is gratefully acknowledged.
Finally I would like to thank my colleges and supervisors in Bergen who helped me with all my questions and the Nansen Center and my supervisors in Berlin for making my studies in Norway possible.

# Table of Contents

# List of Tables



# List of Figures

# List of Equations

# Acronym Glossary

| | |
|---|---|
| 2-D | two dimensional |
| 3-D | three dimensional |
| ADEOS | Advanced Earth Observing Satellite |
| BATS | Bermuda Atlantic Time Series |
| BBOP | Bermuda Bio-Optics Project |
| BOFS | British Ocean Flux Study |
| CDOM | Coloured Dissolved Organic Matter |
| CHORS | Center for Hydro-Optics and Remote Sensing |
| COADS | Comprehensive Ocean-Atmosphere Data Set |
| CTD | Conductivity, Temperature, Depth |
| CZCS | Coastal Zone Colour Scanner |
| DIC | Total dissolved inorganic carbon |
| DOM | Dissolved Organic Matter |
| EOS-A | Earth Observing Satellite-A |
| ERS-1 | European Remote Sensing Satellite |
| ESA | European Space Agency |
| FNOC | Fleet Numerical Oceanography Center |
| GAC | Global Area Coverage |
| GCP | Ground Control Point |
| GEOSEC | Geochemical Ocean Sections Study |
| GFF | Glass Fiber Filter by Whatman |
| GMT | Greenwich Mean Time |
| GSFC | Goddard Space Flight Center |
| HPLC | High Pressure Liquid Chromatography |
| IR | Infrared |
| IOCCG | International Ocean Colour Co-ordinating Group |
| JGOFS | Joint Global Ocean Flux Study |
| L0 | Level-0, Raw Data |
| L1a | Level-1a, calibrated radiances |
| L2 | Level-2, derived products |
| L3 | Level-3, gridded and averaged derived Products |
| LAC | Local Area Coverage |
| MERIS | Medium Resolution Imaging Spectrometer |
| MICOM | Miami Isopycnic Coordinate Ocean Model |
| ML | Mixed Layer |
| MOBY | Marine Optical Buoy |
| MOCE | Marine Optical Characterisation Experiment |
| MODIS | Moderate Resolution Imaging Spectrometer |
| MOS | Modular Optoelectronic Scanner |
| MPDATA | Multidimensional Positive Definite Advection Transport Algorithm |
| NABE | North Atlantic Bloom Experiment |
| NASDA | National Space Development Agency (Japan) |
| NET | NIMBUS Experimental Team |
| NIMBUS | Not an acronym, a series of NASA experimental weather satellites |
| NMC | National Meteorological Center |
| NOAA | National Oceanic and Atmospheric Administration |
| NRT | Near Real Time |
| OCM | Ocean Colour Monitoring |
| OCTS | Ocean Colour Temperature Sensor |
| OGCM | Ocean General Circulation Model |
| OPT | Ozone Processing Team |
| OWS | Ocean Weather Station |
| POLDER | Polarisation and Directionality of the Earth's Reflectance |
| ROSIS | Reflecting Optics System Imaging Spectrometer |
| SAVE | South Atlantic Ventilation Experiment |
| SBRC | Hughes / Santa Barbara Research Center |

| | |
|---|---|
| SeaWiFS | Sea-Viewing Wide Field-of-View Sensor |
| SIRREX | SeaWiFS Intercalibration Round-Robin Experiment |
| SMI | Standard Mapped Image |
| SO | Southern Ocean |
| SPIE | Society of Photo-optical Instrumentation Engineers |
| SPM | Suspended Particulate Material |
| TIROS | Television Infrared Observation Satellite |
| TOMS | Total Ozone Mapping Spectrometer |
| TOVS | TIROS Operational Vertical Sounder |
| TTO/NAS | Transient Tracers in the Ocean / North Atlantic Study |
| WOCE | World Ocean Circulation Experiment |

# Abbreviations

| | |
|---|---|
| approx. | approximately |
| atm. | atmosphere |
| betw. | between |
| Chl a | Chlorophyll a |
| Chl | Chlorophyll |
| eq | charge equivalents |
| i.e. | *id est* |
| kg-sw | kilogram seawater |
| l.h.s. | left hand side |
| min. | minutes |
| Phaeo | Phaeophytin |
| ppm | parts per million |
| r.h.s. | right hand side |
| stand. | standard |
| Sv | Sverdrup = $10^6$ $m^3/s$ |
| w.r.t. | with regard to |

# Glossary

| | |
|---|---|
| attenuation | "The reduction in level of a quantity, such as the intensity of a wave, over an interval of a variable such as the distance from a source" (Parker 1984: 122); additive consequence of absorption and scattering that occur between the photons and the organic and inorganic materials present (including the pure water) |
| chlorophyll | "The generic name for any of several (…)plant pigments which function as photoreceptors of light energy for photosynthesis" (Parker 1984: 292); in this study only chlorophyll a |
| climatological | based on data which is averaged over a long time period (opposite to synoptic) |
| coccolith | "One of the small, interlocking calcite plates covering members of the Coccolithophorida." (Parker 1984:319) |
| coccolithophorids | "Coccolithophorida: A group of unicellular, biflagellate, golden-brown algae characterised by a covering of coccoliths." (Parker 1984: 319) |
| diapycnal | non-equal or non-constant density (opposite to isopycnal) |
| diatom | "The common name for algae composing the class Bacillariophycea; noted for the symmetry and sculpturing of the silicious cell walls."(Parker 1984: 444) |
| euphotic | "Of or constituting the upper levels of the marine environment down to the limits of effective light penetration for photosynthesis." (Parker 1984: 568) |
| irradiance | radiant flux density; "The amount of radiant power per unit area that flows across or onto a surface." (Parker 1984: 1317) |
| isopycnal | of equal or constant density (opposite to diapycnal) |
| phaeophytin | "A derivative of chlorophyll in which $Mg^{2+}$ is replaced by two protons." (Singleton and Sainsbury 1989: 657) |
| photic | synonym with euphotic |
| phycobilin | phycobiliproteins; "Pigment which occurs in cyanobacteria, in algae of the Rhodophyta, and in cryptophytes." (Singleton and Sainsbury 1989: 669) |
| phycoerythrin | "A red phycobilin" (Parker 1984: 1209) |
| pigment | "Any colouring matter in plant or animal cells" (Parker 1984: 1214); in this study chlorophyll a + phaeophytin together are called pigment |
| radiance | "The radiant flux per unit solid angle per area of projected area of the source. (…) Also known as steradiance." (Parker 1984: 1317) |
| synoptic | based on data which is gathered instantaneously or simultaneously (opposite to climatological) |

# Symbols

| | |
|---|---|
| $\alpha_d$ | ocean surface albedo for direct sun light |
| $\alpha_s$ | ocean surface albedo for diffusive sun light |
| $\alpha$ | initial slope of the photosynthesis-irradiance curve |
| $\beta$ | solar noon altitude [radians] |
| $\rho$ | chlorophyll to pigment ratio, $\rho$=Chl/C |
| $\zeta$ | normalised depth, $\zeta=z/z_e$ |
| $\mu$ | mean cosine of the zenith angles of perfect diffuse skylight after refraction at the sea surface |
| $\gamma$ | non-dimensional empirical coefficient |
| $\varepsilon$ | turbulent kinetic energy dissipation rate in the oceanic upper mixed layer [$m^2/s^3$] |
| $\varepsilon$ | small number to prevent division by zero |
| $\tau$ | transmission coefficient (0.7) |
| $\theta_d$ | sun zenith angle in water |
| $\sigma_0$ | dimensionless density |
| $\lambda$ | wavelength |
| $\lambda$ | decay rate (0.1 1/d) |
| $\nu$ | detrital regeneration exponent (0.858) |
| $\nabla$ | two-dimensional gradient operator [1/m] |
| (aq) | liquid phase (dissolved) |
| (g) | gaseous phase |
| (s) | solid phase |
| $(H^+)$ | activity of the hydrogen ion |
| [x] | concentration of x [mol/kg-sw] |
| x [y] | dimension y of unit x |
| $A_T$ | total alkalinity [$eq/m^3$] |
| A | absorption by water and ozone (0.09) |
| B | bacteria [$mmol\text{-}N/m^3$] |
| $B_T$ | total dissolved borate [mol/kg-sw] |
| C | pigment concentration [$mg/m^3$] |
| C | Cloudiness fraction |
| Chl | chlorophyll concentration [$mg/m^3$] |
| $Chl_{model}$ | chlorophyll concentration of the model [$mg/m^3$] |
| $Chl_{surface}$ | surface chlorophyll concentration derived from the satellite [$mg/m^3$] |
| $Chl_{subsurface}$ | subsurface chlorophyll concentration derived from the satellite [$mg/m^3$] |
| $\overline{C}_{ze}$ | mean pigment concentration within the euphotic layer [$mg/m^3$] |
| $\overline{C}_{sat}$ | weighted mean pigment concentration within the surface layer [$mg/m^3$] |
| $\overline{C}_{pd}$ | mean pigment concentration within the surface layer [$mg/m^3$] |
| $\overline{C}_z$ | mean pigment concentration within a layer with the depth z [$mg/m^3$] |
| $\langle C \rangle_{tot}$ | total pigment within the euphotic layer [$mg/m^2$] |
| $C^i$ | one of the nine biochemical compartments (P, Z, B, $N_n$, $N_r$, $N_d$, D, $C_T$, $A_T$) |
| $C_T$ | total dissolved inorganic carbon (DIC) [$mmol\text{-}C/m^3$] |
| D | particulate organic nitrogen (detritus) [$mmol\text{-}N/m^3$] |
| $E_d(0^-,\lambda)$ | surface incident spectral irradiance |
| $E_d(z,\lambda)$ | downwelled spectral irradiance |
| F | photosynthesis-irradiance relationship |
| F | flux of particulate material |
| $f_{CaCO3}$ | $CaCO_3$ temperature inhibition factor |
| $G_1$ | grazing rate of zooplankton on phytoplankton |
| $G_2$ | grazing rate of zooplankton on bacteria |
| $G_3$ | grazing rate of zooplankton on detritus |
| $h_k$ | layer thickness [m] |
| i | numbering index |
| J(t,z) | light limited growth rate of phytoplankton at time t and depth z |
| K (490) | diffuse attenuation coefficient at 490 nm |

| | |
|---|---|
| k | numbering index |
| $K_0$ | Henry's law constant, solubility of $CO_2$ in seawater [mol-C/$m^3$] |
| $K_1$ | equilibrium constant |
| $K_2$ | equilibrium constant |
| $K_B$ | equilibrium constant |
| $K_h$ | isopycnal diffusivities [$m^2$/s] |
| $k_l$ | empirical coefficient [m/s] |
| $K_{sp}$ | equilibrium constant |
| $k_t$ | total vertical attenuation coefficient |
| $k_w$ | attenuation coefficient for water |
| $k_c$ | attenuation coefficient for phytoplankton |
| $K_v$ | diapycnical diffusivities [$m^2$/s] |
| $K_w$ | equilibrium constant |
| $L_u(z,\lambda)$ | upwelled spectral irradiance |
| $L_{WN}(443)$ | normalised water leaving radiance at 443 nm [W/$cm^2$ µm sr ] |
| $L_{WN}(490)$ | normalised water leaving radiance at 490 nm [W/$cm^2$ µm sr ] |
| $L_{WN}(520)$ | normalised water leaving radiance at 520 nm [W/$cm^2$ µm sr ] |
| $L_{WN}(550)$ | normalised water leaving radiance at 550 nm [W/$cm^2$ µm sr ] |
| $L_{WN}(555)$ | normalised water leaving radiance at 555 nm [W/$cm^2$ µm sr ] |
| LAT | latitude |
| N | buoyancy frequency [1/s] |
| $N_d$ | dissolved organic nitrogen (DON) [mmol-N/$m^3$] |
| $N_n$ | nitrate [mmol-N/$m^3$] |
| $\tilde{N}_n$ | nutrient limitation factor (nitrate) |
| $N_r$ | ammonium [mmol-N/$m^3$] |
| $\tilde{N}_r$ | nutrient limitation factor (ammonium) |
| $m_N$ | molar mass of nitrogen [g/mol] |
| P | phytoplankton [mmol-N/$m^3$] |
| PAR | photosynthetically available radiation [W/$m^2$] |
| $pCO_2$ | partial pressure of carbon dioxide |
| $pCO_2^{air}$ | atmospheric concentration of $CO_2$ at 100% relative humidity and the temperature of the sea surface |
| Q | irradiance |
| $Q_0$ | irradiance at the top of the atmosphere |
| $Q_{surface}$ | total irradiance field at the surface of the ocean |
| $Q_d$ | irradiance (direct sunlight) |
| $Q_s$ | irradiance (diffuse sky light) |
| $R_b$ | C : N ratio for bacteria |
| $R_p$ | C : N ratio for phytoplankton, zooplankton, detritus, and DON |
| $R_{Chl}$ | C : Chl ratio |
| S | salinity |
| $S_0$ | solar constant (1365 W/$m^2$) |
| Sc | Schmidt number of $CO_2$ in seawater |
| SPM | suspended particulate material, dry weight [mg/l] |
| SST | sea surface temperature [°C] |
| t | time [s] |
| $T_K$ | absolute temperature [K] |
| T | temperature [°C] |
| $U_1$ | bacterial uptake rates of DON |
| $U_{10}$ | wind speed at a height of 10 m over the sea surface [m/s] |
| $U_2$ | bacterial uptake rate of ammonium |
| $\mathbf{u}_k$ | two-dimensional fluid velocity vector [m/s] |
| $V_p$ | maximum phytoplankton growth rate |
| z | depth [m] |
| z | sun zenith angle [radians] |
| $z_e$ | euphotic layer depth [m] |
| $z_{ml}$ | mixed layer depth [m] |
| $z_{90}$ | depth of the layer that contributes 90 % of the radiant energy emerging from the sea [m] |

| | |
|---|---|
| Z | zooplankton [mmol-N/$m^3$] |

# 1 Introduction

## 1.1 Background and motivation

An increasing human population, increased pollution of our earth and the possibility of global warming are some of the main motivating factors for improving our understanding of the dynamics of global environment and climate systems, to monitor these systems, and also to assess the likelihood for changes in the systems over the next century and beyond. One interesting question in this field is, if the ocean acts as a carbon sink and how much carbon is exported. Two processes govern the capacity of the ocean to act as a carbon sink. Carbon dioxide is dissolved in sea water and is transported downward by the global thermohaline circulation. The other export flux is biologically mediated. Dead or living organisms sink to the bottom of the sea.

Obviously, improved knowledge of how the earth's environment and climate systems operate require globally distributed and high quality information about said systems. For the world's oceans, observations have been limited to *in situ* observations from a few time series stations and from national and international cruises. Recently, a large number of remotely sensed data sets have become available from the many Earth observing satellite programs. Earth observing satellites have the advantage that the coverage is global or quasi-global, and that the Earth is mapped on a regular basis. For calibration of the satellite sensors *in situ* data has to be gathered and algorithms have to be developed that convert the remotely sensed signal to the desired observing parameter. Such corrections are generally complicated. Thus, the major problem with remotely sensed data is the correction that has to be applied to the signal, and that the satellite sensors only give information of the surface properties of the Earth.

By their very nature satellite images are descriptive and they do not give us an impression of the forces which govern natural systems. Numerical models can be used to simulate the underlying processes of our global environment. Physical models reproduce environmental forcing, and biological models reproduce the response of the biological system to this forcing as well as the response to biological interactions. Combined physical and biological models can then be used to understand the various responses of marine ecosystems. It is also possible to use a combined model to forecast ecosystem behaviour and to estimate biological primary production and associated material fluxes. However, this requires that physical-biological models be verified with space- and-time-dependent distributions of biological properties.

In the present study, satellite chlorophyll data from different ocean colour sensors will be compared with phytoplankton biomass simulated with a 3-dimensional physical and biogeochemical model available at the Nansen Center to assess the quality of the model's results.

## 1.2 Objectives and thesis organisation

Available data sets from the OCTS (Ocean Colour and Temperature Scanner), SeaWiFS (Sea-Viewing Wide Field-of-View Sensor), and CZCS (Coastal Zone Colour Sensor) ocean colour sensors and *in situ* data will be analysed for the North Atlantic Ocean. This analysis will lead to an estimation of the seasonal distribution of chlorophyll in the region. The satellite chlorophyll data obtained will be compared with phytoplankton biomass simulated with a 3-dimensional physical and biogeochemical model available at the Nansen Center. Therefore phytoplankton biomass has to be calculated from the chlorophyll concentration or vice versa. As the satellite sensors can only "see" the chlorophyll concentration in the upper layer of the ocean, the subsurface chlorophyll concentration has to be calculated from the satellite/surface value. The comparison between satellite chlorophyll data and the model results shall lead to a quantification of the quality of the simulated phytoplankton biomass and an improved estimation of primary production and the downward flux of carbon in the North Atlantic Ocean. Thus, the objectives in detail are:

- Acquisition of the necessary data products
- Conversion of the different data formats and integration into a common software
- Calculation of chlorophyll concentration from phytoplankton biomass
- Calculation of subsurface chlorophyll concentrations from the surface / satellite values

- Comparison of the surface / satellite and the subsurface chlorophyll values with the model results in time and space
- Assessment of the qualitative implications for primary production estimates of the North Atlantic Ocean

In the next two chapters a brief introduction to ocean colour monitoring and the numerical model used at the Nansen Center will be given. This shall show how the two quantities which are compared are derived. Emphasis is put on the calibration efforts for the different ocean colour sensors because this has a big influence on the sensors' accuracy. In chapter 4 the methods which were chosen to compare the modelled biomass fields with the satellite measurements are outlined. Finally, the results and the problems with the comparison between the satellite chlorophyll data and the model, as well as the implications for primary production estimates for the North Atlantic ocean, are given in chapter 5 and 6.

# 2 Ocean Colour Monitoring

## 2.1 Historical Overview

Ocean Colour Monitoring with the help of satellites began with CZCS on Nimbus 7 launched in 1978. CZCS has been operating until 1986 (Duchossois 1987). Many activities in this field of studies were evaluated later. OCM was planned for ERS-1 but was not retained in the final payload configuration. It is now planned for the polar platform for the Columbus Space Station (Duchossois 1987). Other proposals included MERIS which shall be launched on ENVISAT-1 at the end of the decade (ESA) and MODIS which shall be launched on EOS in 1998. ROSIS is being evaluated but is not expected to be launched soon. The Japanese OCTS on the ADEOS satellite measured ocean colour from August 1996 until June 1997 when it went out of operation. The French POLDER sensor was also on this satellite and measured ocean colour but it had a different concept than OCTS and its main objective was the measurements of the polarisation of light and bi-directional effects. It also had a lower resolution. The German MOS sensor was launched on the IRS-P3 satellite in 1996 and mainly gathers data from European coastal waters and parts of the Arabian sea. So there exists ocean colour data with world wide coverage mainly from CZCS (1978-1987) and OCTS (1996-1997). With the launch of SeaWiFS on the OrbView-2 (formerly SeaStar) satellite on August 1, 1997 a new satellite for Ocean Colour Monitoring was in the orbit. Thus, SeaWiFS fills the gap between CZCS and the proposed launch of the next generation of ocean colour sensors which will have more bands and a narrower bandwidth (e.g. MERIS or MODIS). CZCS lacked rapid global coverage capability, and also several basic improvements in the areas of calibration and sensor characterisation, spectral bands, and radiometric sensitivity are included in SeaWiFS (Hooker *et al.*. 1992; Homepage of the IOCCG: http://www.ioccg.org). But CZCS had the advantage of a long operation period. Therefore, a climatological average over the time of CZCS-operation could be produced which is used in this study together with the data from OCTS and SeaWiFS.

**Table 1** Operating period of ocean colour sensors used in this study

| Ocean colour sensor | Platform | Operation period |
|---|---|---|
| CZCS | Nimbus-7 | 1978-1986 |
| OCTS | ADEOS | August 1996 - June 1997 |
| SeaWiFS | OrbView-2 | August 1997 - present |

## 2.2 Principles of Ocean Colour Monitoring

### 2.2.1 Overview

Since Chlorophyll is a green pigment and the colour of sea water changes from blue to green as the concentration of chlorophyll increases, the amount of chlorophyll in ocean waters can be derived from ocean colour. When visible light from the sun illuminates the ocean surface, it is subject to several optical effects. Foremost among these effects are light reflection and absorption. Absorption selectively removes some wavelengths of light while allowing the transmission of other wavelengths. In the ocean light reflects off particulate matter suspended in the water, and absorption is primarily due to the photosynthetic pigments (e.g. chlorophyll) present in the phytoplankton and dissolved organic matter. The net result of these optical interactions is light radiated from the ocean surface, which is termed the water-leaving radiance. The measured radiance may then be quantitatively related to various constituents in the water column that interact with visible light, such as chlorophyll (Gordon and Morel 1983). Unfortunately, the amount of radiance emitted from the sea surface is very small compared to the atmospheric radiance arriving at the sensor due to Rayleigh scattering. In fact, 90% or more of the signal measured by satellites over oceans is due to atmospheric radiance (Hooker *et al.*. 1992). Furthermore, clouds and sea ice directly reflect light. Therefore, the ocean colour cannot be measured if clouds or sea ice interfere with the path of light between the sensor and the ocean. Other problems arise in coastal waters where light can be reflected from the bottom of the sea because this reflectance changes the spectral composition of the water-leaving radiance. At certain angles of view sun glint can

also be a problem because the sea surface can act like a mirror and the amount and spectral composition of the water-leaving radiance will be changed.

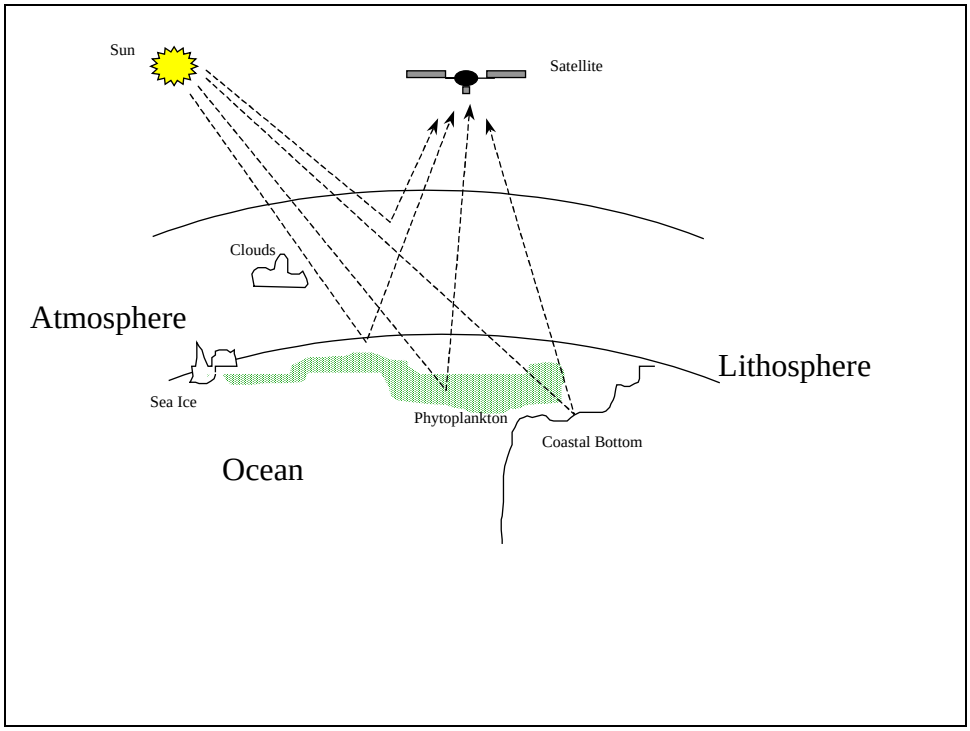


**Figure 1** Principles of ocean colour measurements

Therefore the radiation which can be measured at the sensor (raw count) must be corrected regarding atmospheric influences, sea glint, etc. to derive the amount and spectral distribution of the water-leaving radiance. The chlorophyll concentration can then be calculated from the water-leaving radiance in case 1 waters (see below) if it is compared and calibrated with sea-truth data. Calibration is not only important for the comparison of the water-leaving radiance with the actual chlorophyll a concentration in the ocean but also to take into account that the space-born sensor ages because carbon and silicon-based substances can gas out and coat the instrument's optics or atomic oxygen and harsh ultraviolet radiation from the sun can cause changes in the sensor's performance (Hooker et al. 1992). In chapter 2.3 the calibration efforts for SeaWiFS are briefly summarised as an example for ocean colour sensors and the differences in comparison to OCTS and CZCS are pointed out in chapter 2.4 and 2.5.

### 2.2.2 Definition of case 1 and case 2 waters

The algorithms to calculate chlorophyll a concentrations from the composition of the water-leaving radiance generally perform well in the open ocean whereas the calculation of chlorophyll in waters which are rich in yellow substances (Gelbstoff) or sediments, for example near the mouths of rivers, is much more difficult. This problem leads to the distinction between case 1 and case 2 waters. According to the definition of Morel and Prieur "An ideal case 1 water would be a pure culture of phytoplankton and an ideal case 2 water a suspension of nonliving material with a zero concentration of pigments." (Morel and Prieur 1977: 715) Generally, case 1 waters are open ocean waters with low pigment concentrations whereas case 2 waters are coastal, turbid waters with higher productivity. It is important to distinguish between case 1 and case 2 waters because algorithms for chlorophyll a prediction tend to fail in case 2 waters, e.g. CZCS performed poorly in regions of high chlorophyll a concentrations, high coloured dissolved organic materials concentration and coccolithophorid blooms. There are different definitions for the classification of watermasses into class 1 and 2. For CZCS case 1 water was

- clear, open-ocean water with a
- pigment concentration of less than 0.25 mg/m$^3$

(Mueller and Austin 1992)

For SeaWiFS another definition is used: "Case-1 will be considered to refer to what might be called ordinary open ocean Case-1 waters, wherein scattering and absorption are dominated by phytoplankton, pigments, and Gelbstoff concentrations, and where global blue-green colour ratio algorithms for chlorophyll a concentration and K(490) work well." (Mueller and Austin 1995a: 43) This means that:

- Gelbstoff absorption at 380 nm, $a_g(380)$, is less than 0.1 $m^{-1}$
- total suspended particulate matter concentration is less than 0.5 mg/l
- measured satellite $L_W(\lambda)$ values predict measured sea-truth chlorophyll a concentration within ±35%
- measured satellite $L_W(\lambda)$ values predict measured sea-truth K(490) within ±20%

(Mueller and Austin 1995a)

### 2.2.3 Algorithms for chlorophyll a estimation

A critical component in the performance of an ocean colour sensor is the biooptical algorithm which is used for the calculation of pigment concentration. The conditions in the world's oceans are very different. Therefore one single biooptical algorithms cannot be applied on a global basis because of the following reasons:

- variations in the relationship between ocean reflectance and chlorophyll concentration at different latitudes (changes of the solar irradiance or the depth of the mixed layer)
- changes in the reflection/absorption characteristics of the main algae groups
- special problems for coastal waters (yellow substances, suspended particulate matter)

(Holligan and Morel 1987)

Nevertheless, this is done. Generally the biooptical algorithms used for CZCS, OCTS and SeaWiFS are established by linear regression analysis of the log-transforms of sea-truth data. And a recent comparison showed that these empirical algorithms still performed better than semi-analytical ones (Reilly et al. 1998).

The CZCS algorithm calculated the pigment concentration (chlorophyll a and phaeophytin) as given by Equation 1. But because of difficulties in the performance of the algorithms other algorithms were developed and used, too.

$$C = 10^{0.053 - 1.705 \cdot \log\left[\frac{L_{WN}(443)}{L_{WN}(550)}\right]} \quad if < 1.5 \frac{mg}{m^3}$$

$$C = 10^{0.522 - 2.440 \cdot \log\left[\frac{L_{WN}(520)}{L_{WN}(550)}\right]} \quad if > 1.5 \frac{mg}{m^3}$$

**Equation 1** CZCS pigment algorithm (Reilly *et al.* 1998)

The OCTS and SeaWiFS algorithms calculate the chlorophyll concentration directly.

$$Chl = 10^{-0.55006 + 3.497 \cdot \log\left[\frac{L_{WN}(520) + L_{WN}(565)}{L_{WN}(490)}\right]}$$

**Equation 2** OCTS chlorophyll a algorithm (Reilly *et al.* 1998)

$$Chl = -0.40 + 10^{0.341 - 3.001 \cdot \log\left[\frac{L_{WN}(490)}{L_{WN}(555)}\right] + 2.811 \cdot \left(\log\left[\frac{L_{WN}(490)}{L_{WN}(555)}\right]\right)^2 - 2.041 \cdot \left(\log\left[\frac{L_{WN}(490)}{L_{WN}(555)}\right]\right)^3}$$

**Equation 3** SeaWiFS chlorophyll a algorithm (Darzi 1998a and Reilly et al. 1998)

For the conversion of chlorophyll concentrations to pigment concentrations (for the CZCS-like pigment concentration, a data product available for SeaWiFS) the following equation is used.

$$C = 1.34 \cdot Chl^{0.98}$$

**Equation 4** SeaWiFS CZCS-like pigment concentration (Darzi 1998a)

## 2.3 SeaWiFS

### 2.3.1 Overview

The primary optics of SeaWiFS consist of an off-axis folded telescope and a rotating half-angle mirror. Radiation backscattered by the Earth's surface and atmosphere is collected by the telescope and reflected onto the mirror. The beam path is then directed through beam splitters to separate the radiation into four wavelength regions. Spectral bandpass filters are used to narrow these regions to 20 nm bandwidth requirement of the SeaWiFS spectral bands. The radiation then falls on silicon detector elements. The electronics module amplifies the detector signal, performs analog-to-digital conversion, time delay and integration for data transmission. The instrument may be tilted forward or backward 20° along the spacecraft orbital trajectory to minimise the effects of sun glint (Hooker *et al.*. 1992).

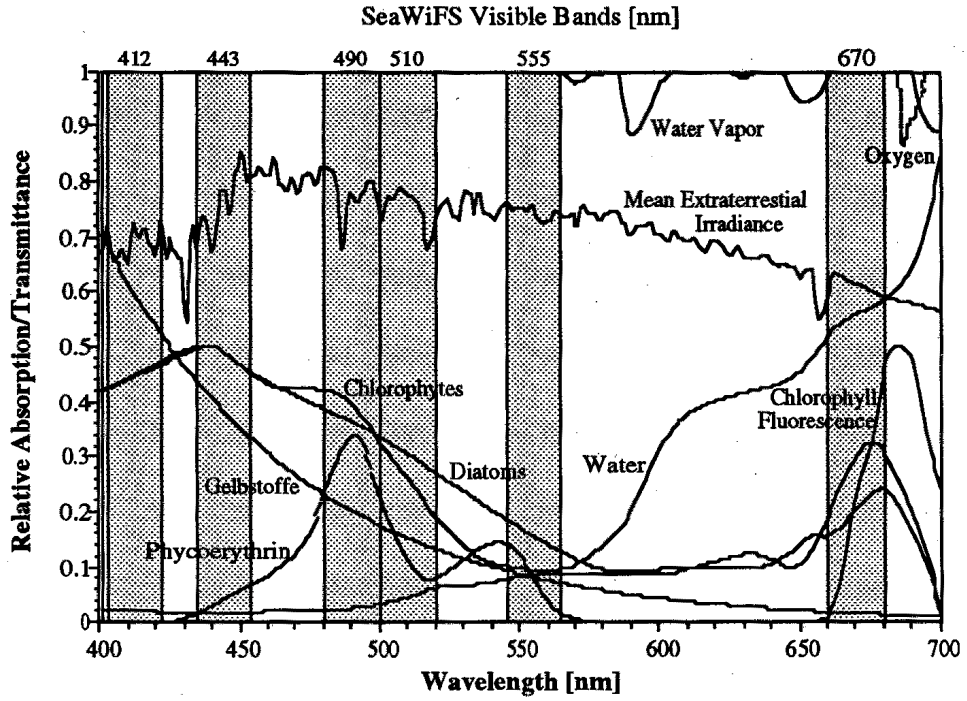


**Figure 2** SeaWiFS bands and some absorption characteristics (Hooker *et al.* 1992)

The water-leaving radiance shall be measured with a radiometric accuracy to within ± 5%, the chlorophyll a concentration to within ±35% over the range of 0,05-50,0 mg/m$^3$ in open water with relatively low pigment concentrations and a minimum depth of 100 m (Case 1 waters). In other than case 1 waters (case 2 waters) errors will be much larger, because of high concentrations of particulate matter or yellow substance (Gelbstoff) and bottom reflectance in shallow waters (Darzi *et al.* 1998b).

**Table 2** Major instrument parameters and characteristics for SeaWiFS (Hooker *et al.*. 1992)

| **Spectral Resolution** | | |
|---|---|---|
| **Band** | **Wavelength [nm]** | **Primary Use** |
| 1 | 402-422 (violet) | Yellow substance |
| 2 | 433-453 (blue) | Chlorophyll absorption |

| | | |
|---|---|---|
| 3 | 480-500 (blue-green) | Pigment absorption (Case 2 waters), K (490) |
| 4 | 500-520 (blue-green) | Chlorophyll absorption |
| 5 | 545-565 (green) | Pigments, optical properties, sediments |
| 6 | 660-680 (red) | Atmospheric correction |
| 7 | 745-785 (near IR) | Atmospheric correction, cloud and ice detection, aerosol radiance |
| 8 | 845-885 (near IR) | Atmospheric correction, aerosol radiance |
| **Sensor accuracy** | Radiance accuracy | <5% absolute each band |
| | Relative precision | <1% linearity |
| | Between band precision | <5% relative band-to-band |
| | Polarisation | <2% sensitivity (all angles) |
| **Orbit parameters** | Orbit-type | Sun Synchronous at 705 km |
| | Equator crossing | Noon ± 20 min., descending node |
| | Inclination | 98° 20" |
| | Orbital period | 98.9 min. |
| **Mission characteristics** | Swath width (at equator) | 2801 km LAC (± 58.3°)<br>1502 km GAC (±45.0°) |
| | Pixels along scan | 1285 (LAC), 248 (GAC) |
| | Nadir resolution | 1.13 km LAC; 4.5 km GAC |
| | Scan period | 0.124 s |
| | Scan plane tilt | +20°, 0°, -20° |
| | Digitisation | 10 bits |

## 2.3.2 Calibration and validation

Experience with CZCS has shown that it is very difficult to determine a sensor's calibration once it has been launched. Because of the very large atmospheric contribution to the total observed radiances and the great sensitivity of the bio-optical algorithms to the estimated water-leaving radiances, small errors in the calibration can induce sizeable errors in derived geophysical parameters, e. g. chlorophyll a concentration. To guarantee a high quality and accuracy of the satellite data big efforts are to be made. The calibration and validation procedures can be broadly grouped into the following areas.

- orbital calibration
- atmospheric correction
- calibration with sea-truth data

Each of the above mentioned areas is connected with another and many different techniques are used to ensure the desired quality of the data (Hooker *et al.*. 1992 and Darzi *et al.* 1998b):

- using correlative data for validating higher-level products like the chlorophyll a concentration
- analysing trends and anomalies
- selecting ancillary data sets that are used in data processing, such as winds, ozone, and atmospheric pressure
- direct statistical and interactive examination of the archived products
- comparison with field measurements for validation and algorithm evaluation
- matchups between sea-truth observations and satellite data
- comparison of calibration procedures for radiometers (SIRREX)

Therefore, only a brief summary of the procedures and algorithms which have been used is given here with the appropriate references.

### 2.3.2.1 Orbital calibration

Once a satellite sensor is in space degradation begins. The sensor will age with time and its performance will change over time. Ageing can be caused by outgassing of carbon and silicon-based substances which can coat the instrument's optics or by atomic oxygen and harsh ultraviolet radiation from the sun. Therefore calibration of the sensor is needed to accurately measure the incoming radiation (Level-0 data). This is done by pointing the sensor towards a radiation source of known characteristics. For SeaWiFS the sun and the moon are used. Dark count data has to be gathered and other corrections are to be applied also (Darzi *et al.* 1998):

- lunar calibration data is taken once per month when the moon is at a phase of 7 degrees
- solar diffusor calibration data is taken once per week while the spacecraft is over the south pole
- on-orbit dark count

**Table 3** Algorithms for orbital calibration according to McClain *et al.*. 1994b

| **Algorithm** | **Reference** |
|---|---|
| Moon calibration | Voss 1994 |
| Extraterrestrial solar irradiance $E_S$ | Neckel and Labs 1984 |
| Pre-flight solar-based calibration | Bigger *et al.*. 1984 |

### 2.3.2.2 Atmospheric correction

The measured incoming radiation at the satellite must now be calculated into the water-leaving radiance. Only a small part of the measured radiance at the satellite is actually from the surface of the sea, 80-90% of sensor received total radiance is due to scattering in the atmosphere (André and Morel 1989 and Gordon *et al.*. 1988). Furthermore, the composition of the atmosphere is not constant. Atmospheric corrections have to take into account changing concentrations of aerosols or ozone in the atmosphere and changing ground pressure, e.g. aeolian dust creates special problems for atmospheric correction (McClain *et al.*. 1994b). Thus, ancillary data of surface pressure, atmospheric pressure, relative humidity and the ozone optical thickness is necessary to perform an atmospheric correction because all these properties affect the transmission characteristics of the atmosphere. As sun glint depends on the solar and observation viewing geometry and wind speed, the surface values of wind speed is also necessary (McClain *et al.*. 1994a). For the SeaWiFS algorithm near real-time data will be used. Historical data is used for quality control purposes.

**Table 4** Ancillary data used for SeaWiFS calibration and validation (McClain *et al.* 1994c and 1994b)

| **Historical / climatological data** | | |
|---|---|---|
| **Data source** | **Parameter** | **Time frame** |
| COADS | pressure<br>humidity<br>wind speed | 1946-1990 |
| NIMBUS TOMS | ozone | 1978-1992 |
| **Near-real time ancillary data** | | |
| **Data source** | **Parameter** | **Priority** |
| NOAA NMC | meteorological data | primary data |
| FNOC | meteorological data | secondary source |
| GSFC OPT | ozone | primary data |
| TOVS | ozone | secondary data |

**Table 5** Algorithms for atmospheric and other corrections according to McClain *et al.*. 1994a, McClain *et al.*. 1994b, McClain *et al.*. 1995, Gordon and Wang 1994 and Mueller *et al.*. 1995b

| **Algorithm** | **Reference** |
|---|---|
| **Geometric and electronic correction** | |
| Swath overlap | Gordon *et al.*. 1983<br>Evans and Gordon 1993<br>McClain *et al.*. 1994a |
| Out of band correction | McClain *et al.*. 1995 |
| Sensor ringing mask<br>Mueller<br>SEAPAK<br><br>Miami DSP | <br>Mueller 1988<br>McClain *et al.*. 1991<br>Brock *et al.*. 1991<br>Evans and Gordon 1993 |
| **Atmospheric correction (Scattering)** | |
| Raleigh scattering | Gordon and Castaño 1987<br>Gordon *et al.*. 1988 |
| Aerosol model<br>LOWTRAN-6 aerosol model<br><br>Maritime aerosol model<br>Mie equations | <br>Shettle and Fenn 1979<br>Kneizys *et al.* 1993<br>Jursa 1985<br>Dave 1972 |
| **Atmospheric correction (Absorption)** | |
| Oxygen absorption correction | Eckstein and Simpson 1991<br>McClain *et al.*. 1994a |
| Correction of oxygen absorption on band-7 radiance | Fraser 1995 |
| Pressure and ozone correction | McClain *et al.*. 1994a |
| Interpolated pressure fields | McClain *et al.*. 1995<br>McClain *et al.*. 1994a |
| Optical thickness<br>Scattering optical thickness of stand. atm. gases<br>Absorption optical thickness of water vapour<br>Ozone optical thickness | <br>Kneizys *et al.*. 1983<br>Kneizys *et al.*. 1983<br>Inn and Tanaka 1953<br>Griggs 1968 |
| **Surface reflection and sun glint** | |
| Surface reflection<br>Probability distribution of surface slopes<br>Look-up tables for surface radiance<br>Radiative transfer code | <br>Cox and Munk 1955<br>Cox and Munk 1955<br>Ahmad and Fraser 1982 |
| Sun glint and white caps | Cox and Munk 1954a/1954b<br>Viollier *et al.*. 1980<br>McClain *et al.*. 1991 |
| **Other corrections** | |
| Cloud and ice detection | Eckstein and Simpson 1991<br>McClain *et al.*. 1994a |
| Coccolithophore blooms | Brown and Yoder 1994<br>McClain *et al.*. 1995 |

### 2.3.2.3 Calibration with sea-truth data

The calculated water-leaving radiance derived from the SeaWiFS sensor has finally to be compared with sea-truth data. Therefore, water-leaving radiances are measured by ships, drifting buoys and fixed moorings to gather time series and geographically diverse samples of water leaving radiances data sets. The radiometric accuracy shall be within a 1% error margin. Sea bed reflection influence on the water-leaving radiance shall be avoided for validation. But other error factors remain. Prime problems are the perturbation of the water-leaving radiance by the measuring ship etc., which depends on ship colour and size, instrument deployment, solar zenith angle, or cloud colour, and

atmospherically induced variability in irradiance, which depends on solar elevation, or cloud colour. At longer wavelenghts contributions from phycoerythrin and chlorophyll a fluorescence and water Raman scattering are significant (Mueller and Austin 1992).

**Table 6** Algorithms for correcting sea-truth measurements of water-leaving radiance according to Mueller and Austin (1992)

| **Algorithm** | **Reference** |
|---|---|
| Ship shadow avoidance | Gordon 1985 |
| Instrument self-shading corrections | Gordon and Ding 1992<br>Zibordi and Ferrari 1994 |
| Raman corrections | Marshall and Smith 1990 |
| Normalisation by surface irradiance | Smith and Baker 1984, 1986 |
| K-Analysis | Smith and Baker 1984, 1986<br>Petzold 1988 |
| Above-water radiance | Mueller and Austin 1995a |
| Finite bandwidth correction | Siegel *et al.*. 1986<br>Marshall and Smith 1990 |
| Normalised water-leaving radiance | Gordon 1988<br>Gordon and Clark 1981 |
| Moored radiometry | Smith *et al.*. 1991<br>Dickey *et al.*. 1991 |
| Sky radiance distributions | Voss and Zibordi 1989 |
| Beam attenuation coefficient | Smith and Baker 1981 |
| Hydrographic analysis of CTD files | Fofonoff and Millard 1983 |

Parallel to the sea-truth measurements of the water-leaving radiance, the properties of the water column below are measured to compare these properties to the measured sea-truth water-leaving radiance and the satellite derived calculated water-leaving radiance, respectively. Parameters in the water which have to be measured in time and depth include:

- Chlorophyll a and pigment concentration
- Coloured Dissolved Organic Material (CDOM)
- Coccoliths
- Detritus
- Suspended sediment
- Conductivity
- Temperature

A more complete list of all the necessary sea-truth measurements is given in Table 7.

**Table 7** Required observations for initialisation, calibration, verification and bio-optical algorithm development for SeaWiFS (Mueller and Austin 1992)

| | **Product Verification** | **Radiative Transfer** | **Bio-Optical Algorithms** |
|---|---|---|---|
| **Primary optical measurements** | | | |
| Incident spectral irradiance $E_d(0^-,\lambda)$ | x | x | x |
| Downwelled spectral irradiance $E_d(z, \lambda)$ | x | x | x |
| Upwelled spectral irradiance $L_u,(z, \lambda)$ | x | x | x |
| Spectral solar atmospheric transmission $\tau_s(\lambda)$ | x | x | x |
| Submerged upwelled radiance distribution $L(z,\theta,\phi)$ | x | x | x |
| Spectral sky radiance distribution | x | x | x |
| Upwelled spectral irradiance $E_u(z, \lambda)$ | | x | x |
| **Calculated or derived variables** | | | |
| Water-leaving radiance $L_w(0^-,\lambda)$ | x | x | x |
| Attenuation coefficient downwelled irradiance $K_E(z, \lambda)$ | x | x | x |
| Attenuation coefficient upwelled radiance $K_L(z, \lambda)$ | x | x | x |
| Spectral reflectance $R_L(z, \lambda)$ | x | x | x |
| **Ambient properties** | | | |

| | | | |
|---|---|---|---|
| Sea and sky state photographs | x | x | x |
| Wind velocity | x | x | x |
| *In situ* fluorescence profiles | | x | x |
| Aerosol samples | | x | x |
| Temperature and salinity profiles | | | x |
| Secchi depth | | | x |
| **Primary biogeochemical measurements** | | | |
| Phytoplankton pigments (HPLC technique) | | x | x |
| Phytoplankton pigments (fluorometric technique) | | x | x |
| Total suspended material (TSM) concentration | | x | x |
| Coloured dissolved organic material (CDOM) | | x | x |
| **Inherent optical properties** | | | |
| Spectral beam attenuation coefficient $c(z,\lambda)$ | | x | x |
| Spectral absorption coefficient $a(z,\lambda)$ | | x | x |
| Spectral backscattering coefficient $b_b(z,\lambda)$ | | x | x |
| Spectral volume scattering function $\beta(z,\lambda,\theta)$ | | x | x |
| **Algorithm specific research measurements** | | | |
| Airborne fluorescence and radiances | | x | x |
| Coccolith concentration | | | x |
| Detritus absorption coefficient | | x | x |
| Humic and fulvic acids (Gelbstoff) | | | x |
| Inorganic suspended material | | | x |
| Organic suspended material | | | x |
| Particle absorption coefficient | | x | x |
| Particle fluorescence | | | x |
| Particle size spectra | | x | x |
| Particulate organic carbon (POC) | | | x |
| Particulate organic nitrogen (PON) | | | x |
| Phycobilin pigments concentration | | | x |
| Phytoplankton species counts | | | x |
| Primary productivity ($^{14}C$) | | | x |
| Total dissolved organic carbon (DOC) | | | x |

The sea-truth measurements have to be done according to standard procedures (for references see Table 8). In general, the pigment concentration is determined as chlorophyll-like pigment concentration (Chlorophyll a and phaeophytin). The amount of historical data suitable for developing and validating the algorithms employed is very limited because of the specific suite of simultaneous observations and the radiometric accuracies required (within less than 5%). The historical database used for SeaWiFS (SeaBASS) includes 330.000 independent pigment observations (50 data sets) between 1956 and 1994 (historical pigment database) so new measurements had to be carried out for validation and calibration. These measurements were done using ships (Marine Optical Characterisation Cruises: MOCE) and buoys (Marine Optical Buoy: MOBY). The MOBYs are deployed near Hawaii in the Pacific and Liverpool in the Atlantic. To ensure comparability of the sea-truth measurements the instruments were regularly compared with each other (SeaWiFS Intercalibration Round-Robin Experiments: SIRREX)
(Hooker *et al.*. 1994)

**Table 8** Standard measurement procedures for sea-truth data according to Mueller and Austin (1992)

| **Measurement procedure** | **Reference** |
|---|---|
| Standard fluorometric method for chlorophyll measurement | Yentsch and Menzel 1963<br>Strickland and Parsons 1972 |
| Measurement of chlorophyll with HPLC | JGOFS 1991<br>Goericke and Repeta 1993 |
| Phycoerythrin concentration | Wyman 1992 |
| DOM measurements | Bricaud *et al.*. 1981 |
| Humic/Fulvic acid | Carder *et al.*. 1989 |
| Absorption spectrum of suspended particles (GFF dual beam spectrometer) | Mitchell and Kiefer 1984 |
| SPM dry weight | Strickland and Parsons 1972 |

As can easily be observed, the calibration effort for SeaWiFS is extensive. The calibration effort for CZCS for example was much lower. Thus, the accuracy of the SeaWiFS data is much higher than that of CZCS. But of course the advances in sensor technology are a reason for SeaWiFS higher accuracy, too.

### 2.3.3 Generated data

During the SeaWiFS mission a lot of data is generated. Following are the descriptions of several classes of data and the level of processing applied to them:

Level-1: Earth located data sets and sea-truth data which are available in GAC (approx. 4,5 km) and LAC (approx.1,1 km) resolutions

Level-1a: Raw satellite measurements which are available in GAC and LAC resolutions
- raw radiance count
- orbital calibration and navigational data
- selected instrument and telemetry data

Level-2: Processed data at GAC resolution; derived geophysical parameters produced using the Level-1a radiances as input data
- pigment and chlorophyll concentration
- diffuse attenuation coefficient at 490 nm (K(490))
- normalised water-leaving radiances
- aerosol radiances
- an error field

Level-3: Global gridded data (at approx. 9 km resolution) of the above listed parameters that has been statistically collected into daily, weekly, monthly, or annual grid cells corresponding either to 9 x 9 km equal area grid squares (binned product) or 0.09 x 0.09° squares (standard mapped image product)

(Mueller and Austin 1995a)

## 2.4 OCTS

All information which is presented in this chapter is derived from online-documentations of the OCTS-sensor or the ADEOS satellite, respectively, which are provided by the National Space Development Agency of Japan, NASDA (http://www.nasda.go.jp).

### 2.4.1 Overview

.

OCTS was designed to observe the entire earth with 8 channels in the visible band and 4 channels using atmospheric windows in the infrared band, all of which used suitable wavelengths to observe the ground surface and/or sea surface. Because of its specifications, it was expected that OCTS would not only prove useful for ocean colour measurements but also to monitor the optical thickness of atmospheric aerosols and the changing state of deserts, snow cover, ice cover and suspended substances in the ocean and to estimate the radiation balance. The spectroscopic measurement of ocean colour and sea surface temperature by the OCTS involved 12 channels, ranging from the visible and near-infrared bands to the thermal infrared band. A Ritchey-Chretien optical reflection system was employed as the collecting system for the OCTS. The aperture diameter was 27 cm and the system has a silver deposited aluminium mirror as in the case of the scanning mirror. For spectral separation, a crystal depolarizer was installed as the base for a dichroic filter to separate the visible band and infrared band in the separation component to achieve polarisation specification. While Si photodiodes were used as the detector for the visible and near-infrared band, an InSb PV type detector and HgCdTe PC type detector were used for Band 9 (3.7 µm) and Band 10 through Band 12 (8.5 µm - 12 µm) of the infrared band respectively. The desired accuracy of the sensor was to predict the water-leaving radiation $L_{WN}$ within ± 5 % and the chlorophyll a concentration within ± 30 %.

**Table 9** Major instrument parameters and characteristics for OCTS

| **Spectral Resolution** | | |
|---|---|---|
| **Band** | **Wavelength** | **Primary Use** |
| 1 | 402 - 422 nm (violet) | Yellow substance |
| 2 | 433 - 453 nm (blue) | Pigment concentration, coccolithophorids |
| 3 | 480 - 500 nm (blue-green) | Chlorophyll and pigment concentration, K(490) |
| 4 | 500 - 520 nm (blue-green) | Chlorophyll and pigment concentration |
| 5 | 555 - 575 nm (green) | Chlorophyll concentration, coccolithophorids |
| 6 | 660 - 680 nm (red) | Atmospheric correction, vegetation index |
| 7 | 745 - 785 nm (near IR) | Atmospheric correction, cloud and ice detection, aerosol radiance, vegetation index |
| 8 | 845 - 885 nm (near IR) | Atmospheric correction, aerosol radiance, vegetation index |
| 9 | 3.55 - 3.88 μm (IR) | Vegetation stress |
| 10 | 8.25 - 8.80 μm (IR) | Sea surface temperature |
| 11 | 10.3 - 11.4 μm (IR) | Sea surface temperature |
| 12 | 11.4 - 12.7 μm (IR) | Sea surface temperature |

| | | |
|---|---|---|
| **Sensor accuracy** | Calibration accuracy of visible bands | ± 10 % absolute<br>± 3 % relative |
| | Calibration accuracy of infrared bands | ± 0.8 K |
| | Linearity | ± 5 % |
| | Inter band registration | within ± 0.5 pixel |
| | Polarisation sensitivity | < 2 - 5 % |
| **Orbit parameters** | Orbit type | Sun-synchronous sub-recurrent at 796.75 km |
| | Descending node time | 10:15 to 10:45 am |
| | Inclination | 98.59° |
| | Orbital period | 100.92 min. |
| **Mission characteristics** | Minimum swath width | 1400 km |
| | Nadir resolution | 700 m |
| | Scanning rate | 0.905 s |
| | Scanning angle | approx. 40° |
| | Scan plane tilt | -20°, 0°, 20° |
| | Digitisation | 10 bit |

## 2.4.2 Calibration and validation

Calibration and validation for OCTS was probably as thorough as for SeaWiFS. A full description cannot be given here, and only the more significant differences between OCTS and SeaWiFS are pointed out. Orbital calibration was achieved using sunlight (weekly) and an internal light source (weekly) which itself is subject to change because of the harsh orbital conditions. It failed shortly after launch. Additional aircraft underflights off the coast of California were planned to be carried out annually. For the sea-truth calibration a radio buoy (similar to the MOBYs for SeaWiFS) was constantly used, but it was located in the central part of the Sea of Japan. Ocean campaign acquisition of data on chlorophyll-a, water-leaving radiance, etc. through cruising supplemented the radio buoy measurements.

### 2.4.3 Generated data

Following is a list of data which was generated during the OCTS mission. The final GAC resolution at nadir was about 4 x 4 km.

| | |
|---|---|
| Level-0: | Raw satellite measurements |
| Level-1a: | Uncorrected image: Level 0 data are cut out by unit scene and the radiometric / geometric correction factor required for subsequent processing is added |
| Level-2: | Data having undergone radiometric and registration correction and transformation to physical quantities<br>• Luminance of radiation<br>• Aerosol scattering<br>• Optical thickness<br>• Pigment density<br>• Chlorophyll a<br>• K (490)<br>• Vegetation<br>• Sea surface temperature |
| Level-3 MAP | Map projection of Level-2 transformed data<br>• Sea surface temperature<br>• Pigment density<br>• Chlorophyll a<br>• K (490) |
| Level-3 binned | Level 2 data are binned (with time and spatial references) on a daily, weekly, monthly and yearly basis<br>• Luminance of radiation<br>• Aerosol scattering<br>• Sea surface temperature<br>• Pigment density<br>• Chlorophyll a<br>• K (490) |
| Level-3 binned map | map projection of binned data<br>• Vegetation<br>• Sea surface temperature<br>• Pigment density<br>• Chlorophyll a<br>• K (490) |

## 2.5 CZCS

### 2.5.1 Overview

The Coastal Zone Colour Scanner (CZCS) was a multi-spectral line scanner dedicated principally to measurements of ocean colour. It was launched aboard Nimbus-7 in October 1978. Due to the power demands of the various on-board experiments the CZCS operated on an intermittent schedule. The thermal infra-red sensor (band 6 10.5-12.5 microns) failed within the first year. Sometime in 1981 it was determined that the sensitivity of the other CZCS sensors was degrading with time, in particular band 4. Sensitivity degradation was persistent and increased during the rest of the mission. In mid 1984 NIMBUS-7 Mission personnel experienced turn-on problems with the CZCS system which were related to power supply problems and the annual lower power summer season of NIMBUS-7. The CZCS system also began to shut down occasionally. This continued to occur the rest of the mission. From March 9, 1986 to June, 1986 the CZCS system was given highest priority for the collection of a contemporaneous data set of ocean colour. It was turned off in June at the start of the low power season with the intention of turning it back on in December when power conditions would be

more favourable. Attempts to reactivate the CZCS system in December 1986 failed. The CZCS sensor was officially declared non-operational as of 18 December 1986 (Evans and Gordon 1994).

**Table 10** Major instrument parameters and characteristics for CZCS

| **Spectral Resolution**<br>**Band** | **Wavelength** | **Primary Use** |
|---|---|---|
| 1 | 433 - 453 nm (blue) | chlorophyll absorption |
| 2 | 510 - 530 nm (green) | chlorophyll concentration |
| 3 | 540 - 560 nm (yellow) | Gelbstoff concentration |
| 4 | 660 - 680 nm (red) | aerosol absorption |
| 5 | 700 - 800 nm (near IR) | land and cloud detection |
| 6 | 10.5 - 12.5 µm (IR) | surface temperature |
| **Sensor accuracy** | Water-leaving radiance | ±10 % |
| | Overall accuracy | Pigment prediction ± 80 % |
| **Orbit parameters** | Orbit type | Sun-synchronous at 955 km |
| | Equator crossing | Noon (ascending) |
| | Inclination | 104.9° |
| | Nodal period | 104 min. |
| | Nodal increment | 26.1° |
| **Mission characteristics** | Scan width (on nadir) | 1556 km |
| | Pixels along scan | 1970 |
| | Nadir resolution | 0.825 km |
| | Scan period | 0.0275 s |
| | Scanning angle | approx. 40° |
| | Digitisation | 8-bit |

## 2.5.2 Calibration and validation

Calibration and validation of the CZCS-data was the worst in comparison to OCTS and SeaWiFS. There was no orbital calibration and for sea-truth calibration no measurements of the water-leaving radiance were conducted. Instead calibration relied solely on chlorophyll measurements from ship cruises. As the sensitivity of the instrument decreased with time calibration became more and more difficult. There were artefacts due to sensor degradation (short-term fluctuations) and the loss of sensitivity in band 1 was 40 %, for example. It was possible to measure the water leaving radiance with an accuracy of ±10 % (Evans and Gordon 1994) and the overall algorithm accuracy for pigment prediction was ± 80 % (Campbell 1995a).

## 2.5.3 Generated data

In addition to the regular data, which is outlined below, a climatological average over the whole operating period of CZCS was produced from Level 2 data..

Level 1 Raw radiance counts
Level 1a Calibrated radiances
Level 2 Derived geophysical parameters for each CZCS scene:

- Pigment concentration
- Diffuse attenuation coefficient
- Normalised water-leaving radiance at 440 nm
- Normalised water-leaving radiance at 520 nm
- Normalised water-leaving radiance at 550 nm
- Aerosol radiance at 670 nm

Level 3 Global or regional composites representing a daily, weekly, monthly or annual average of the geophysical parameters.

## 2.6 Conclusions

Although there are differences in the algorithms and the band selection, all sensors principally work in the same way which makes it possible to use all three sensors in this study. But there are big differences in accuracy. SeaWiFS and OCTS have the highest accuracy. Unfortunately, OCTS ceased operation after less than a year in orbit. CZCS on the other hand had a long time of operation, in fact the longest of all ocean colour sensors, and therefore it was possible to compute a climatological average from the CZCS-images. But the accuracy is much lower than that from SeaWiFS and OCTS.

# 3 Carbon Cycle Modelling for the Ocean

## 3.1 The global carbon cycle

The general facts about the global carbon cycle are well known today. But it is still difficult to exactly quantify the relevant carbon fluxes. The present estimates cannot explain the gap between the release of $CO_2$ by the combustion of fossil fuel and deforestation on the one hand and the accumulation of $CO_2$ in the atmosphere, which is well documented in the Mauna Loa time series, and the uptake of $CO_2$ in the ocean on the other hand. Thus, the current estimates have to be refined to get a more accurate quantification of the global carbon cycle.

**Table 11** Current estimates of global carbon fluxes (Quay 1996)

| **Carbon fluxes** | **Amount [gigatons C/year]** |
|---|---|
| Combustion of fossil fuels | $5.4 \pm 0.5$ |
| Biomass burning (Deforestation) | $1.6 \pm 0.8$ |
| Accumulation of $CO_2$ in the atmosphere | 3.4 |
| Ocean uptake | $2.1 \pm 0.8$ |
| Missing | 1.6 |

## 3.2 The carbon and nitrogen cycle in the ocean

One possible carbon sink is the ocean. The amount of $CO_2$ uptake depends for example on the temperature of the sea (solubility of gases in the sea) or the primary production of marine algae. But the variations in estimates of global marine production range from $20 - 44 \times 10^{15}$ g C/yr (Schlesinger 1991). Furthermore, phytoplankton is fed upon by zooplankton or bacteria which themselves are predated by fish and other higher organisms. At some point in time these organisms will die and be degraded by other organisms or the dead organic matter will sink to the bottom. Thus this sinking organic material forms a sink in the global carbon cycle. Eventually, all organisms are situated in a complicated food chain / food web and the quantification of this food web in the ocean is not easy. For example Cole et al. (1988) found that bacterial growth is about twice that of zooplankton and consumed 40% of NPP in the photic zone. Cho and Azam (1988) also concluded that free-living bacteria were more important than zooplankton in the consumption of particulate organic carbon in the ocean. About 90% of the NPP is degraded to inorganic compounds in the surface waters, and the remainder sinks below the euphotic zone to the deep ocean. The mean sinking rate is about 350m/day, so the average particle spends about 10 days in transit to the bottom (Honjo et al. 1982). The approximation of this flux of dead biomass to the bottom ranges from $3.4 - 6.0 \times 10^{15}$ g C/yr (Martin et al. 1987 and Eppley and Peterson 1979). But these figures show the importance of the biologically mediated flux of carbon to the bottom of the ocean.

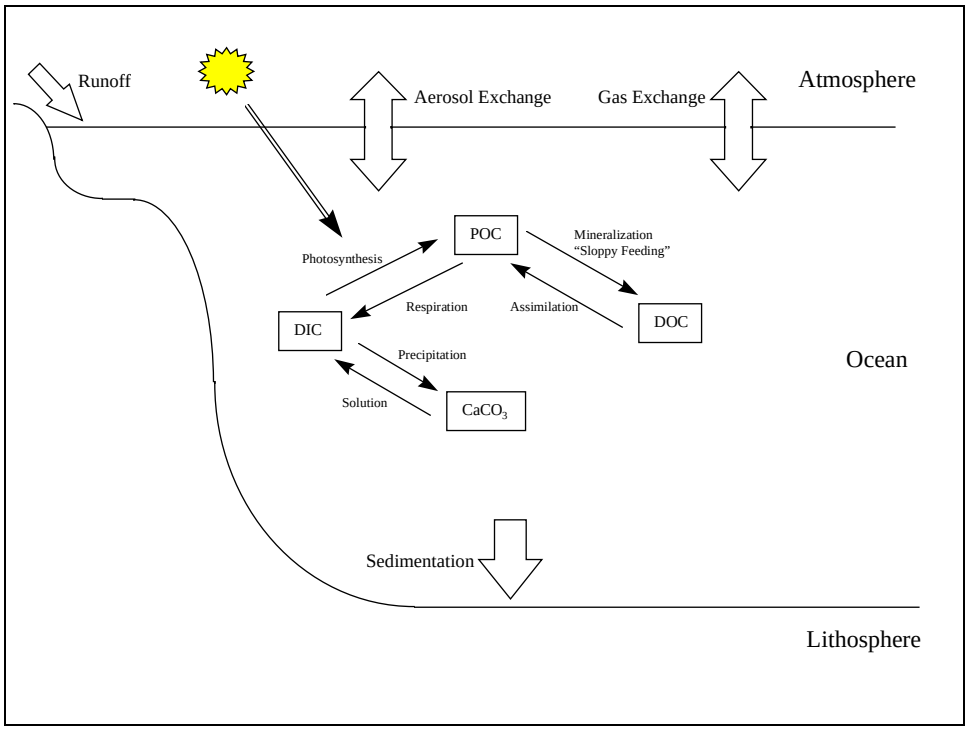


**Figure 3** Carbon cycle in the ocean

Obviously the downward flux of carbon in the oceans depends on the concentration of phytoplankton in the upper ocean and the primary production. According to the nutrient light hypothesis phytoplankton will grow if there is enough light and nutrients (Yentsch 1993). The most important nutrient in the sea seems to be nitrogen. In most regions of the ocean, nitrate supply is thought to limit the production of organic matter, but in vast areas the concentration of nitrate is well in excess of that required to sustain growth (Chrisholm and Morel 1991). The extend of nutrient rich areas and nutrient poor areas is largely governed by the ocean dynamics (currents, upwelling, downwelling, tidal waves, etc.).

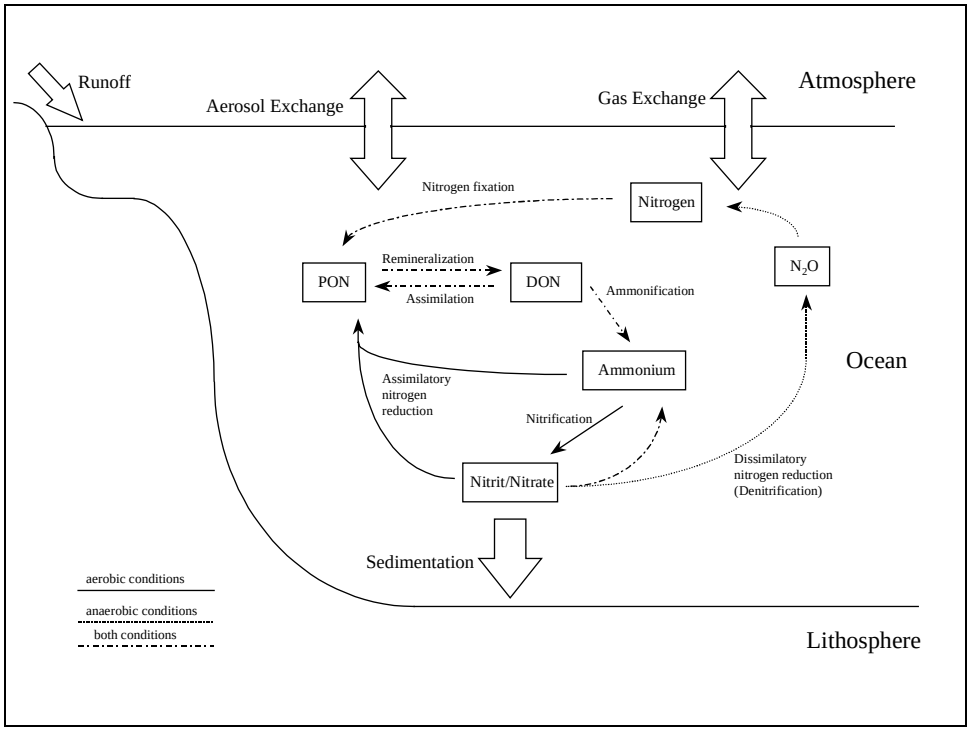


**Figure 4** Nitrogen cycle in the ocean

## 3.3 Overview of the ocean dynamics in the North Atlantic

The ocean dynamics themselves are largely governed by wind, irradiance (heat), and the rotation of the earth (coriolis force). Poleward heat transport by atmospheric and oceanic currents power the world's climate system. In the atmosphere much of this heat transport is accomplished by transient eddies (cyclones and anticyclones) embedded in strong, hydrodynamically unstable zonal currents circling the earth in west to east directions. Ocean currents cannot move along a latitude circle (except around Antarctica) without sooner or later running into a continent. As a result, oceanic circulation systems tend to form close loops ("gyres") within individual basins. Hence, the ocean exhibits a phenomenon not generally seen in the atmosphere, namely, strong persistent currents flowing in meridional directions (Ingmanson and Wallace 1995).

Sunlight, the source of oceanic heating penetrates the ocean only to a depth of a few hundred meters. Thus, the ocean is essentially heated from above. In most oceanic locations, a thin warm layer of warm water overlies a massive layer of cold water. The cold bottom water is being replenished continuously from relatively small polar regions where atmospheric circulation anomalies or other factors allow the formation of masses that possess sufficient density to sink to the bottom (downwelling areas). Centuries or millennia later, this water comes into contact with the surface again (upwelling areas) because it eventually fills up the basin.

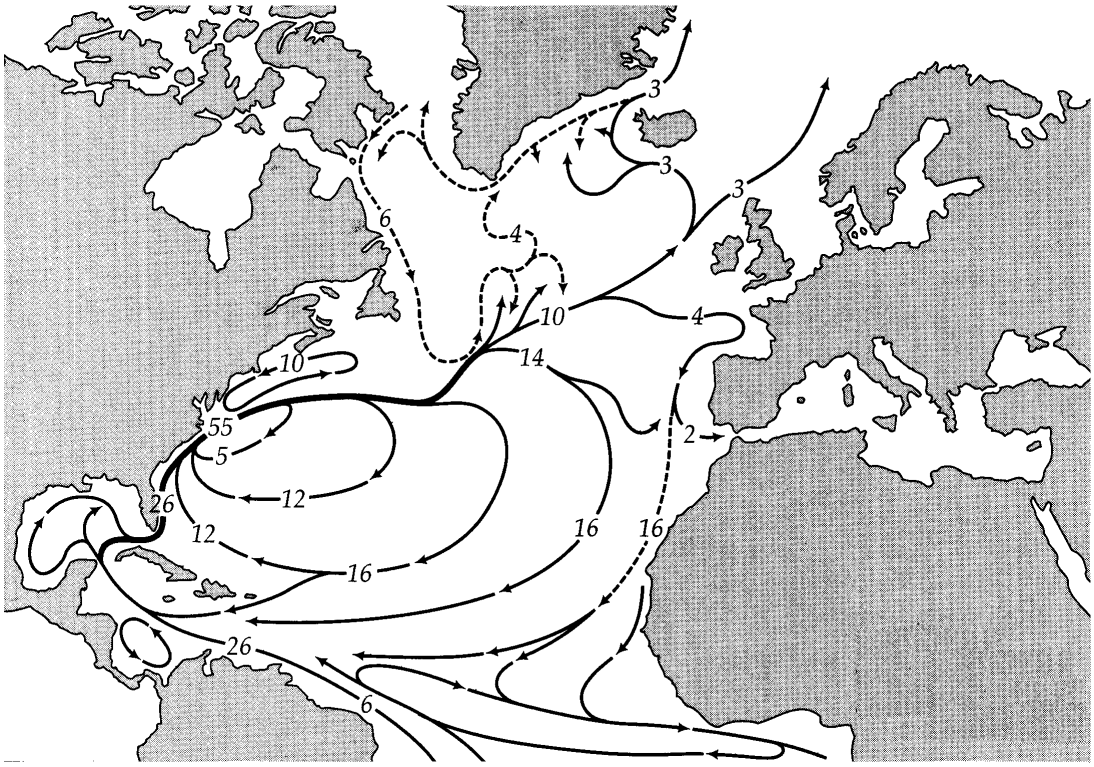


**Figure 5** The general surface circulation of the North Atlantic (solid lines: warm currents; dashed lines: cold currents). The numbers indicate flow rates in Sverdrup (1 Sv = $10^6$ $m^3/s$) from Ingmanson and Wallace 1995: 155

The main features of the North Atlantic are the subtropical gyre, the Golf Stream, which is the most prominent and important current of the North Atlantic, the Mauritanian upwelling area at the coast of Africa and the downwelling area in the Greenland Island Norwegian Sea which is an important part of the global thermohaline circulation. Figure 5 gives an overview over other surface currents in the North Atlantic.

# 3.4 The isopycnic coordinate carbon cycle model (Drange 1994)

## 3.4.1 Overview

The Nansen Center Carbon Cycle Model (N3CM) as described by Drange (1994 and 1996) is based on the isopycnic coordinate OGCM "MICOM" described by Bleck *et al.* (1992), in the Atlantic implementation of New *et al.* (1995a). The chemical model of Peng *et al.* (1987), and a slightly modified version of the nitrogen based 1-D ecosystem model described by Fasham *et al.* (1990) and Fasham (1993), which was extended to a 3-D framework by Sarmiento *et al.* (1993), have been coupled to the physical model.

Following are the most important equations and references. A more detailed description is given by Drange (1994 and 1996). A general overview over biogeochemical models is given by Evans and Garçon (1997). The model description is divided into three parts, one part each for the equations which govern the physical, the chemical and the ecological part of the model. Following then is the numerical solution technique and the boundary conditions.

## 3.4.2 The physical model

The modelation of the ocean physics is the most important part of the model because it resolves the strength and direction of currents, the mixed layer dynamics and deep water formation or upwelling. The preferred direction of movement of watermasses in the ocean is along, rather than across, planes of constant density (isopycnals). The mixing is orders of magnitude weaker in the diapycnal than in the isopycnal direction and this is embedded into the isopycnal concept per se, only two dimensional prognostic equations have to be solved so there is no numerical smoothing of the dynamic fields in the diapycnal direction. The Achilles heel of isopycnic models is that layers may disappear and reappear wherever and whenever called for by the dynamics, which puts severe constraints on the numerical treatment of the layers and the actual solution technique employed. The most important parameter for an isopycnic coordinate OGCM is the density of the water which changes according to temperature and salinity.

On top of the model ocean the mixed layer (ML) formulation incorporates the integral effect of wind stirring and buoyancy fluxes (evaporation etc.) at the surface. The prognostic variables for the ML are the horizontal velocity vector, the layer thickness, temperature and salinity. Thus, the mixed layer formulations are governed by surface forcing. The equations can be found in Drange (1994). Below the mixed layer there are 19 layers of prescribed and constant density with the horizontal velocity vector, the layer thickness and the salinity as prognostic variables. The potential densities of the isopycnic layers in the dimensionless $\sigma_0$-units (reference pressure at surface) are 24.70, 25.28, 25.77, 26.18, 26.52, 26.80, 27.03, 27.22, 27.38, 27.52, 27.64, 27.74, 27.82, 27.88, 27.92, 28.00, 28.06, 28.09, and 28.12. Unstable stratification is removed by mixing the actual water masses and all of their physical and biogeochemical properties uniformly in the vertical (Drange 1996). The mixed layer was split into two biochemical layers. In the euphotic zone the ecosystem model as described in chapter 3.4.4 was solved, and in all layers below the euphotic zone, the regeneration model given in chapter 3.4.4.5 is solved. The euphotic zone was defined as the penetration depth of 0.75 % of the surface irradiance, with a minimum of 40m. In the case of a thick mixed layer relative to the euphotic zone, four of the biochemical layers are placed in the euphotic zone, and the fifth layer covers the rest of the mixed layer. If a physical layer below the mixed layer became thicker than 12m and was positioned in the euphotic zone, the physical layer was split into two or more biochemical sublayers.

The basic equations to be solved were the mass continuity equation and transport equations for the biochemical compartments. The mass continuity equation in terms of the layer thickness $h_k$ for layer k reads:

$$\frac{\partial h_k}{\partial t} + \nabla \cdot (\mathbf{u}_k h_k) - \nabla \cdot (K_h \nabla h_k) - \frac{\partial}{\partial z}\left( K_v \frac{\partial h_k}{\partial z} \right) = \left( \frac{\partial h_k}{\partial t} \right)_{diap}$$

**Equation 5** Mass continuity equation (layer thickness)

The first term of Equation 5 describes the local change in the thickness of layer k, the second term gives the advective change of $h_k$, whereas the third and fourth terms give the change in $h_k$ due to non-modelled fluctuations in the dynamic fields, parameterized as diffusive mixing. The isopycnal diffusivity is constant in the interior of the model domain and assumes the value $10^3$ $m^2/s$. The diapycnal diffusivity is inversely proportional to the square of the local buoyancy frequency N [1/s] in the physical mixed layer, and proportional to $N^{-1}$ in the interior ocean.

$$K_v = \gamma \varepsilon N^{-2}$$

**Equation 6** Diapycnical diffusivity in the physical mixed layer

$$K_v = \frac{10^{-7}}{N} m^2 s^{-1}$$

**Equation 7** Diapycnical diffusivity in the interior ocean (Gargett expression)

**Table 12** Algorithms implemented in the physical part of N3CM according to Drange (1994)

| **Algorithms** | **References** |
|---|---|
| Reynolds averaging of the non-linear flux term | Bleck *et al.*. 1992 |
| Mixed-layer of the Kraus-Turner type | Bleck *et al.*. 1989<br>Kraus and Turner 1969<br>Niiler and Kraus 1977 |
| Gargett expression | Gargett 1984 |

The transport equations to be solved for each of the biochemical compartments $C^i$ in each of the physical and biochemical (see section 3.3.4) layers k can be put in the following form:

$$\frac{\partial h_k C_k^i}{\partial t} + \nabla \cdot (\mathbf{u}_k h_k C_k^i) - \nabla \cdot (K_h \nabla h_k C_k^i) - \frac{\partial}{\partial z}\left( K_v \frac{\partial h_k C_k^i}{\partial z} \right) = \left( \frac{\partial h_k C_k^i}{\partial t} \right)_{diap} + h_k \frac{\delta C_k^i}{\delta t}$$

**Equation 8** Transports equations for the biochemical compartments $C^i$

The concentration of compartment $C^i$ in each of the physical and biochemical layers k is given by dividing $h_k C^i_k$ from Equation 8 by $h_k$ from Equation 5. The integrated carbon cycle model preserves the total inventory of the biochemical compartments $C^i$ if and only if Equation 5 and Equation 8 are solved simultaneously and consistently. The last term in Equation 8 denotes all sources and sinks that act on $C^i$, and depends, in general, on all of the compartments.

## 3.4.3 The chemical model

The thermodynamic and chemical properties of seawater are, to first order, governed by the properties of pure water and 13 major dissolved components. Several of the major dissolved components are conservative, i.e., the abundance varies in a linear way with salinity.

**Table 13** Major ion composition of seawater, their chlorinity ratio and mean residence times for the elements (Schlesinger 1991 and Holland 1978)

| **Constituent** | **Concentration in Seawater [mg/kg]** | **Chlorinity Ratio** | **Mean Residence Time [$10^6$ years]** |
|---|---|---|---|
| Sodium | 10760 | 0.5561 | 75 |
| Magnesium | 1294 | 0.0668 | 14 |
| Calcium | 412 | 0.0213 | 1.1 |
| Potassium | 399 | 0.0206 | 11 |
| Strontium | 7.9 | 0.00041 | 12 |

| | | | |
|---|---|---|---|
| Chloride | 19350 | 1.0000 | 120 |
| Sulphate | 2712 | 0.1400 | 12 |
| Bicarbonate | 145 | 0.0075 | 0.10 |
| Bromide | 67 | 0.0035 | 100 |
| Silicate | 2.9 | 0.00015 | 0.02 |
| Boron | 4.6 | 0.00024 | 10.0 |
| Fluoride | 1.3 | 0.000067 | 0.5 |
| Water | | | 0.036 |

Once the numerical value of the alkalinity and dissolved inorganic carbon (DIC) compartments are known in the surface layer, the partial pressure of $CO_2$ can be computed based on analytical expressions of the equilibrium that governs the carbonic acid system in seawater, because temperature and salinity are known from the physical fields:

$$pCO_2^{sea} = pCO_2^{sea}(C_T, A_T, T, S)$$

**Equation 9** Partial pressure of $CO_2$ in the sea

The carbonic acid system in sea-water is mainly determined by the following reactions (Stumm and Morgan 1981 and Millero and Sohn 1992):

$$\begin{aligned}
CO_2(g) &\leftrightarrow CO_2(aq) && K_0\\
CO_2(aq) + H_2O &\leftrightarrow HCO_3^- + H^+ && K_1\\
HCO_3^- &\leftrightarrow CO_3^{2-} + H^+ && K_2\\
B(OH)_3 + H_2O &\leftrightarrow B(OH)_4^- + H^+ && K_B\\
H_2O &\leftrightarrow OH^- + H^+ && K_w\\
CaCO_3(s) &\leftrightarrow Ca^{2+} + CO_3^{2-} && K_{sp}
\end{aligned}$$

In the above, expression $K_0$ is the Henry's law constant and the Ks denote the equilibrium constants for the reactions considered. All these constants depend on temperature, salinity, and the pressure of the system. In addition, $K_1$, $K_2$, $K_B$, $K_w$ and $K_{sp}$ depend on the pH scale. In some expressions the activity of the hydrogen ion ($H^+$) is needed which is determined by the pH scale used (Bates and Culberson 1977). Thus, the equilibrium constants are calculated with empirical formulas which take these dependencies into consideration. A very simple example is the equation for total borate which is only dependent on the salinity (see Equation 10). All the empirical formulations are given by Peng *et al.* (1987).

$$\begin{aligned}
K_0 &= \frac{pCO_2}{[CO_2(aq)]}\\
K_1 &= \frac{[HCO_3^-](H^+)}{[CO_2(aq)]}\\
K_2 &= \frac{[CO_3^{2-}](H^+)}{[HCO_3^-]}\\
K_B &= \frac{[B(OH)_4^-](H^+)}{[B(OH)_3]}\\
K_W &= (H^+)[OH^-]
\end{aligned}$$

$$\begin{aligned}
C_T &= [CO_2(aq)] + [HCO_3^-] + [CO_3^{2-}]\\
B_T &= [B(OH)_3] + [B(OH)_4^-] = 1.212 \cdot 10^{-5} S\\
A_T &= [HCO_3^-] + 2[CO_3^{2-}] + [B(OH)_4^-] + [OH^-] - [H^+]_T
\end{aligned}$$

**Equation 10** Equations for the chemical part of the model

The contribution from the phosphorus, nitrogen, and silicon components on the carbonic acid system are included in a way similar to Borate.

**Table 14** Algorithms implemented in the chemical part of N3CM according to Drange (1994)

| **Algorithms** | **References** |
|---|---|
| Concentration of total dissolved borate $B_T$ | Millero 1979<br>Millero and Sohn 1992 |
| Carbonic acid system | Stumm and Morgan 1981<br>Millero and Sohn 1992 |
| Total alkalinity | Dickson 1981<br>UNESCO 1987 |
| Relation between the total and free $H^+$ | Dickson and Millero 1987 |
| Contribution of phosphorus on the carbonic acid system | Peng *et al.* 1987<br>Dickson 1981 |
| Contribution of nitrogen species on the carbonic acid system | Stumm and Morgan 1981<br>Brewer and Goldman 1976<br>Goldman and Brewer 1980 |
| Distribution of sinking $CaCO_3$ | Archer and Maier-Reimer 1994 |
| Dissolution curve for calcite and aragonite | Broecker and Takahashi 1978 |
| Concentration profiles of $CO_3^{2-}$ | Takahashi *et al.* 1981 |
| Exchange of $CO_2$ across the air-sea interface | Wanninkhof 1992 |
| Calculation of Temperature and Salinity from the off-line physical fields | Peng *et al.*. 1987 |

## 3.4.4 The ecosystem model

### 3.4.4.1 Overview

The model is a seven-compartment model with phytoplankton, zooplankton and bacteria as the living biota, the nutrients are ammonium and nitrate. In addition, there is one pool of dissolved organic nitrogen and one pool of particulate organic nitrogen. The model has been designed for the annual cycle of nitrogen at Station "S" near Bermuda (32° North 65° West) and was later adjusted and tested against observations from both Station "S" and the Ocean Weather Station "India" (59° North 19° West). It is divided in two parts, one that describes the exchange of nitrogen between compartments in the euphotic zone, and a second part that parameterizes the decay of particulate and dissolved organic nitrogen below the euphotic zone. The ecosystem is only modelled explicitly in the euphotic zone, below the euphotic zone all the organic matter is gradually turned over to ammonium and then to nitrate. An overview of the ecological part of the model and its coupling to the chemical model can be seen in Figure 6.

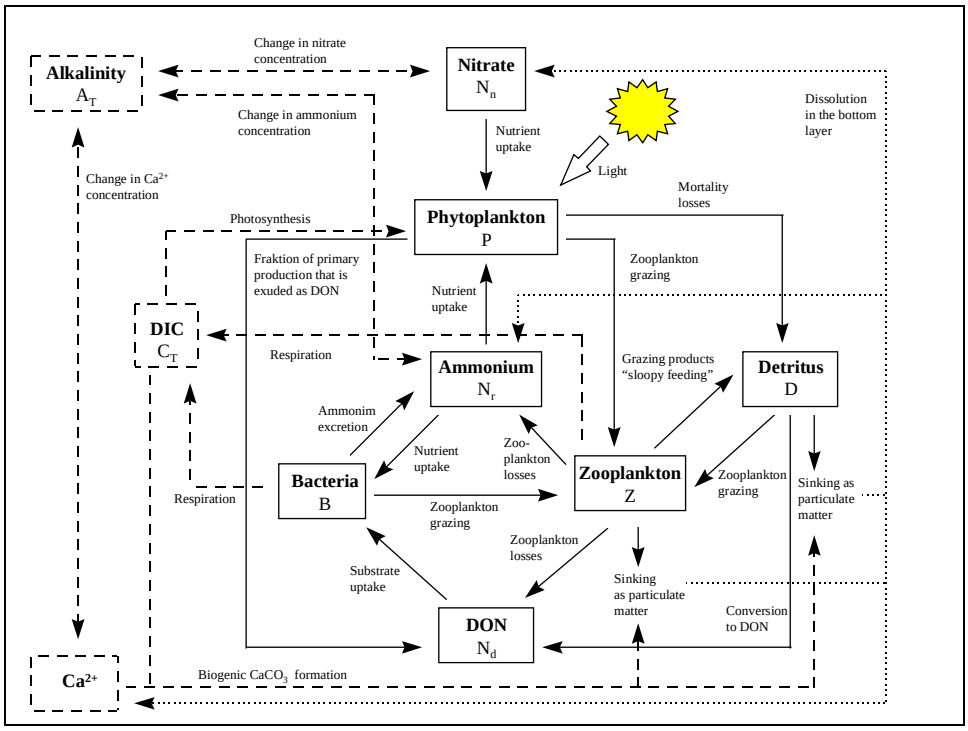


**Figure 6** The ecosphere model for the euphotic zone (solid lines), its link to the chemical model (dashed lines) and processes in the bottom layer (dotted lines)

The model is based on nitrogen as the "currency" of the ecosystem model. Constant ratios are used to calculate the carbon content from the nitrogen content or vice versa. These Redfield ratios (carbon to nitrogen ratio) are assumed as follows: 7.5 for phytoplankton, 5.5 for zooplankton, and 5 for bacteria. The carbon to nitrogen ratio for DON and detritus varies according to the sources and sinks of these compartments.

### 3.4.4.2 Phytoplankton

Phytoplankton is the only carbon fixing compartment in the model. The first term on the right hand side in Equation 11 is the light and nutrient limited growth rate of the phytoplankton. $\gamma$ is the fraction of primary production that is exuded as dissolved organic nitrogen. In general, the light limited growth rate J (t, z) depends on the irradiance field, the sun angle, the quantum yield of photosynthesis, temperature, light attenuation in the water (which in itself depends on the phytoplankton concentration), and depth. The exact formulation for J (t, z) and the nutrient limitation factors are given in chapter 3.5. The second term on the right hand side symbolises zooplankton grazing and the last term phytoplankton mortality.

$$\frac{\delta P}{\delta t} = (1-\gamma)\, J(t,z)\, (\tilde{N}_n + \tilde{N}_r)\, P - G_1 - \mu_1 \frac{P}{k_5 + P}$$

**Equation 11** Phytoplankton equation

### 3.4.4.2 Zooplankton

The zooplankton grazes on phytoplankton (first term on r.h.s.), bacteria (second term), and detritus (third term). A part of it dies or is eaten up by higher predators, like fish (fourth term). The fifth term takes into account that the carbon to nitrogen ratio for bacteria and zooplankton is not the same. The grazing functions are defined in a way that the zooplankton is feeding on the most abundant food source (see Drange (1994) for details).

$$\frac{\delta Z}{\delta t} = \beta_1 G_1 + \beta_2 G_2 + \beta_3 G_3 - \mu_2 \frac{Z^2}{k_6 + Z} - \eta(R_b / R_p) G_2$$

**Equation 12** Zooplankton equation

### 3.4.4.3 Bacteria

The bacteria obtain carbon from the dissolved organic nitrogen pool (constant N to C ratio) and their nitrogen from ammonium uptake. Special consideration has to be given to the carbon to nitrogen ratios. They are not the same for all biochemical compartments. To maintain constant ratios for each of the biochemical compartments, ammonium is taken up or exuded as necessary (see Equation 16). Thus, for the growth of bacteria the uptake of carbon and nitrogen from the dissolved organic nitrogen pool (DON) and additional nitrogen uptake from the ammonium pool is necessary. The exact description of $U_1$ and $U_2$, the bacterial uptake rates for DON and ammonium, is given by Drange (1994). The third term on the right hand side is the bacterial specific excretion rate and the last one the loss because of zooplankton grazing.

$$\frac{\delta B}{\delta t} = U_1 + U_2 - \mu_3 B - G_2$$

**Equation 13** Bacteria equation

### 3.4.4.4 Detritus, Nitrate, Ammonium, DON

Detritus is produced by sloppy feeding (term 1-3 on r.h.s.) and by dying phytoplankton (5th term). It is consumed by zooplankton (4th term). A fraction of the detritus pool is converted to DON (6th term) and another part sinks to the bottom (7th term).

$$\frac{\delta D}{\delta t} = (1-\beta_1) G_1 + (1-\beta_2) G_2 + (1-\beta_3) G_3 - G_3 + \mu_1 \frac{P^2}{k_5 + P} - \mu_4 D - w \frac{\partial D}{\partial z}$$

**Equation 14** Detritus equation

The nitrate equation is only governed by the uptake of nitrate through phytoplankton. The only source for nitrogen is its regeneration below the euphotic zone (see chapter 3.4.4.5).

$$\frac{\delta N_n}{\delta t} = -J(t,z) \tilde{N}_n P$$

**Equation 15** Nitrate equation

Ammonium is taken up by phytoplankton and zooplankton (term 1 and 2 on r.h.s) and is gained from bacteria (3rd term) and zooplankton (4th term). The last term on the right hand side is necessary because of the changing carbon to nitrogen ratios as mentioned above.

$$\frac{\delta N_r}{\delta t} = -J(t,z) \tilde{N}_r P - U_2 + \mu_3 B + \varepsilon \mu_2 \frac{Z^2}{k_6 + Z} + \eta(R_b / R_p) G_2$$

**Equation 16** Ammonium equation

DON is produced by phytoplankton, zooplankton (term 1 and 2 on r.h.s.) and through the degradation of detritus (3rd term). It is used by bacteria as a source of energy (4th term).

$$\frac{\delta N_d}{\delta t} = \gamma J(t,z)(\tilde{N}_n + \tilde{N}_r)P + \delta\mu_2 \frac{Z^2}{k_6 + Z} + \mu_4 D - U_1$$

**Equation 17** DON equation

### 3.4.4.5 Regeneration below the euphotic zone

The equations described in the previous section are only solved in the euphotic zone. Below the euphotic zone the model of Sarmiento *et al.* (1993) is followed that all biogenic compartments decay to ammonium, and then to nitrate with the decay constant λ. All of the particulate material (detritus) that falls out of the euphotic zone, i.e. $w(\partial D/\partial z)_{ez}$ and the accumulated amount of zooplankton losses $(1-\varepsilon-\delta)\ \mu_2 Z^2/(k_6+Z)$ is distributed in the vertical according to the following empirically derived expression (Martin *et al.* 1987):

$$F(z) = F(z_{ez})(\frac{z}{z_{ez}})^{-\nu}$$

**Equation 18** Distribution below the euphotic zone

In Equation 18 F is the flux of particulate material, and the subscript ez denotes that the quantity is evaluated at the base of the euphotic zone. Once the material is distributed according to Equation 5 the material is remineralized to ammonium with the decay constant λ. Particulate material that ends up on the ocean floor is immediately remineralized.

### 3.4.4.6 Coupling to the chemical model

It is assumed that photosynthesis is the only inorganic carbon fixing compartment, the only autotroph organism in the biological system. DIC (total dissolve inorganic carbon) is therefore lost during photosynthesis (1st term on r.h.s) and gained through respiration of bacteria and zooplankton 3rd and 4th term). DIC is also lost by the formation of $CaCO_3$ (2nd term).

$$\frac{\delta C_T}{\delta t} = -J(t,z)(\tilde{N}_n + \tilde{N}_r)PR_p - \frac{\delta CaCO_3}{\delta t} + \mu_3 BR_b + \varepsilon\ \mu_2 \frac{Z^2}{k_6 + Z} R_p$$

**Equation 19** Dissolved Inorganic Carbon equation

The alkalinity is governed by the uptake of nitrate and ammonium (1st and 2nd term on r.h.s) and the formation of $CaCO_3$.

$$\frac{\delta A_T}{\delta t} = -\frac{\delta N_n}{\delta t} + \frac{\delta N_r}{\delta t} - 2\frac{\delta CaCO_3}{\delta t}$$

**Equation 20** Total alkalinity equation

### 3.4.4.7 Biogenic formation and dissolution of calcium carbonate

Both phytoplankton and zooplankton species produce calcium carbonate shells. On global average 80% of the carbon atoms that sinks out of the euphotic zone is in the form of organic tissue and 20% is in the form of $CaCO_3$ (Broecker and Peng 1982: p. 11 and 269). The formation of $CaCO_3$, which depends on temperature (see Equation 21), reduces the alkalinity and thereby increases the partial

pressure of $CO_2$ in seawater (and vice versa). The flux of $CaCO_3$ is assumed to be proportional to the flux of organic matter out of the euphotic zone (proportionality factor: 0.2).

$$f_{CaCO_3} = \frac{\exp[0.6(T-10)]}{1+\exp[0.6(T-10)]}$$

**Equation 21** Temperature dependence of $CaCO_3$ formation

Instead of solving the chemical model in each of the biochemical layers it has been assumed that the sinking $CaCO_3$ is distributed in the vertical with an e-folding length of 4000m, and is then dissolved into seawater. All of the $CaCO_3$ that ends up on the seabed is dissolved in the bottom layer.

#### 3.4.4.8 Silicon

The silicid acid system has not been included in the model, since the biogenic uptake of Si generally differs from that of N and P due to the formation of biogenic silica shells. Proper inclusion of the silicid acid would therefore require explicit modelling of for instance planktonic diatoms which is not done in the ecological part of the model.

### 3.4.5 Numerical solution techniques

It is an absolute requirement for an isopycnic layer model to use a positive definite numerical advection scheme. The layer thickness fields have to remain positive just like the biochemical compartments. The upstream advection scheme is positive definite but suffers from large numerical diffusion. It is possible, however, to construct numerical advection schemes that are positive definite and almost free of numerical diffusion by defining so called anti-diffusive velocities. MPDATA developed by Smolarkiewicz and co-workers (Smolarkiewicz 1984, Smolarkiewicz and Clark 1986, and Smolarkiewicz and Grabowski 1990) is an algorithm which incorporates this method. The basic version of the MPDATA scheme is of second order accuracy and is based on forward-in-time and upstream-in-space discretisation of the transport equation.

Thus, the exchange of the water masses in the vertical among the physical layers in the model is a result of the ventilation of the mixed layer, diapycnical mixing and convection. Since the exchange of water masses directly affects only the upper and lower biochemical layers in the physical layers under consideration, interior biochemical layers can remain isolated from the neighbouring biochemical layers for a long time but this is unrealistic. Thus vertical mixing between biochemical layers in the mixed layer is resolved by a parameterization of the vertical turbulent diffusion within the mixed layer.

**Table 15** Numerical solution algorithms

| **Algorithm** | **Reference** |
|---|---|
| Method of successive over-relaxation | Golub and van Loan 1983 |
| MPDATA | Smolarkiewicz 1984<br>Smolarkiewicz and Clark 1986<br>Smolarkiewicz and Grabowski 1990 |
| Sublayer splitting algorithm | Drange 1994 |
| Off-line time integration procedure | Drange 1994 |

### 3.4.6 Model domain and boundary conditions

#### 3.4.6.1 Geographical boundaries

The model equations were formulated on a Mercator grid (126 by 104). The Mediterranean Sea, the Hudson Bay, the Barents Sea, and the North Sea were excluded from the model domain but these boundary seas were passively present in the initialisation fields. The Greenland Iceland

Norwegian Seas are covered by 12 by 13 grid cells, which means that this region should be considered as a boundary zone for the Atlantic. Furthermore, the northern and southern model boundaries were solid walls, and the along isopycnical diffusivity was increased linearly by an order of magnitude over the ten grid cells closest to the walls. There is no exchange of water through the northern and the southern model boundaries.

### 3.4.6.2 Initialisation

The model was initialised with the September values of the Levitus (1982) data sets. The integrated carbon cycle model was initialised with a nitrate, a total dissolved inorganic carbon, and a total alkalinity field (see Table 16 for references). For the initial concentration of phytoplankton, zooplankton, bacteria, ammonium, dissolved organic nitrogen and detritus the values of Sarmiento *et al.* (1993) were used.

The forcing fields were climatological averages from different data sets which are given in Table 16. Algorithms which were also used for the forcing are given in Table 16 as well. The carbon dioxide concentrations begin in 1979 with 336 ppm and an annual increase of 1.6 ppm. The latitudinal dependency of the $CO_2$ concentration has been neglected. It must be noted that the accuracy of the forcing fields might not be as good as would be desired. Thus, the model results can have huge errors just because of inaccurate forcing fields, e. g. contains the irradiance model together with the uncertainty associated with the prescribed cloudiness fraction an expected error of about 20% in the irradiance field.

**Table 16** Measurements and algorithms necessary for initialisation, boundary conditions, and forcing fields (Drange 1994)

| | **Comment** | **Reference** |
|---|---|---|
| **Initialisation** | | |
| Nitrate | interpolated annual mean values | Levitus *et al.* 1993 |
| DIC<br>Alkalinity | interpolated values | GEOSECS<br>TTO/NAS<br>AJAX<br>SAVE<br>NABE<br>Hudson-82 expedition<br>Mosby-93 expedition |
| Phytoplankton<br>Zooplankton<br>Bacteria<br>Ammonium<br>DON<br>Detritus | $P = 0.14$ mmol/m$^3$<br>$Z = 0.014$ mmol/m$^3$<br>$B = 0.014$ mmol/m$^3$<br>$N_r = 0.1$ mmol/m$^3$<br>$N_d = 0.1$ mmol/m$^3$<br>$D = 0.1$ mmol/m$^3$ | Sarmiento *et al.* 1993 |
| Salinity<br>Temperature | | Levitus 1982 |
| **Forcing fields** | | |
| Wind | climatological data | Hellerman and Rosenstein 1983 |
| Heat fluxes | climatological data | Esbensen and Kushnir 1981 |
| Precipitation | climatological data | Jaeger 1976 |
| Evaporation | climatological data | Esbensen and Kushnir 1981 |
| **Carbon dioxide** | | |
| $CO_2$ (atmosphere) | monthly mean concentrations<br>algorithm for seasonal variation | Boden *et al.* 1991<br>Drange 1994 |
| Calculation of $pCO_2$ (at water saturation pressure) from $pCO_2$ (in dry air) | algorithm | Siegenthaler 1986<br>Sarmiento *et al.* 1992 |
| Exchange of $CO_2$ across the air- | algorithm | Liss and Slater 1974 |

| | | |
|---|---|---|
| sea interface | | |
| Transfer velocity for $CO_2$ transfer | algorithm | Wanninkhof 1992<br>Jäne *et al.* 1987 |
| **Solar irradiance** | | |
| Atmospheric effect on solar irradiance field | algorithm | Rosati and Miyakoda 1988<br>Gill 1982<br>Hsiung 1986 |
| Effects of clouds | algorithm | Reed 1977, 1981 |
| Cloud cover | monthly mean fractional cloud cover | COADS<br>Woodruff *et al.* 1987 |
| Irradiance field in the ocean | algorithm | Kirk 1986<br>Sathyendranath and Platt 1988 |
| Sun zenith angle in water | algorithm | Snell's law |
| **Other** | | |
| Bathymetry | Scripps 1° database | |

#### 3.4.6.3 Sea ice

A sea ice model is not included yet, but the presence of sea-ice was mimicked by setting the surface wind stirring and the heat fluxes to zero where the modelled ML temperature went below -1.8°C.

#### 3.4.6.4 Time step

The integrated carbon cycle model used a year of 365 days, and a time step of 10512 s. To keep the output fields within reasonable limits, one model year was divided into twenty-five 14.6 days intervals (each interval corresponds to 120 time steps). The simulation started at day 58.4, since the generally deep mixed layer at this time of year would tend to smooth out localised biological signals in the surface $C_T$, $A_T$ and nitrate fields. In addition, February is well before the planktonic blooms start at high latitudes. The atmospheric concentration of $CO_2$ depends on time and the integration started in year 1981 (i.e. at day 58.4 in year 1981)

The model reached an annual quasi steady state circulation in model year 15. The annual quasi steady state circulation was deemed sufficiently realistic to be used as a driver for the carbon cycle model. The ecosystem and chemical models were run fully coupled with the physical model for 5 years, starting on January 1 of year 20 of the physical model run. A quasi-annual cycle was obtained after 2-3 years.

However, the present dynamical model which is forced with observed salinity and heat fluxes on a closed model domain, will never reach a true annual steady-state circulation. It has been verified that if the present version of the model is run for more than a couple of decades, dense water produced at high latitudes starts to accumulate in the deepest parts of the model domain (New *et al.*. 1994a).

## 3.5 Calculation of primary production

Primary production is governed by phytoplankton concentration and the availability of light and nutrients. The net primary production in the model is governed by the first term on the r.h.s. of Equation 11. Nitrate and ammonium are the only relevant nutrients for primary production in the model. The light limited growth rate J (t, z) is dependant on the irradiance field, the sun angle, the quantum yield of photosynthesis, temperature, light attenuation in the water (which is itself dependant on the phytoplankton concentration), and depth. In the model the following formulations were used:

$$\tilde{Q}_0 = S_0 \cos z$$
$$Q'_d = \tilde{Q}_0 \cdot \tau^{\frac{1}{\cos z + \varepsilon}}$$
$$Q_d = Q'_d\,(1-\alpha_d)(1-0.62C-0.0019\beta)$$
$$Q'_s = \frac{(1-A)\tilde{Q}_0 - Q'_d}{2}$$
$$Q_s = Q'_s\,(1-\alpha_s)(1-0.62C-0.0019\beta)$$
$$\alpha_d = \max\left(0.15, \frac{0.05}{\cos z + 0.15}\right)$$
$$\alpha_s = 0.065$$
$$\beta = \arcsin\cos z$$
$$Q_{surface} = Q_d + Q_s$$

**Equation 22** Irradiance field at the top of the ocean

First the irradiance field at the top of the ocean was calculated from the solar constant ($S_0$), the zenith angle (z) and the cloudiness fraction (C) from the COADS data set according to Equation 22 and additional equations given by Drange (1994). Thus the computed radiance field represents a climatological irradiance field.

From the irradiance field on the surface of the ocean the irradiance field within the ocean is computed as given in Equation 23. The irradiance at any given depth depends on the solar elevation (β), the depth (z) and phytoplankton self shading (P). Only the photosynthetically active radiation is used for photosynthesis.

$$Q' = Q_d \cdot e^{\frac{-k_t z}{\cos\theta_d}} + Q_s \cdot e^{\frac{-k_t z}{\mu}}$$
$$k_t = k_w + k_c \cdot P(z)$$
$$\cos\theta_d = \sqrt{1-\left(\frac{\cos\beta}{1.33}\right)^2}$$
$$\mu = 0.83$$
$$Q = f_{PAR} \cdot Q'(z)$$
$$f_{PAR} = 0.43$$

**Equation 23** Irradiance field in the ocean

The photosynthesis-irradiance relationship is the final expression with which to calculate phytoplankton growth or primary production, respectively. As shown in Equation 24 photosynthesis is dependent on temperature and irradiance.

$$J = V_p \cdot \frac{\alpha Q}{\sqrt{V_p^2 + \alpha^2 Q^2}}$$
$$V_p = 0.6 \cdot 1.066^{\frac{T}{^\circ C}}$$

**Equation 24** Photosynthesis-irradiance relationship

## 3.6 Conclusions

During tests the model generally performed well, it was a reasonable approximation of the real ocean. The modelled seasonal variation of the nitrate and phytoplankton concentrations, and the surface $pCO_2$ seem reasonable and are in general agreement with observations. However, along the Equator, strong upwelling in the model generates far too high surface nitrate and total dissolved inorganic carbon concentrations. In addition, the model's winter mixed layer is too deep at the Bermuda station "S", leading to a surface water $pCO_2$ value that is about 40 ppm above the observed value.

As the nutrient concentration in the upper ocean strongly depends on the mixed layer dynamics, the seasonal evolution of the mixed layer depth is very important. Generally the mixed layer dynamics follow the observation in summer but the mixed layer in the southern part of the suptropical gyre is to deep and extends too far to the west during winter.

Another important point is the proper placement and magnitude of ocean currents. Unfortunately, the modelled Gulf Stream is to diffusive and does not separate from the coast of Cape Hatteras as observed. This is a common problem for OGCMs with horizontal resolutions of about 1° by 1°.

# 4 Material and Methods

## 4.1 Overview

The basis of this work is formed by a comparison. In a good comparison the same attributes should be compared with each other at the same time and at the same place. This is not always trivial, as in the case of this study. The chlorophyll concentrations derived from satellite images are averaged for a different time than the model results. The model results were calculated on a non-standard grid, which must be transformed to a standard geographical projection. The model results are computed as biomass in mol-N/$m^3$ which has to be transformed into chlorophyll concentrations in order to be able to compare both values. Special consideration has to be given to the conversion of surface chlorophyll concentrations into subsurface chlorophyll concentrations. Thus, in the following chapters (4.2 - 4.4) a description is given how these problems were dealt with in this study.

In principal, there are two approaches to compare the model results with the satellite data. One is a spatial comparison of the values at a fixed time, and the other one is a comparison at a fixed place to gain a time series. Both approaches are covered in this study. For the time series the Bermuda station was chosen in order to use sea-truth data from the Bermuda-Atlantic-Time-Series. The sea-truth values there are compared with satellite chlorophyll concentrations from OCTS, CZCS and the model results. The spatial comparison is conducted using SeaWiFS-,and CZCS-data. OCTS images have also been rectified for future comparisons between OCTS and model results from a model run with synoptic forcing.

## 4.2 Time

### 4.2.1 Data sets used for the spatial comparison

The model data and the satellite data is averaged over a different period of time. The model output is averaged for every 15 model days, the SeaWiFS-data (Level 3) used in this study was averaged over a period of 8 days or one month, OCTS-data (Level 3 binned) was averaged over a period of 7 days and the monthly climatological data from CZCS is averaged over 6 years. So there is a mismatch in the averaging time. The match-ups which were chosen to make the comparison are given in Table 17.

**Table 17** List of data sets which have been compared with each other

| **Weekly averages** | | | |
|---|---|---|---|
| **Number of match-up** | **Model data [days]** | **SeaWiFS image [days, year]** | **OCTS images [days, year]** |
| R 18 | 255 - 270 | 257 - 264, 1997 | |
| R 19 | 270 - 285 | 273 - 280, 1997 | |
| R 20 | 285 - 300 | 289 - 296, 1997 | |
| R 21 | 300 - 315 | 305 - 312, 1997 | 308 - 315, 1996 |
| R 22 | 315 - 330 | 321 - 328, 1997 | 315 - 322, 1996 |
| R 23 | 330 - 345 | 337 - 344, 1997 | 329 - 336, 1996 |
| R 24 | 345 - 360 | 353 - 365, 1997 | 350 -357, 1996 |
| R 1 | 1 - 15 | 1 - 8, 1998 | 364, 1996 - 5, 1997 |
| R 2 | 15 - 30 | 17 - 24, 1998 | 19 - 26, 1997 |
| R 3 | 30 - 45 | 33 - 40, 1998 | 40 - 47, 1997 |
| R 4 | 45 - 60 | 49 - 56, 1998 | 47 - 54, 1997 |
| R 5 | 60 - 75 | 65 - 72, 1998 | 61 - 68, 1997 |
| R 6 | 75 - 90 | 81 - 88, 1998 | 75 - 82, 1997 |
| R 7 | 90 -105 | 97 - 104, 1998 | 88 - 95, 1997 |
| R 8 | 105 - 120 | 113 - 120, 1998 | 110 - 117, 1997 |

| | | | |
|---|---|---|---|
| R 9 | 120 - 135 | 121 - 128, 1998 | 124 - 131, 1997 |
| R 10 | 135 - 150 | | 138 - 145, 1997 |
| R 11 | 150 - 165 | | 152 - 159, 1997 |
| R 12 | 165 - 180 | | 166 - 173, 1997 |
| **Monthly averages** | | | |
| | **Model data [days]** | **SeaWiFS image [days, year]** | **CZCS data [month, years]** |
| January | 1 - 30 | 1 - 31, 1998 | January, 1979-1986 |
| February | 30 - 60 | 32 - 59, 1998 | February, 1979-1986 |
| March | 60 - 90 | 60 - 90, 1998 | March, 1979-1986 |
| April | 90 - 120 | 91 - 120, 1998 | April, 1979-1986 |
| Mai | 120 - 150 | 121 - 151, 1998 | Mai, 1979-1986 |
| June | 150 - 180 | | June, 1979-1985 |
| July | 180 - 210 | | July, 1979-1985 |
| August | 210 - 240 | | August, 1979-1985 |
| September | 240 - 270 | | September, 1979-1985 |
| October | 270 - 300 | 274 - 304, 1997 | October, 1979-1985 |
| November | 300 - 330 | 305 - 334, 1997 | November, 1979-1985 |
| December | 330 - 360 | 335 - 365, 1997 | December, 1978-1985 |

### 4.2.2 Data sets used for the time series

For the time series sea-truth data from the Bermuda-Atlantic-Time Series is used. This data is not averaged but a measurement at a fixed time. The model results are averaged over a period of 15 days as in the spatial comparison and the satellite data in the time series is also averaged over the same period of time as in the spatial comparison. Unfortunately there is no pixel in the GAC-resolution for OCTS which is sufficiently close to the Bermuda station (approximately 31° 40’ North 64° 10’ West). Thus OCTS-data is averaged over the four nearest pixels to the station to get the data for the position of the Bermuda station.

## 4.3 Space

### 4.3.1 Map projection

Instead of projections which are often used, like the Lambert Conformal Conical Projection or the Universal Transverse Mercator projection, the Lambert Azimuthal Equal Area projection is used. The reason for this is that the Lambert Azimuthal Equal Area projection is an equal area projection which is sensible for this kind of comparison, and not less important because it was supported by the software used (Maling 1991).

**Table 18** Map projection used

| | | |
|---|---|---|
| **Projection** | Lambert Azimuthal Equal Area | |
| **Spheroid and Datum** | Clark 1866 | |
| **Center of projection** | Latitude | 25° North |
| | Longitude | 40° West |
| **Original scale** | $1:1.6 \cdot 10^8$ | (not retained in images) |
| **Map boundaries [m]** (in meters from the center of projection) | Upper Left x | -5993218.1980 |
| | Upper Left y | 5993218.1980 |
| | Lower Right x | 5953263.41101 |
| | Lower Right y | -5953263.41101 |
| **Pixel size [m]** | Pixel size x | 39954.787990 |
| | Pixel size y | 39954.787990 |
| **Map boundaries** | Northernmost latitude | 81° 6’ 51.30’’ North |

| | |
|---|---|
| Southernmost latitude | 36° 0’ 45.87’’ South |
| Westernmost longitude | 145° 19’ 48.70’’ West |
| Easternmost longitude | 65° 19’ 48.75’’ East |

### 4.3.2 Resolution differences and resampling

As the resolutions of the different data sets are different, a common resolution is defined. The resolution of the model varied between 20 x 20 km in the Nordic Sea and about 200 x 200 km in the South Atlantic. The satellite images had a resolution of about 6 x 6 km to 40 x 40 km. Thus, a resolution of the approx. 40 x 40 km per pixel was chosen. Therefore, the data sets had to be resampled. To keep the original values the nearest neighbour method was chosen and no interpolation performed.

### 4.3.3 File conversions and rectifications

To fit the original data to the desired map projection and the desired resolution, the different data files are converted, rectified and resampled with the help of commercially available software packages (see Table 19).

**Table 19** Software used

| **Software** | **Version** | **Purpose** |
|---|---|---|
| Imagine | 8.2 | File conversions, rectifications, resampling, and calculations |
| SeaDAS | 3.1 | File conversion of original SeaWiFS files, original georeference |
| Tecplot | 7.0 | Graphics and interpolation of the time series |

The basis for giving a correct spatial position of the data is formed by a SeaWiFS image which has been produced with a known projection and map boundaries using the SeaDAS software. This file was then imported into Imagine and all other data files are rectified onto this image with the help of Ground Control Points (GCPs). The CZCS images are rectified with the help of 35 GCPs and a third order polynomial transformation. OCTS images are rectified with 24 GCPs and a third order polynomial transformation. The biggest challenge forms the rectification of the model data because of its non-standard grid and changing resolution. An initial group of 28 GCPs is chosen on the coastlines of America, Africa and Europe, such as Land’s End or Cape Hatteras, and a third order polynomial transformation is performed. But the root mean square error (RMS) is deemed still too high (Fisher 1991). Thus, the positions of another 22 GCPs along the northern and southern map or model boundaries are predicted using the 3$^{rd}$ order transformation and a higher order transformation, first 4$^{th}$ order then 5$^{th}$ order, is carried out. Between each transformation the position of the 22 additional GCPs is again predicted with the higher order transformation. The final transformation uses 50 GCPs, the 28 original points and the 22 additional ones, and a 5$^{th}$ order polynomial transformation.

**Table 20** Transformations for the rectification of the data sets

| **Data-set** | **Number of GCPs** | **Order of transformation** | **RMS-error [m]** | | |
|---|---|---|---|---|---|
| | | | x | y | total |
| CZCS-images | 35 | 3$^{rd}$ order | 28515 | 34186 | 44517 |
| Model-data | 28 | 3$^{rd}$ order | 139254 | 82658 | 161939 |
| | 50 | 5$^{th}$ order | 53362 | 51731 | 74322 |
| OCTS-images | 24 | 3$^{rd}$ order | 32394 | 34905 | 47621 |

# 4.4 Attribute

## 4.4.1 Calculation of chlorophyll and pigment from biomass

To compare the correct attributes with each other, the model phytoplankton biomass (P) had to be transformed to chlorophyll concentration ($Chl_{model}$). This was done by assuming constant ratios between carbon and nitrogen, the so called Redfield ratio, and carbon to chlorophyll. For the Redfield ratio the value given by Drange (1994) $R_P = 7.5$ is used. For the carbon to chlorophyll ratio the value of Sarmiento *et al.* (1993) $R_{Chl} = 50$ is used. This leads to the following formulation:

$$Chl_{\text{model}} = \frac{P \cdot m_N \cdot R_P}{R_{Chl}}$$

$$R_P = 7.5$$

$$R_{Chl} = 50$$

$$m_N = 14.01 \frac{g}{mol}$$

**Equation 25** Calculation of model chlorophyll from biomass

In some cases it is necessary to exchange chlorophyll with pigment concentrations. This is done by assuming a constant ratio of $\rho$=0.76 (Balch *et al.* 1992)

## 4.4.2 Calculation of subsurface chlorophyll

The calculated chlorophyll concentration can now be compared with the surface / satellite chlorophyll data as has been done by Sarmiento *et al.* (1993) who reasoned that the penetration depth, i. e. the depth of the water column that can bee actually “seen” by the satellite, is within a scale of the order of 10m (Gordon *et al.* 1982). As the upper two layers of their model down to 23 m (bottom depth) were generally well mixed, they concluded that a reasonable comparison with satellite observations could be made with the mean properties of the upper two layers of their model. But the model of Drange (1994) is different to that of Sarmiento *et al.* (1993) in so far that the depth of the biological layer varies with the mixed layer depth. The model output is averaged over the upper biochemical layers. The averaging depth is actually half the mixed layer depth. Therefore, the depth over which the chlorophyll concentration is averaged in the model varies considerably with the depth of the mixed layer. The difference between the different depths is exemplified in Figure 7. As has been mentioned before the different depths can vary considerably, the penetration depth from approx. 3 - 50m, the euphotic depth from 7 - 150 m, and the mixed layer from 10 - 600 m.

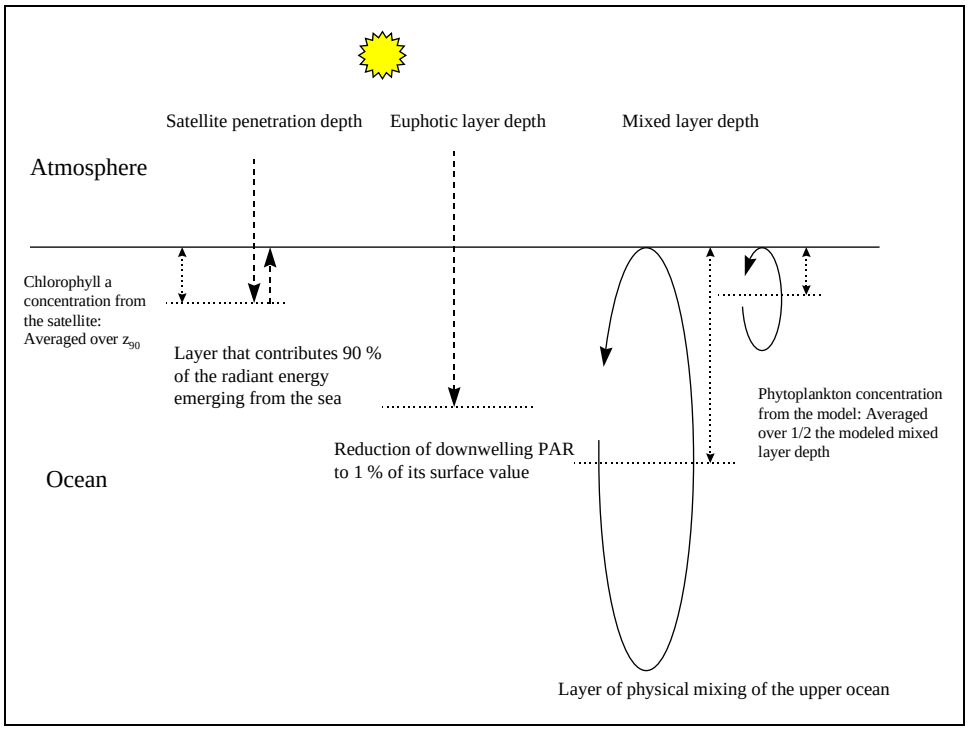


**Figure 7** Comparing different averages

For the calculation of the mean subsurface chlorophyll concentration an empirical relationship of Morel and Berthon (1989) was used. Morel and Berthon (1989) computed average chlorophyll profiles for seven different trophic situations for stratified waters in the ocean from *in situ* data (see Figure 8). They statistically examined the chlorophyll profiles of about 4000 stations which were representative of case 1 waters. The geographical distribution of these stations was uneven. The East Atlantic and the Southwest Pacific were well documented whereas other zones were poorly represented.

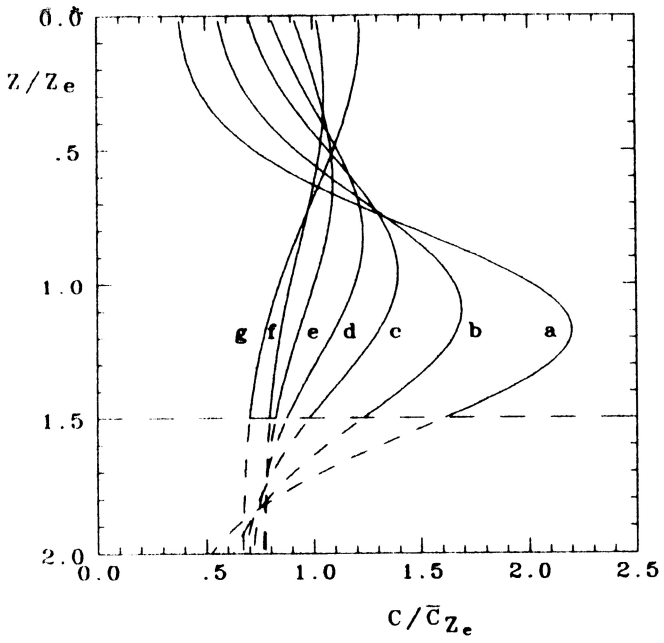


**Figure 8** Idealised chlorophyll profiles from Morel and Berthon (1989)

Their algorithm is only valid in case 1 waters. But as the satellite data which is used in this study excludes values for case 2 waters, because chlorophyll algorithms tend to fail in these waters, no problem arises from this. Unfortunately, the equations given by Morel and Berthon (1989) are based on pigment concentrations. To convert the chlorophyll concentrations to pigment concentrations the average chlorophyll to pigment ratio of ρ=0.76 given by Balch *et al.* (1992) is used. First Morel and Berthon (1989) calculated the total pigment content per square meter in the euphotic zone, the depth of the euphotic zone, and the average concentration in the euphotic zone based on the following equations:

$$\langle C \rangle_{tot} = 38.0 \bar{C}_{sat}^{0.423} \quad if \;\; \bar{C}_{sat} \le 1.0 \frac{mg}{m^3}$$

$$\langle C \rangle_{tot} = 40.3 \bar{C}_{sat}^{0.505} \quad if \;\; \bar{C}_{sat} > 1.0 \frac{mg}{m^3}$$

**Equation 26** Total pigment content in the euphotic layer

$$z_e = 568.2 \langle C \rangle_{tot}^{-0.746} \; if \;\; z_e < 102\, m \; or \; \langle C \rangle_{tot} > 10 \frac{mg}{m^2}$$

$$z_e = 200.0 \langle C \rangle_{tot}^{-0.293} \; if \;\; z_e > 102\, m \; or \; \langle C \rangle_{tot} \le 10 \frac{mg}{m^2}$$

**Equation 27** Euphotic layer depth

$$\bar{C}_{ze} = \frac{\langle C \rangle_{tot}}{z_e}$$

**Equation 28** Mean pigment concentration in the euphotic layer

A numerical analysis of the pigment profiles led to a possible parameterization where $C_b$ is a background over which a gaussian curve is superimposed with a maximum value given by $C_{max}$, occurring at $\zeta_{max}$ and having a thickness controlled by $\Delta\zeta$. This parameterization is restricted to the range of $\bar{C}_{pd}$ values (average chlorophyll concentration in the penetration depth) extending from about 0.02 mg/m$^3$ to 10 mg/m$^3$ and to a depth of two times the depth of the euphotic zone. Equation 29 gives the parameterization in its dimensionless form.

$$\frac{C(\rho)}{\bar{C}_{ze}} = C_b + C_{\max} e^{-\left[\frac{(\varsigma - \varsigma_{\max})}{\Delta\varsigma}\right]^2}$$

$$C_b = 0.768 + 0.087 \log \bar{C}_{pd} - 0.179 (\log \bar{C}_{pd})^2 - 0.025 (\log \bar{C}_{pd})^3$$

$$C_{\max} = 0.299 - 0.289 \log \bar{C}_{pd} + 0.579 (\log \bar{C}_{pd})^2$$

$$\varsigma_{\max} = 0.600 - 0.640 \log \bar{C}_{pd} + 0.021 (\log \bar{C}_{pd})^2 + 0.115 (\log \bar{C}_{pd})^3$$

$$\Delta\varsigma = 0.710 + 0.159 \log \bar{C}_{pd} + 0.021 (\log \bar{C}_{pd})^2$$

**Equation 29** Parameterization of the pigment profiles

It is assumed that the chlorophyll concentration estimate $\bar{C}_{sat} \approx \bar{C}_{pd}$ (Error ≈ 2.5 % according to Morel and Berthon (1989)) and the dimensionless depth is replaced with the actual depth z. Then the mean pigment concentration for a layer with the depth z can be computed as following:

$$\bar{C}_z = \frac{\int_0^z C(z)\,dz}{z}$$

**Equation 30** Mean pigment concentration in a layer with the depth z

For the integration which is necessary to calculate $\bar{C}_z$, an equation given by Prudnikov *et al.* (1986) of the following type is used.

$$\int e^{-(ax^2+bx+c)}dx = \frac{1}{2}\sqrt{\frac{\pi}{a}}\; e^{\frac{b^2-4ac}{4a}}\; erf\left(x\sqrt{a}+\frac{b}{2\sqrt{a}}\right)$$

**Equation 31** Integration formula

This leads to the following formulation:

$$\bar{C}_z = \bar{C}_{ze}\,C_b + \frac{\bar{C}_{ze}\,C_{\max}}{2\cdot z}\sqrt{\frac{\pi}{a}}\,e^{\frac{b^2-4ac}{4a}}\left[erf\left(z\sqrt{a}+\frac{b}{2\sqrt{a}}\right)-erf\left(\frac{b}{2\sqrt{a}}\right)\right]$$

$$a = \frac{1}{z_e^2\,\Delta\varsigma^2}$$

$$b = -\frac{2\varsigma_{\max}}{z_e\cdot\Delta\varsigma^2}$$

$$c = \frac{\varsigma_{\max}^2}{\Delta\varsigma^2}$$

**Equation 32** Mean pigment concentration in a layer with the depth z

For the approximation of the error function an equation given by Abramovitz and Stegun (1965) is used.

$$erf\ x = 1-(a_1t+a_2t^2+a_3t^3+a_4t^4+a_5t^5)e^{-x^2}+\varepsilon(x)$$

$$t = \frac{1}{1+px}$$

$$p = 0.3275911$$

$$a_1 = 0.254829592$$

$$a_2 = -0.284496736$$

$$a_3 = 1.421413741$$

$$a_4 = -1.453152027$$

$$a_5 = 1.061405429$$

$$|\varepsilon(x)| \le 1.5\ 10^{-7}\ \ truncation\ error$$

**Equation 33** Approximation of the error function

With Equation 32 and Equation 33 the mean pigment concentration for every depth can be calculated. The pigment concentration is again recalculated to a chlorophyll concentration with the constant ration of ρ=0.76 given by Balch *et al.* (1992). The equations are then used to calculate the mean chlorophyll concentration for a layer with the depth of the modelled mixed layer. Thus, the

averaging depths of the subsurface chlorophyll concentration derived from the satellite is the same as the averaging depth of the model.

### 4.4.3 Comparison between climatological CZCS data and synoptic SeaWiFS data

Another problem is the comparison between model results which have been obtained with climatological forcing fields and synoptic satellite images. The reason to do this is the higher accuracy of the synoptic SeaWiFS-data compared with the climatological CZCS data. Thus the SeaWiFS data for 1997/1998 is compared with the climatological average of the CZCS data (1979-1986) to examine if 1997/1998 was significantly different from the climatological average.

## 4.5 The final comparisons

The final comparisons are done in a qualitative way to see if the model results and the satellite images show the same spatial pattern, and in a quantitative way to examine if the model results and the satellite data are in the same order of magnitude. The actual quantitative comparison is done on a procentual basis. If the satellite and model are compared the satellite value is assumed to be correct and the model results are shown in % of the satellite values. Thus, a higher percentage than 100 in the comparison results symbolises an overestimation of the chlorophyll concentration by the model, whereas a lower percentage than 100 symbolises an underestimation of the chlorophyll concentration by the model. Finally, two main comparisons are maid:

- time series: synoptic OCTS data, climatological CZCS data and *in situ* measurements are compared to model results which have been obtained with climatological forcing (only qualitative)
- spatial: synoptic SeaWiFS data and climatological CZCS data are compared to model results which have been obtained with climatological forcing (qualitative and quantitative)

# 5 Results

In the presentation of the results, it is now assumed that the satellite values are mostly correct despite of the problems which have been pointed out in chapter 2. Thus, the comparisons are always relative.

## 5.1 Colour Coding used in the Presentation of the Results

The results of the comparison have been colour coded according to Figure 9. A legend to the single images has not been added because the software used was not appropriate for generating individual legends.

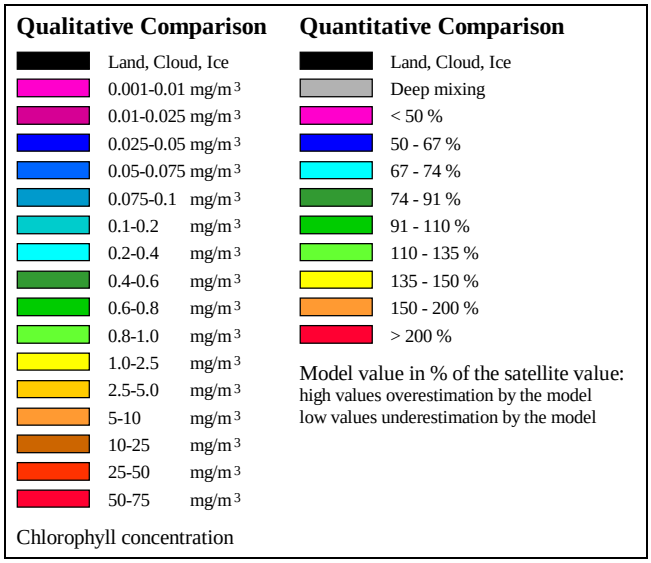


**Figure 9** Colour coding for the qualitative and quantitative comparison

## 5.2 Time Series with OCTS-, BATS- and Model-Data

Figure 10 shows *in situ* data from BATS. A small blooming event can be seen at the end of 1996. Afterwards, the surface chlorophyll concentration decreases and the development of a subsurface chlorophyll maximum can be observed. The figure shows that the chlorophyll concentration is not uniform with depth. It is good proof that some sort of chlorophyll profile, like the one used in this study, has to be used to calculate the average chlorophyll concentration for a water column with a given depth from the surface / satellite values.

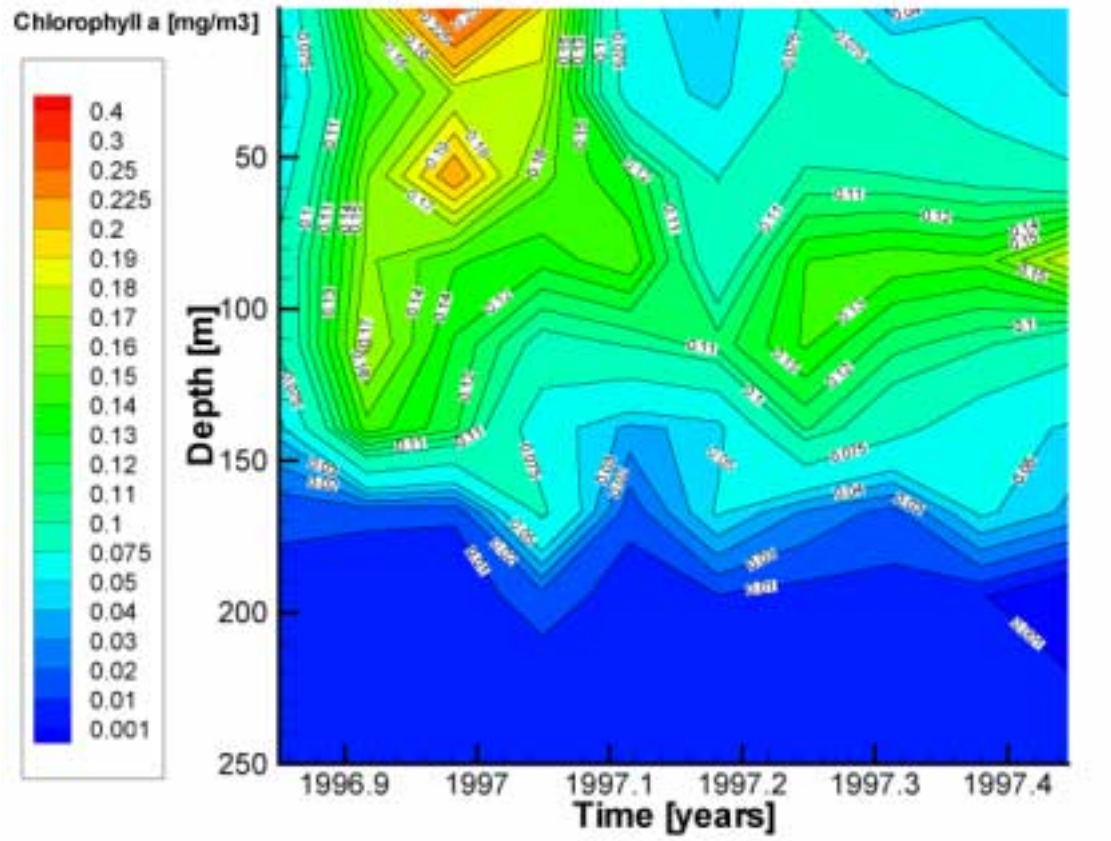


**Figure 10** Depth profile of *in situ* chlorophyll a measurements from the Bermuda Atlantic Time Series (BATS; 32° N, 64° W); time is given in decimal years

For the comparison with the model results and the satellite data only the surface chlorophyll value from the *in situ* data was used. The satellite values were either the plain surface values or the averaged chlorophyll concentration for the depth of the model's biochemical layer. Furthermore, it must be mentioned that the satellite results are averaged over 7 days, whereas the *in situ* data are discrete measurements in time. Thus, conclusions about the quality of the satellites performance cannot be made.

- It can be seen that there exists a difference between the surface chlorophyll value from the satellites and the calculated average subsurface chlorophyll concentration, although the difference is not big at all times.
- Notable, is the difference between the climatological CZCS data and the synoptic OCTS data. The blooming event at the end of the year was apparently only a one year event. The CZCS data does not show a peak.
- At the beginning of the time series the model followed the value of the climatological CZCS chlorophyll concentration but then it diverged from the climatological CZCS value and was nearer to the synoptic OCTS value.
- The difference between the model results which have been obtained with climatological forcing are up to an order of magnitude

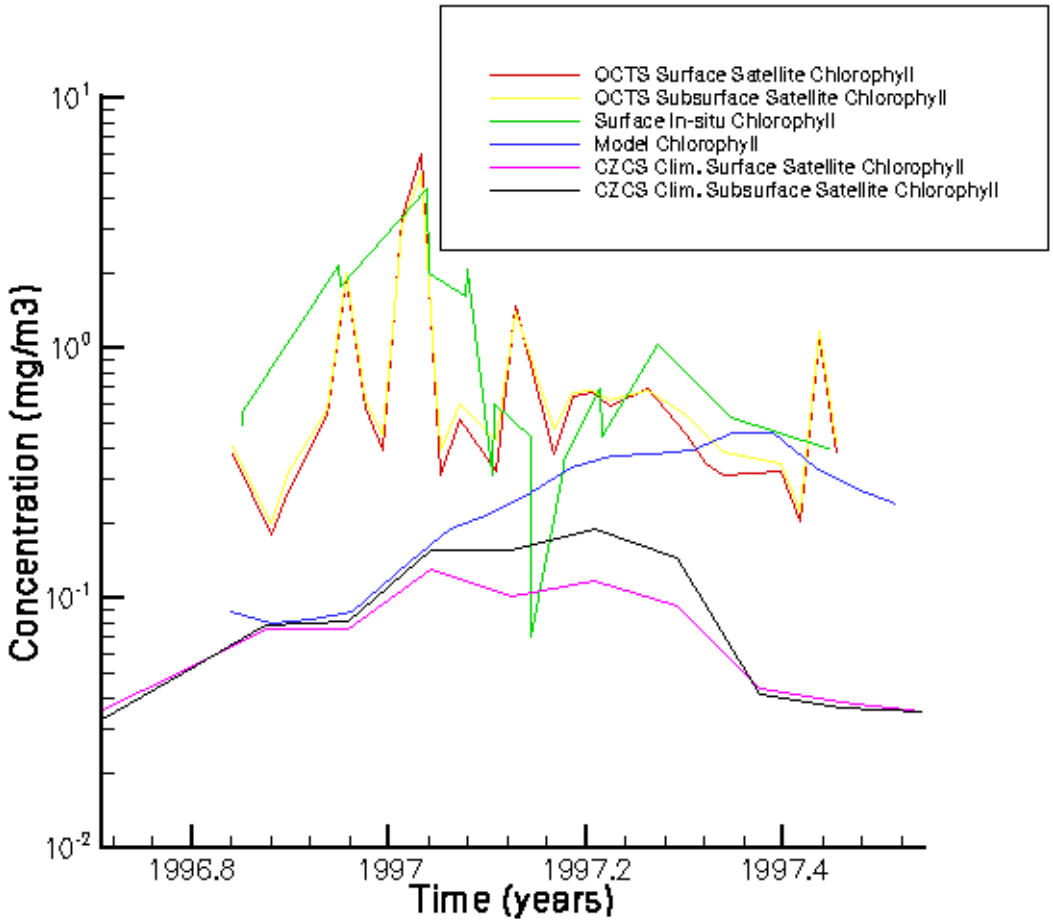


**Figure 11** Chlorophyll a time series with *in situ* data from BATS, OCTS, CZCS, and the model at the location of the Bermuda Atlantic Time Series 32° N, 64° W); time is given in decimal years

## 5.3 Synoptic SeaWiFS data, climatological CZCZ data and climatological model data

### 5.3.1 Qualitative comparison

For this comparison three monthly averaged images have been chosen for the presentation, one from September, one from February and one from April (see Figure 12). The comparison shows that the satellite values from SeaWiFS and CZCS (climatological average) and the model results are in good general agreement but there are some notable differences between the model and the satellite values.

- A band of high chlorophyll concentration in the model extends from Spain westward (February and April scene). High concentrations can already bee seen in February and the concentrations are even higher in April. This band structure of high chlorophyll concentration is not clearly observed by the satellites but there might be some fainter band structure further to the north, approx. at the latitude of France or Great Britain.
- The Mauritanian upwelling at the coast of Africa can be identified by the high chlorophyll concentrations in both the model and satellite images. But the extend of the upwelling zone seems to be smaller in the model.
- Especially at the coast of North America higher chlorophyll concentrations are visible in the satellite images but not in the model results. This is also the case for the September and February scene for the waters surrounding Great Britain.
- The modelled concentration south of Greenland is lower than in the satellite images (April images)

- Along the coast of South America larger areas of high chlorophyll concentration can be observed in the September scene which are not represented in the model.
- The modelled chlorophyll concentration in the west of the Gulf of Guinea (Westafrica) is lower than the concentration observed by the satellites.
- The extend of the very low chlorophyll concentrations in the subtropical gyre varies. And especially in the April scene the model result does not closely match the satellite images.
- The chlorophyll concentrations at the southern boundary of the model is higher than it can be seen in the satellite images.
- The direct comparison between the climatological CZCS images and the SeaWiFS data for 1997-1998 show a good qualitative agreement.

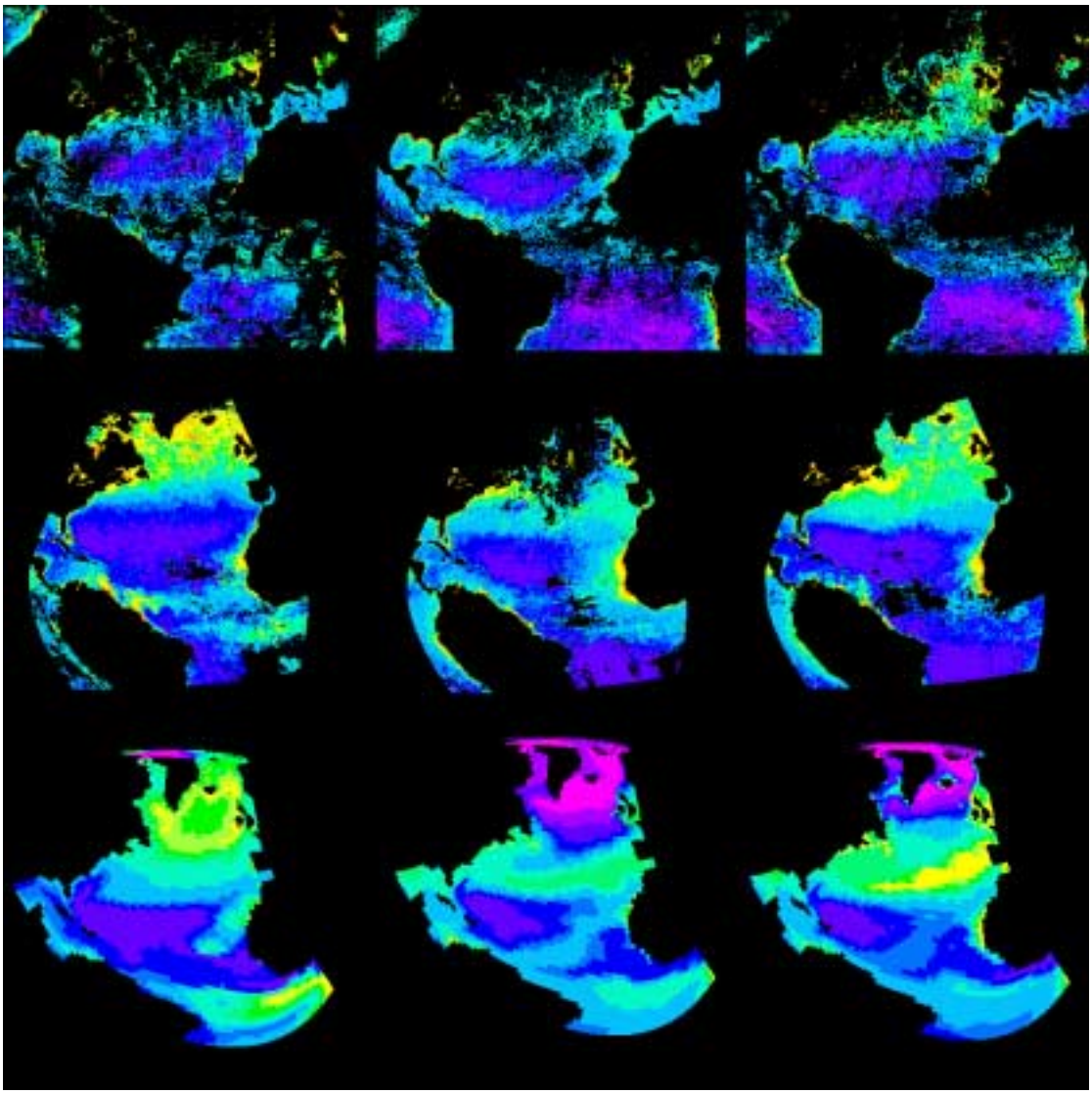

**Figure 12** Qualitative Comparison: SeaWiFS (upper row), CZCS (middle row) and model (lower row) chlorophyll data for September / R18 (left column), February / R 4 (middle column) and April / R 8 (right column)

### 5.3.2 Quantitative comparison

Three different quantitative comparisons have been conducted. First the simple surface values from SeaWiFS have been compared with the model results (lower row in Figure 13). This comparison does not take a changing chlorophyll profile into account. Thus, the algorithm which is laid out in chapter 4.4.2 is not used in the comparison. It is a comparison of surface values. The more correct approach of comparing the subsurface satellite values of the climatological CZCS data (upper row in

Figure 13) and the SeaWiFS images (middle row in Figure 13) with the model results has been done in the other two comparisons.

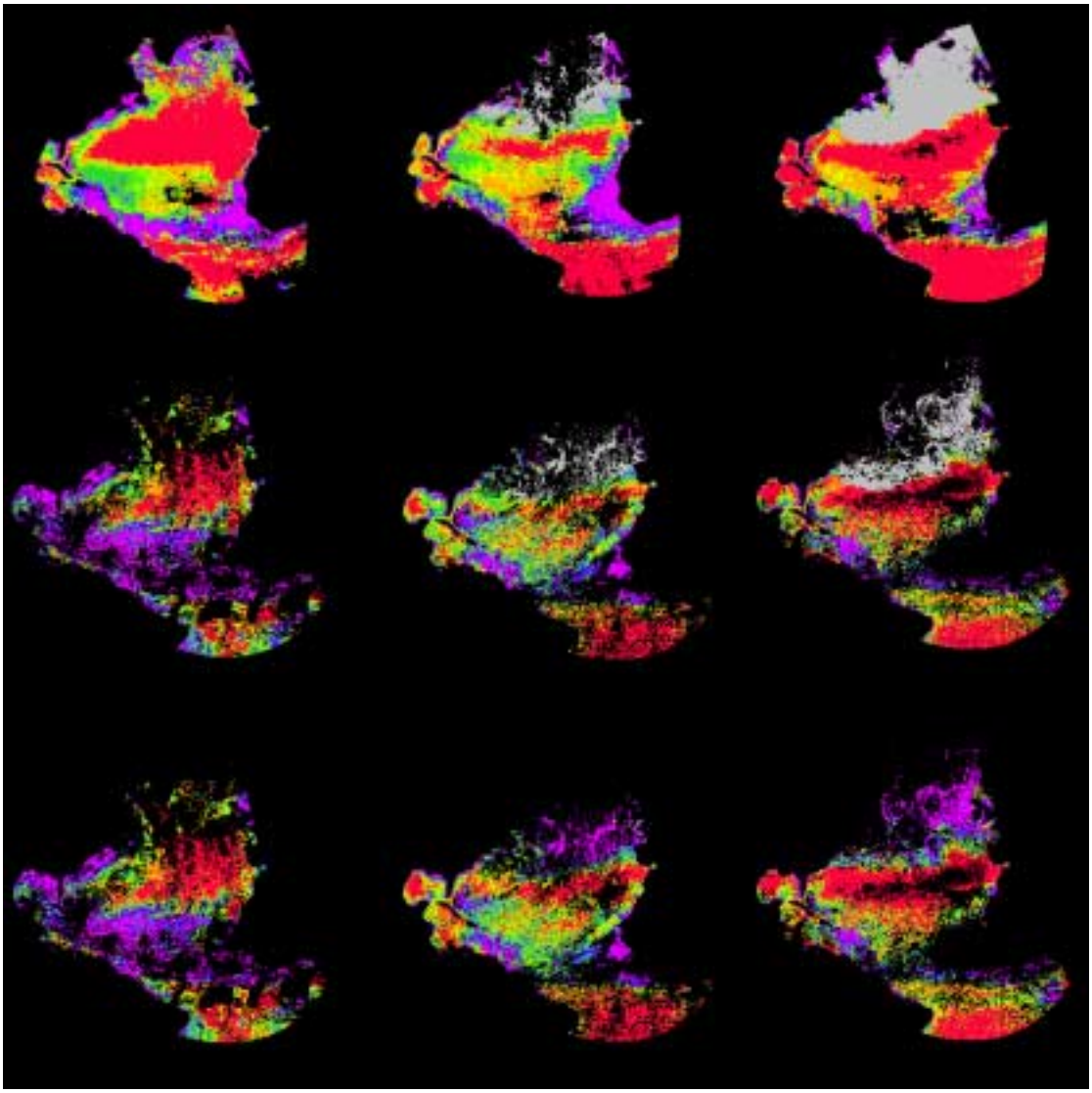

**Figure 13** Quantitative Comparison between subsurface CZCS / model chlorophyll (upper row), subsurface SeaWiFS / model chlorophyll (middle row) and surface SeaWiFS / model chlorophyll (lower row) for September / R18 (left column), February / R 4 (middle column) and April / R 8 (right column)

On the first glance, the difference between the three comparisons are not very obvious but some features are noticeable:

- The comparison between surface SeaWiFS images (lower row in Figure 13) and subsurface SeaWiFS data (middle row in Figure 13) with the model results do not produce a vastly different picture but in some small areas and in areas with deep mixing a difference can be noticed. A big area in the February and April scenes is not used in the subsurface comparison because of the deep mixing in this area. In the surface comparison these areas are underestimated by the model. Other differences between the surface and subsurface comparison with SeaWiFS can only be seen in the February scene (middle column in Figure 13) east of the Florida coast. Here the surface and subsurface comparisons lead to different results.
- The differences in the model results and the satellite values are especially big in the areas where the qualitative distribution of chlorophyll in the model does not resemble the pattern which is observed in the satellite images. Good examples are the band structure of a high chlorophyll concentration west of Spain in the February and April scenes, the overestimation of chlorophyll at the southern

boundary of the model, or the too low concentrations of the model along the coast of North America, Great Britain and South America.

- Even in areas where the model reproduced the right pattern of chlorophyll concentration (e.g. the low chlorophyll concentration in the subtropical gyre), the model results do not always match the chlorophyll concentration measured by the satellites.
- Over the whole timeframe evaluated in this study a look at the quantitative comparison between surface chlorophyll / model (see Figure 14) and subsurface chlorophyll / model (see Figure 15) reveals that there are no big differences between these two comparisons. An exception is the size of the deep mixing area in the North Atlantic which is underestimated in the surface comparison and not compared at all in the subsurface comparison.
- The development over time (see Figure 14 and Figure 15) gives a hint of the overall accuracy of the model. Even though the general patterns of the chlorophyll concentration are reproduced by the model, the difference between the modelled chlorophyll values and the values measured by SeaWiFS is within an error margin of 35 % only in approx. one fourth of the North Atlantic. Another forth is overestimated by a factor higher than 2 and another fourth underestimated by a factor higher than 2.

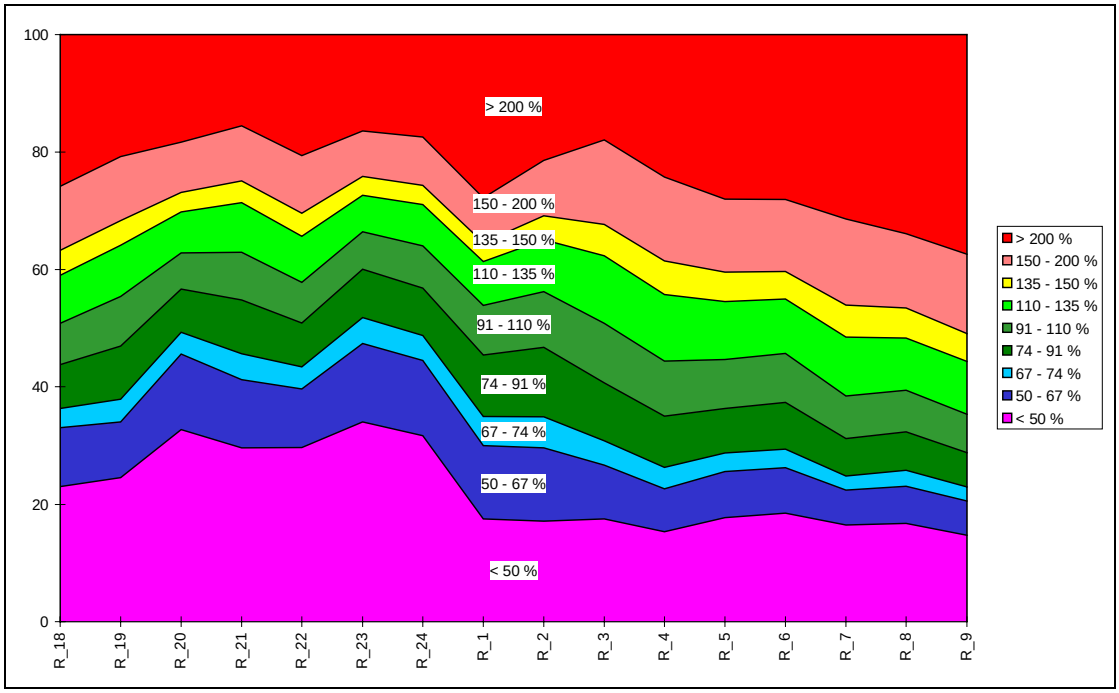


**Figure 14** Quantitive comparison between SeaWiFS surface chlorophyll and model results beginning in September 1997 (R 18) and ending in Mai 1998 (R 9); on the y-axis the percentage of the covered area is shown

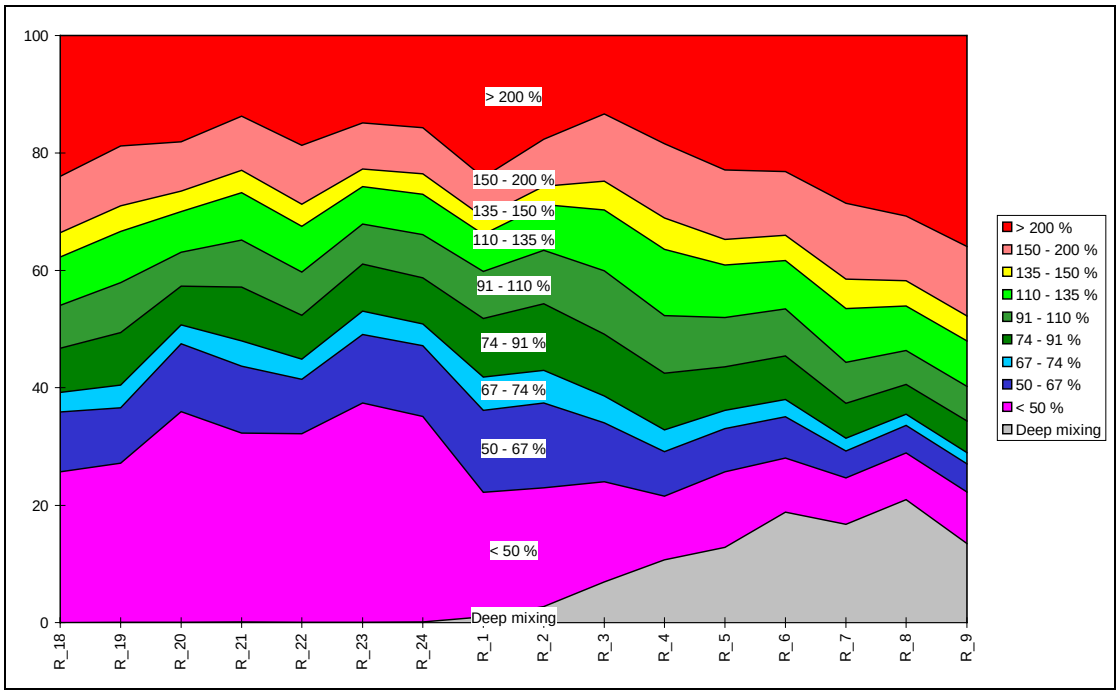


**Figure 15** Quantitive comparison between SeaWiFS subsurface chlorophyll and model results beginning in September 1997 (R 18) and ending in Mai 1998 (R 9); on the y-axis the percentage of the covered area is shown

The comparison of the climatological CZCS data with the model results obtained with climatological forcing might have been more sensible than a comparison with the SeaWiFS data of just one year (1997-1998). But the qualitative comparison does not reveal big differences between SeaWiFS and CZCS. In the quantitative comparison the picture is different.

- Larger areas seem to be overestimated by the model / CZCS comparison than in the comparison with SeaWiFS. This is especially obvious in a comparison between Figure 15 and Figure 16.

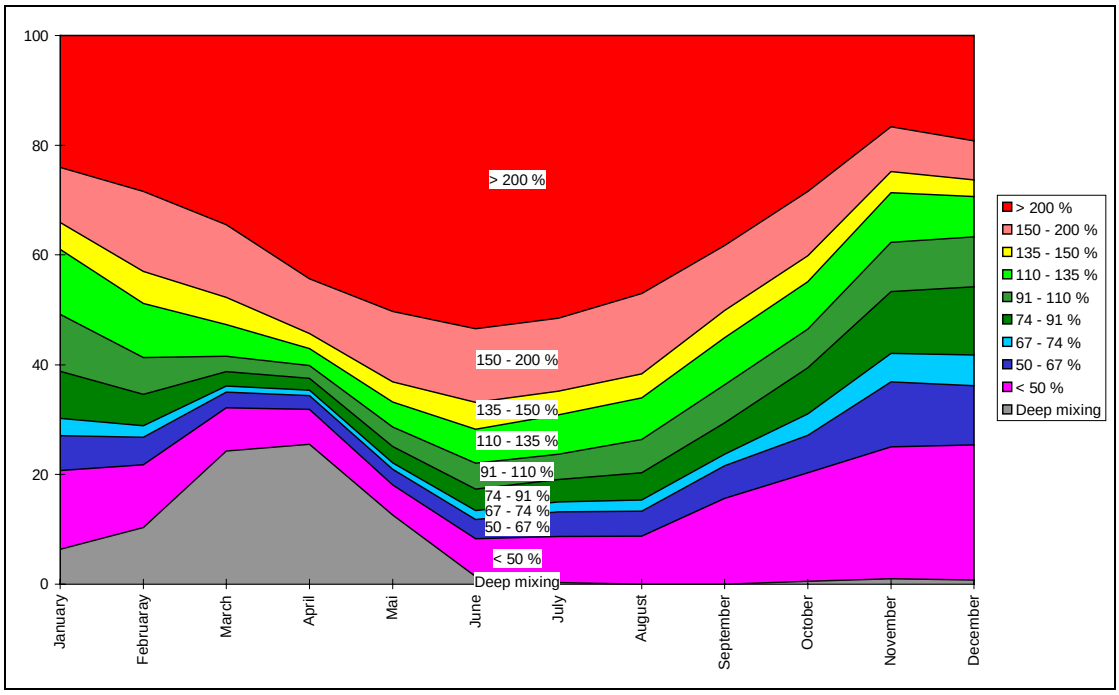


**Figure 16** Quantitive comparison between CZCS subsurface climatological chlorophyll and model results from January to December; on the y-axis the percentage of the covered area is shown

But this difference can be attributed to differences between CZCS and SeaWiFS. A direct comparison between monthly averaged SeaWiFS images from 1997/98 and the climatological CZCS data shows a big underestimation of the chlorophyll concentration by CZCS compared to SeaWiFS (see Figure 17).

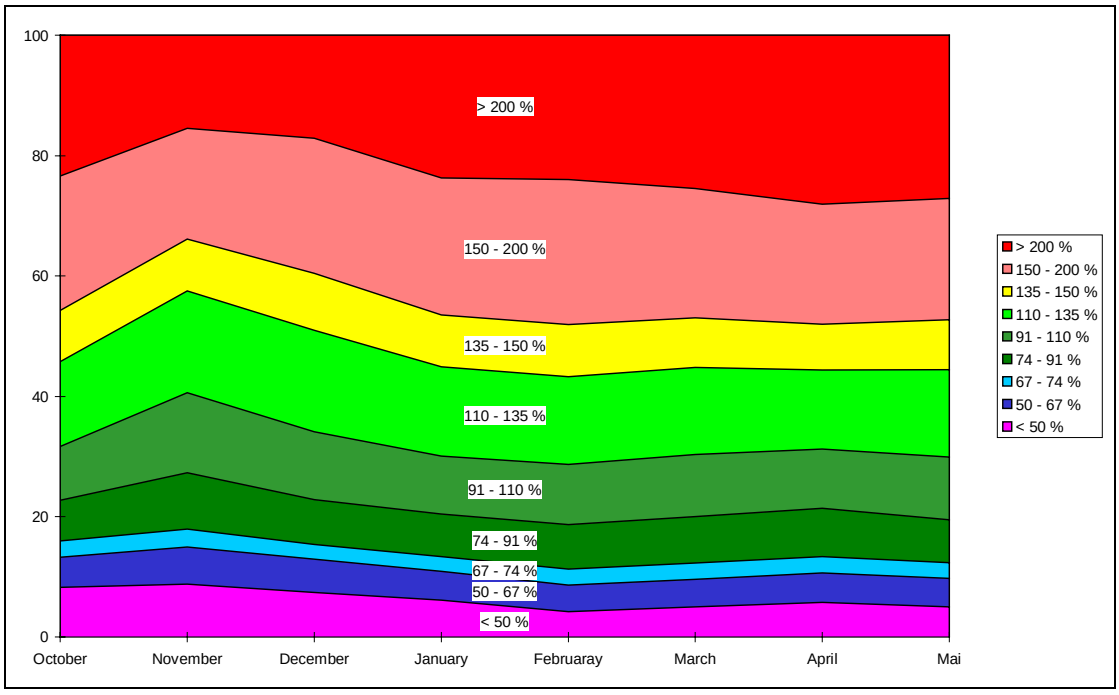


**Figure 17** Quantitive comparison between CZCS climatological chlorophyll and SeaWiFS chlorophyll from October 1997 to Mai 1998; the percentage in the legend is the SeaWiFS chlorophyll value in % of the climatological CZCS value.; on the y-axis the percentage of the covered area is shown.

# 6 Discussion

## 6.1 Error estimations

The errors associated with the chlorophyll measurements and the algorithms used in this comparison are generally very high (see Table 21). The error in time is not estimated here at all and the error in space is minor compared to the error in the attribute. The associated error with *in situ* measurements is deemed to be 10-30 % (Balch *et al.* 1992) and the error for the satellite values for chlorophyll varies between 30 and 80 % (see Table 21 for references). The SeaWiFS data set will be recalculated, because a review of the data showed that the present chlorophyll algorithm overestimated concentrations above around 2 mg/m$^3$. Values at the maximum value of 64 mg/m$^3$ will be reduced by a factor of 3-4. Values between 0.03 and 2 mg/m$^3$ are essentially the same but values previously below 0.03 mg/m$^3$ will be increased by as much as 50 % (e-mail notification from the SeaWiFS team). It is assumed however that in most cases the satellite data is more reliable and accurate than the model data. The calculations to get the average chlorophyll concentration for any given depth up to two times the euphotic layer depth as outlined in chapter 4.4.2 introduces another big error. Balch *et al.* (1992) estimated the error for the calculation of integrated biomass as of 60 - 80 % using standard error expansion techniques (Liebelt 1967). The error in this study might be of the same order of magnitude.

The calculation of integrated biomass in the euphotic zone or, as in this case, the calculation of an average chlorophyll concentration is often the first step in primary production estimates. If the calculation of primary production from the chlorophyll-light curve (see chapter 6.5) were well known the final calculation of primary production would be easy. But unfortunately this is not the case because for instance the light absorption properties differ for each taxonomic phytoplankton group (Aguirre-Gómez *et al.* 1995). Algorithms which use only the satellite chlorophyll concentration to derive primary production are assumed to have an approx. error of 100-300 % (see Table 21 for references). Vastly more than the error with standard *in situ* measurements (17-40 %). But this shows at least that the error made in this study is still within the range of present scientific studies.

**Table 21** Error estimates

| | **Correlation coefficient $r^2$** | **Relative Error [%]** | **Reference** |
|---|---|---|---|
| **Geographical transformations** | | | |
| Importation of SeaWiFS images from SeaDAS to Imagine | | < 0.5 % | |
| Rectification of CZCS images | | < 0.5 % | |
| Rectification of OCTS images | | | |
| Rectification of model data | | < 1.5 % | |
| **Satellite data** | | | |
| SeaWiFS Water leaving radiance | | < 5 % | Hooker *et al.*. 1992 |
| SeaWiFS Surface / Satellite chlorophyll a concentration | | 35 % | Hooker *et al.*. 1992 |
| SeaWiFS K(490) | | 20 % | Hooker *et al.*. 1992 |
| CZCS Water leaving radiance | | 10 % | Evans and Gordon 1994 |
| CZCS Surface / Satellite pigment concentration | | 80 % | Campbell 1995a |
| OCTS Water leaving radiance | | < 5 % | |
| OCTS Surface / Satellite chlorophyll concentration | | 30 % | |
| | | | |
| ***In situ* chlorophyll measurements** | | | |
| Fluorometric method | | 10 - 30 % | Balch *et al.* 1992 |
| | | | |
| **Calculation of subsurface chlorophyll** | | | |
| Calculation of mean pigment concentration in the euphotic layer | 0.681 - 0.767 | 30 - 40 % | Morel and Berthon 1989<br>Balch *et al.* 1992 |

| | | | |
|---|---|---|---|
| Calculation of euphotic layer depth | 0.914 | | Morel and Berthon 1989 |
| Assumption: $\overline{C}_{sat} \approx \overline{C}_{pd}$ | | 2.5 % | Morel and Berthon 1989 |
| Assumption: $\rho \approx 0.76$ | 0.68 | 20 % | Morel and Berthon 1989<br>Balch *et al.* 1992 |
| **Primary Production** | | | |
| Standard carbon 14 technique | | 17 - 40 % | Balch *et al.* 1992 |
| Empirical algorithms | 0.06 | 200 - 300 % | Balch *et al.* 1989a |
| PTL algorithm | 0.12 | 100 - 200 % | Balch *et al.* 1989a |

## 6.2 Problem areas

The results of the comparison which are outlined in chapter 5 showed that the model predictions have problems in some areas. Of course the reason for discrepancies in the comparison must not be caused by the model, wrong satellite measurements could also be a reason. The SeaWiFS data set will be recalculated, but nevertheless it is assumed in this study that in most cases the satellite data is more reliable and accurate than the model data and that the reasons for differences between the satellite values and the model results are mainly due to the model parameterizations, formulations or boundary conditions.

### 6.2.1 Coastal areas of North America and Great Britain

The high chlorophyll concentrations along the coast of North America and Great Britain which can be seen in the satellite pictures are not present in the model results. This might be due to an overestimation of the chlorophyll concentration in these coastal areas by the satellites. As said above the SeaWiFS data is expected to be recalculated because some of its algorithms did not perform well enough. One of the algorithms to be modified is the one which distinguishes between case 1 and case 2 waters. The present algorithm declares to many areas to be of case 1 water than it is true. Coastal waters have high concentrations of yellow substances and suspended sediments due to land drainage (Carder *et al.* 1989). Thus a part of the high concentrations along the coast might be due to misinterpretation of the satellite signal. On the other hand coastal areas have a lot of nutrient-rich runoff (Walsh *et al.* 1981) which is a reason for high chlorophyll concentrations in coastal waters. But this nutrient influx is not incorporated into the model yet. Other shelf processes are not modelled, either. For example, tidal mixing is missing.

### 6.2.2 Areas with deep mixed layers

Another problem area is the area of deep mixing in the North Atlantic ocean. In the model the huge mixed layer depth is the reason for a very low chlorophyll concentration at the surface because the phytoplankton in the mixed layer is distributed along a depth of up to several hundred meters which obviously leads to a very small concentration in surface chlorophyll. But the satellite pictures in this high latitudes are not to be believed without doubt, either. The low angle of the sun has lead to severe misinterpretation of the chlorophyll concentration by CZCS. But the SeaWiFS data should be more accurate and it also shows a higher concentration in the Northern Atlantic ocean than the model.

### 6.2.3 The zone south of the deep mixing area

The zone south of the deep mixing area showed a band structure of high chlorophyll concentration. This structure is definitely artificial in its magnitude and placement although there might be a weaker band structure in the satellite pictures. In this area the mixed layer depth becomes shallower. It is the area of outcropping isopycnals in the model. This means that there is a influx of nutrient rich water from the mixed layer into the stratified layers of the model ocean south of the deep mixing area. Thus the concentration of phytoplankton or chlorophyll, respectively, rises. A weaker

form of this band structure can be seen in the satellite images further north than in the model. This might be a hint that the area of deep mixing is extending to much southward.

### 6.2.4 Coastal area of South America

The high concentration of chlorophyll along the coast of South America which can be seen in the satellite images are probably caused by small eddies. They bring nutrients to the surface and the phytoplankton concentrations rises. But these small eddies are not resolved in the model, so the modelled concentrations are lower than the satellite images suggest. But there might be a second reason for the discrepancies in the comparison. With the Amazon and the Orinoco at least two major rivers have their mouth at this coast. The sediments and yellow substances transported by them into the sea might lead to a failure of the satellite algorithm, so that the concentration measured by the satellites might not be too accurate. On the other hand the Amazon and the Orinoco transport a lot of nutrients into the sea although the nitrate concentrations of many tropical rivers, like the Amazon, Congo, Orinoco or Niger are relatively low (Walsh *et al.* 1981). This nutrient influx is not modelled in NC3M.

### 6.2.5 The Mauritanian upwelling area

The high chlorophyll or phytoplankton concentrations of the Mauritanian upwelling area is caused by the high concentrations of nutrients of the upwelling water masses. Apparently, the extend of this area is underestimated by the model. A similar problem was present in the model of Sarmiento *et al.* (1993), which was caused by low model resolution. It might be the same reason in N3CM, too.

### 6.2.6 The southern model boundary

The huge differences between the modelled results and the satellite images are most probably due to the model formulations. The southern model boundary is formulated as a solid wall which is of course not true in the real world. But the way in which these boundary formulations affect the chlorophyll concentration is not clear.

### 6.2.7 The time series

Drange (1994) already showed that the models winter mixed layer is too deep at the Bermuda station “S”. This led to an overprediction of winter nitrate values at Bermuda which was also reported by Fasham *et al.* (1993). The higher nitrate concentration might be a reason for a stronger bloom in spring and thus explain why the modelled chlorophyll concentration diverges from the climatological CZCS average in spring (see Figure 11).

## 6.3 Possible solutions for these problems

Assuming again that the main error in the comparison is due to the model mistakes, possible solutions are based on model reformulations. Problems in the models performance can be caused by a multitude of factors but a general division into model formulations (the equations, boundary conditions), model parameterizations, and model resolution or scale is helpful (Platt and Sathyendranath 1993).

### 6.3.1 Parameterizations

#### 6.3.1.1 Constant ratios

A topic of much debate is the question if the Redfield ratio or other ratios are really constant. And the second question is, if the Redfield ratio can be assumed to be constant, what its concrete value is. Table 22 gives an definitely incomplete overview of Redfield ratios used by different others. It is clear that even if a constant value is assumed science has not yet agreed on a specific value. There is enough evidence that these ratios are not constant at all. The uptake of carbon and nitrate can be temporarily uncoupled entirely (Banse 1994) and this definitely leads to a different Redfield ratio. Another example is given by Sambrotto *et al.* (1993) who showed that the DIC reduction and the $NO_3$ uptake in coastal areas does not correspond to a C:N ratio of 6.6. They concluded that there is a higher carbon export in coastal areas and a more effiecient recycling of nitrogen than carbon in the upper layer. Also McAllister (1969) had already shown that the carbon-to-chlorophyll ratio generally adopted in simulation studies at station Pappa (50° N 145° W) varies seasonally between 15 (winter) and 45 (summer).

**Table 22** Redfield ratios and other related ratios used by different authors

| | **Substances** | **Ratio** | **Reference** |
|---|---|---|---|
| **Redfield ratios** | | | |
| Original Redfield ratio | C:N:P | 106:16:1 | Redfield *et al.* 1963 |
| | C:N:P | 106:16:1 | Toggweiler 1993 |
| | C:N:P | 107:19:1 | Martin and Gordon 1988 |
| | C:N:P | 130:16:1 | Peng *et al.* 1987 |
| **Carbon to nitrogen ratio** | | | |
| Original Redfield ratio | C:N | 6.625 | Redfield *et al.* 1963 |
| | C:N | 7 | Prunet *et al.* 1996b |
| | C:N | 7.5 (varies) | Drange 1994 |
| | C:N | 6.625 | Sarmiento *et al.* 1993 |
| **Carbon to chlorophyll ratio** | | | |
| Start value | C:Chl | 40 | Prunet *et al.* 1996a |
| Optimised value | C:Chl | 38.3 | Prunet *et al.* 1996a |
| Start value | C:Chl | 55 | Prunet *et al.* 1996b |
| Optimised value | C:Chl | 40±5 | Prunet *et al.* 1996b |
| Winter | C:Chl | 15 | McAllister 1969 |
| Summer | C:Chl | 45 | McAllister 1969 |
| | C:Chl | 50 | Sarmiento *et al.* 1993 |
| **Pigment to chlorophyll ratio ρ** | | | |
| Stratified waters | Pig:Chl | 0.67 - 0.81 | Morel and Berthon 1989 |
| Well-mixed waters | Pig:Chl | 0.80 - 0.81 | Morel and Berthon 1989 |
| Average in eutrophic systems | Pig:Chl | 0.8 | Morel and Berthon 1989 |
| Average in oligotrophic systems | Pig:Chl | 0.65 | Morel and Berthon 1989 |
| Average | Pig:Chl | 0.76 | Balch *et al.* 1992 |
| | | | |
| **$C_{org}$ to $CaCO_3$ ratio** | | | |
| | $C_{org}$:$CaCO_3$ | 4 | Prunet *et al.* 1996b |
| | $C_{org}$:$CaCO_3$ | 5 | Drange 1994 |

An interesting approach to this problem was taken by Prunet *et al.* (1996a). One of the problems in primary production estimates is the correct parameterization of the biogeochemical processes, which are complex and highly variable in space and time. In their paper *in situ* chlorophyll data was assimilated into a one dimensional vertical physical-biogeochemical model. This model which is thereby constrained by surface chlorophyll information was used to fit other *in situ* data at station Pappa (50° N 145° W) by the minimisation of a cost function. The fit was done by adjusting the parameters in the model. So Prunet *et al.* (1996a) optimised the parameter values for their model at this station. But of course these parameters can be different at another place than station Pappa.

In any case, a general formulation of possible changing Redfield ratios in the different domains of the ocean is not available. Thus, constant ratios must be assumed. Because the model calculated biomass, which had to be transformed into chlorophyll by a constant ratio (see chapter 4.4.1), a change

in this parameterization would have resulted in a general shift into one direction, either lower or higher model chlorophyll concentration. This would not have changed the qualitative pattern of chlorophyll concentration of the model and only a shift in the quantitative comparison. But anyhow a wrong parameterization of the Redfield ratio is unlikely an explanation for the problems described in chapter 6.2.

#### 6.3.1.2 Other parameterizations

Another parameterization which can be criticised is the downward transport of $CaCO_3$ in the model. It is assumed that in the model 20 % of the sinking organic material in warm waters (the formation of $CaCO_3$ depends on temperature, see Equation 21) is $CaCO_3$ (Drange 1994) but for example Prunet *et al.* (1996b) use a value of 25 %. These differences affect the magnitude of the calculated downward flux of carbon. This type of parameterization can be criticised as a whole, too. As Maier-Reimer (1993) and Heinze *et al.* (1990) pointed out the concentration of $CaCO_3$ in surface waters and the downward flux are highly variable in space and time. This is especially evident in Coccolith blooms. These events are not modelled in N3CM. It is unlikely however that the omission of an explicit $CaCO_3$ modelling is a cause for the problems outlined in chapter 6.2. But the modelling of the downward flux of organic material is very important to estimate the export of carbon into the deep ocean.

The assumption of a constant sinking velocity of 1m/d in N3CM can be challenged, as the sinking velocity is different for particles of different sizes and the size of sinking particles might vary during the year. For example, Wolf and Strass (1993) showed that in order to represent spring bloom (generally diatoms) and summer (generally flagellates) phytoplankton populations the sinking velocity switches between 1m/d during eutrophic conditions (spring) and 0.3 m/d during oligotrophic conditions (summer). Once again these parameterizations will not affect the modelled surface chlorophyll concentration directly but they are decisive in the calculation of the final export of carbon into the deep ocean.

### 6.3.2 Model formulations

#### 6.3.2.1 Boundary conditions

The model formulations are possibly a reason for a too low concentration along the coast of North America and Great Britain. There is no boundary condition in the model with regard to nutrient influx from the coast or from river inputs but there should be one.

Another problem formed the formulation of the southern boundary. It is formulated as a solid wall. In the near future the model will be formulated on a truly global grid (Drange pers. com.), so there will be no need for this kind of boundary condition any more.

Perhaps the most important point is the accuracy of the initialisation and forcing fields. Any error in the forcing fields will have its effect on the model results. Thus, the most accurate data should be used. Unfortunately, the data used has not always the accuracy which would be desirable. Maybe a model driven by synoptic forcing fields and its comparison with OCTS images (which have already been prepared) can show the influence of the forcing fields on the chlorophyll concentrations.

#### 6.3.2.2 Other nutrients

Clearly the most important nutrient for phytoplankton is nitrogen. It can be used by phytoplankton in the form of nitrate and ammonium. A high concentration of ammonium inhibits the uptake of nitrate as has been shown by many authors (Wheeler and Kokkinakis 1990, Metzler *et al.* 1997, Fasham *et al.* 1993 and others). The inhibition of $NO_3$ uptake by $NH_4$ is incorporated in the model and there is no reason to believe that a wrong implementation of the nitrogen mechanism is a reason for the discrepancies between the model results and the satellite values. The addition of other nutrients and their explicit modelation could have an significant impact on the chlorophyll concentrations. But however, the use of other nutrients has been omitted in the model.

The addition of Si as a nutrient is especially important for the modelling of diatoms which use Si for their silica shells. It appears that the growth of silicious phytoplankton such as diatoms is limited by the available silica in seawater (Peng *et al.* 1987).

The addition of coccolithophorids and an explicit modelling of Ca could be a valuable factor. Coccolithophorids are thought to play an important role in the oceanic carbon and sulphur cycles through their production of $CaCO_3$ coccoliths, which sink to the bottom and export carbon from the surface, and dimethyl sulphide (DMS), the dominant precursor for cloud condensation nuclei in the maritime atmosphere (Brown and Yoder 1994). Thus, DMS plays a major role in cloud formation over the oceans which in turn governs global climate (Martin *et al.* 1989). According to Brown and Yoder (1994) areas rich in coccolithophorids include the subarctic latitudes of the North Atlantic, the Gulf of Mexico, the North Sea, and the coast of eastern North America. Coccolithophorids have different needs of nutrients and grow in areas of low Si-concentrations which is why a simultaneous introduction of explicit Si and Ca modelling is sensible. What makes the introduction of coccolithophorids into the model very interesting is the fact that at least one of their species (*Emiliaria huxleyi* and maybe *Gephyrocapsa oceanica*) is visible in satellite data (Brown and Yoder 1994). Thus, the compilation of an initialisation field and the verification of the model with satellite data should be possible. But this is not without difficulties because the detection dependants on coccoliths and not the cell concentration. Thus, there is a bias in the satellite data to the declining state of a bloom when the proportion of coccoliths to cells is greatest.

It is also considered that in some environments Fe supplies may be limiting phytoplankton growth, where other major nutrients, like nitrogen, are never depleted (Martin and Gordon 1988). According to Martin *et al.* (1989) these areas include the equatorial Pacific, the North Atlantic, the Gulf of Alaska, and the Southern Ocean. Sources for Fe in the ocean are atmospheric input (dust blown from the continents), runoff and "sea-slides" which cause high concentrations of Fe, Mn and Co in association with alumino-silicate turbidity plumes. It is postulated that atmospheric Fe input rates are not high enough to meet phytoplankton Fe demand in nutrient rich offshore upwelling areas. As a result, major nutrient depletion occurs only along continental margins, where Fe supplies should be adequate.

The omission of an exact modelling of these additional phytoplankton nutrients may have had an effect on the model results concerning phytoplankton concentration. The concentrations of Si, Ca and Fe might all have an impact on the phytoplankton concentration in the North Atlantic ocean. But unfortunately this could not be checked in this study.

### 6.3.3 Scale / Resolution

The resolution of the model is quite coarse. It has already been shown that some of the model's problems are caused by this, e.g. the misplacement of the Gulf Stream (Drange 1994). Another problem caused by a too low resolution might be the seen in the fact that the model was unable to predict and to resolve the eddies along the coast of South America. A higher resolution of the model, i. e. an eddy resolving resolution, should be a remedy of this problem. The outcropping of isopycnals south of the area of deep mixing should also be much smoother with a higher resolution. Thus, the nutrient gradient would not be so sharp and the chlorophyll concentration just south of the mixed layer not so high.

## 6.4 Comparison with the model of Sarmiento *et al.* 1993

The same ecosystem model, which was used by Drange (1994) has also been used by Sarmiento *et al.* (1993) with another physical model. They used a Bryan-Cox OGCM and compared the mean chlorophyll concentration of the upper two boxes (depth: 23m) with the climatological chlorophyll fields from CZCS. To calculate the chlorophyll concentration they used a C:N ratio of 6.625 and a C:Chl ratio of 50 (Slater *et al.* 1993). The forcing of the model was done with similar climatological forcing fields as used by Drange (1994). The results of their qualitative comparison (Slater *et al.* 1993 and Sarmiento *et al.* 1993) showed the following:

- The model spring bloom began too early and predicted too high phytoplankton concentrations.
- After the spring bloom the phytoplankton concentration declined too quickly and during the rest of the year the modelled concentration was too low

- A trough in the chlorophyll concentration appeared at about 50º in the early winter which was most probably caused by a misplaced Gulf Stream.
- In the central subtropical gyre the modelled phytoplankton concentration was so low that zooplankton and bacteria became virtually extinct in this area.
- The modelled concentration of phytoplankton at the equator was too high in the western part of the basin and to low in the eastern part of the basin.
- The chlorophyll values in the Mauritanian upwelling area were too low due the model's low lateral resolution.

In general its seems that the performance of the model of Sarmiento *et al.* (1993) was worse than those of Drange (1994). Most of the effects observed by Sarmiento *et al.* 1993 are different from the ones observed in this study. Only the chlorophyll concentrations in the Mauritanian upwelling area are too low in both models. In any case, it underlines the importance of the underlying physical model and which differences result from it.

## 6.5 Implications for primary production estimates

Marine photosynthetic organisms account for 40 % of global primary production but less than 1 % of plant biomass (Falkowski *et al.* 1998). Thus their contribution to global primary production is really significant. In order to estimate primary production, the concentration of chlorophyll is measured. Then the chlorophyll-light curve is used in the calculation of the amount of carbon fixed in photosynthesis. It is possible to derive ocean primary productivity from surface chlorophyll concentrations measured by space born ocean colour sensors. Estimates of primary production are shown in Table 23. They range from 8.6 PgC/yr to 50.2 PgC/yr. The estimates of the export flux of carbon from the euphotic zone to the deep ocean vary from 23 $mgC/m^2d$ to 98 $mgC/m^2d$. The errors are still very high as has been shown in chapter 6.1 because of several factors such as the limited depth of the phytoplankton visible for the satellite, variable fraction of phaeophytin versus active chlorophyll (Morel and Berton 1989), variable phytoplankton species and varying physiology (Evans *et al.* 1992 and Balch *et al.* 1992). A new estimation for primary production or the downward flux calculated by the model (see also chapter 3.5) is not given here because it is not reasonable to believe that this new estimation would be more accurate than previous ones given the big differences in the quantitative comparison between the satellite images and the model.

**Table 23** Primary production and export flux estimates

| **Area** | **Derived from** | **Annual primary production** | **Reference** |
|---|---|---|---|
| Atlantic | Numerical model | 160 $gC/m^2yr$ | Fasham 1993 |
| Station Pappa (50° N 145° W) | Optimisation of a model with *in situ* data | 90 - 105 $gC/m^2yr$ | Prunet *et al.* 1996a |
| Station Pappa (50° N 145° W) | Optimisation of a model with *in situ* data | 80 ± 12 $gC/m^2yr$ | Prunet *et al.* 1996b |
| Station Pappa (50° N 145° W) | Optimisation of a model with *in situ* data | 100 $gC/m^2yr$ (10-year scale) maximum in summer 0.55 $gC/m^2d$ | Prunet *et al.* 1996b |
| Global | Satellite chlorophyll based algorithm | 43.5 PgC/yr | Falkowski *et al.* 1998 (Algorithm from Behrenfeld and Falkowski 1997b) |
| Global | Satellite chlorophyll based algorithm | 46.9 PgC/yr | Falkowski *et al.* 1998 (Algorithm from Antoine *et al.* 1996) |
| Global | Satellite chlorophyll based algorithm | 50.2 PgC/yr | Falkowski *et al.* 1998 (Algorithm from Longhurst *et al.* 1995) |
| Global | Satellite chlorophyll based algorithm | 27.1 PgC/yr | Falkowski *et al.* 1998 (Algorithm from Eppley and Peterson 1979) |
| Atlantic | Satellite chlorophyll based algorithm | 11.9 PgC/yr | Falkowski *et al.* 1998 (Algorithm from Behrenfeld and Falkowski 1997b) |

| | | | |
|---|---|---|---|
| Atlantic | Satellite chlorophyll based algorithm | 11.3 PgC/yr | Falkowski *et al.* 1998 (Algorithm from *Antoine et al.* 1996) |
| Atlantic | Satellite chlorophyll based algorithm | 13.7 PgC/yr | Falkowski *et al.* 1998 (Algorithm from Longhurst *et al.* 1995) |
| Atlantic | Satellite chlorophyll based algorithm | 8.6 PgC/yr | Falkowski *et al.* 1998 (Algorithm from Eppley and Peterson 1979) |
| | | **Export Flux** | |
| Station Pappa (50° N 145° W) | Optimisation of a model with *in situ* data | 30 gC/m$^2$yr | Prunet *et al.* 1996b |
| Canary Islands | *In situ* measurement | 62 - 98 mgC/m$^2$d (winter) | Neuer *et al.* 1997 |
| Canary Islands | *In situ* measurement | 23 - 41 mgC/m$^2$d (summer) | Neuer *et al.* 1997 |

# 6.6 Outlook

## 6.6.1 Use of other satellite derived data for model verification

The comparison of satellite derived chlorophyll data with the model results is just one method which can be used for model verification. Other variables could be easily checked, too. The sea surface temperature derived from satellite sensors could be easily used for a comparison. Another interesting variable to check is obviously the mixed layer depth because of its influence of the surface nutrient concentration. Balch *et al.* 1992 has developed an empirical algorithm which predicts the mixed layer depth from SST, chlorophyll concentration and the latitude (see Equation 34). But it must be noted that the correlation coefficient is still not very high.

$$\log(z_{ml}) = -0.34 \cdot SST - 0.50 \cdot \log(\bar{C}_{sat}) - 0.036 \cdot LAT + 2.92 \quad r^2 = 0.67$$

**Equation 34** Calculation of mixed layer depth

Another variable which could be checked is the amount of detritus in the surface layer because its concentration is important for the downward flux of carbon. An empirical algorithm to derive the particulate organic carbon (detritus in N3CM) from chlorophyll concentration was devised by Morel (1988):

$$POC = 90\,Chl^{0.57} \quad r^2 = 0.68$$

**Equation 35** Calculation of particulate organic carbon

As has been pointed out in chapter 6.3.2.2 satellite data for coccolithophorids could be used for initialisation and verification if coccolithophorid modelling is introduced into the model. But again it must be pointed out that this is not without difficulties because satellite detection relies on coccoliths and not the cell concentration. Brown *et al.* (1995) showed a method to distinguish between diatoms, coccolithophorids and dinoflagellates which is based on the relation between the euphotic layer depth and the mixed layer depth but is does not work well at the moment. But maybe it can be improved in the future.

As the SeaWiFS data set will be recalculated, and will hopefully be more accurate, a new comparison might yield different results. Also, OCTS images have been rectified for a future comparison of synoptic OCTS data with model results that have been obtained with synoptic forcing. In this comparison the model was forced only with climatological forcing fields.

### 6.6.2 Introduction of other climate relevant gases

The decision to introduce the modelling of other climatically active components, like dimethylsulfide, nitrous oxide or methane are governed by many factors, among them the significance or their importance in coupled ocean atmosphere models. The understanding of the cycling of carbon dioxide, nitrous oxide, or dimethylsulfide, are important and significant because of the major role they play in controlling climate (Sarmiento *et al.* 1993).

Coccolithophorids are thought to be major DMS (dimethyl sulphide) producers. DMS plays a major role in cloud formation over the oceans which in turn governs global climate (Martin *et al.* 1989). The introduction of coccolithophorids and DMS into the model would require an explicit modelling of the S-Cycle which in turn would require the introduction of $O_2$ modelling because several reactions in the S cycle are either aerob or anaerob. Thus, the computational demands of an introduction of coccolithophorids and DMS into the model are high. But on the other hand the significance might not be so big. As Brown and Yoder (1994) pointed out coccolithophorids are regionally but not globally significant for DMS emissions to the atmosphere (0.03 - 0.07 % globally) or downward $CaCO_3$ fluxes (max. 0.03 % globally).

### 6.6.3 Data assimilation

Satellite data can not only be used for verification and initialisation of models but also for assimilation which is defined as the replacement of the simulated phytoplankton distribution with the chlorophyll a fields derived from *in situ* measurements or satellite images. In principal, assimilation schemes can be used to improve the model performance within a short time frame. Obviously, data assimilation is not possible for the future. A forecast using assimilation schemes might only be better than the “simple” model in a timeframe of a few days as Ishizaka and Hofmann (1993) have shown with a chlorophyll data assimilation scheme. There was no significant difference between the results after a few days. Within a few model days following data assimilation, the error in the simulated fields increased and reached the level that was obtained from the model with no data assimilation. Or even worse that some fields, like the nutrient concentrations were totally wrong after data assimilation (Ishizaka 1993). One problem is that not only the phytoplankton concentration needs data assimilation but also the other fields in a simulation, like zooplankton , bacteria or detritus (Ishizaka 1993) in order to be consistent with the assimilated phytoplankton field. But of course there is the possibility of using multiple assimilation schemes (wind, temperature, cloud cover, chlorophyll concentration, light attenuation, etc.) for a longer time which might work better.

# 7 Summary

In the present study, satellite chlorophyll data from different ocean colour sensors have been compared with phytoplankton biomass simulated with a 3-dimensional physical and biogeochemical model to assess the quality of the model's results. Therefore, it was necessary to rectify the images and to devise two algorithms:

- An algorithm has been developed to calculate subsurface chlorophyll concentrations from the surface / satellite values
- Another algorithm was developed to calculate chlorophyll concentration from phytoplankton biomass by the means of constant ratios.

The surface / satellite and the subsurface chlorophyll values were compared with the model results in time and space:

- The qualitative agreement between the satellite images and the model results was generally good.
- Certain features could be seen in the qualitative comparison which showed some drawbacks of the model, i.e. low resolution, and the lack of a boundary condition for nutrient influx at the coast.
- The quantitative comparison showed big differences between the satellite images and the model results.

These differences were deemed so high that a prediction of primary production or the downward flux of carbon which are more accurate than recent estimates made with other methods was not likely and consequently was not carried out.

# 8 References


Abramovitz M., I. A. Stegun (editors), *Handbook of Mathematical Functions*, Dover Publications, New York, 1965

Aguirre-Gómez R., A. R. Weeks, S. R. Boxall, The Identification of Phytoplankton Pigments from Absorption Spectra: *Proceedings of the International Colloquium Photosynthesis and Remote Sensing*, 28-30 August 1995, Montpellier, France, G. Guyot (editor), 516 pp., Paris , Avignon, 1995

Ahmad, Z., and R. S. Fraser, An iterative radiative transfer code for ocean-atmosphere systems, *J. Atmos. Sci., 39*, 656-665, 1982

André, J.-M., and A. Morel, Simulated effects of barometric pressure and ozone content upon the estimate of marine phytoplankton from space, *J. Geophys. Res., 94*, C1, 1029-1037, 1989

André, J.-M., Ocean colour remote sensing and the subsurface vertical structure of phytoplankton pigments, *Deep-Sea Research, 39*, 5, 763-779, 1992

Antoine, D., J.-M. André, and A. Morel, Oceanic primary production 2. Estimates at global scale from satellite (Coastal Zone Colour Scanner) chlorophyll, *Global Biogeochem. Cycles, 10*, 57-69, 1996

Archer, D., and E. Maier-Reimer, Effect of deep-sea sedimentary calcite preservation on atmospheric $CO_2$ concentration, *Nature, 367*, 260-263, 1994

Austin, R. W., T. J. Petzold, Spectral dependence of the diffuse attenuation coefficient of light in ocean waters, *Optical Engineering, 25*, 3, 471-479, 1986

Baker, K. S. and R. C. Smith, Biooptical classification and model of natural waters 2, *Limnol. Oceanogr., 27*, 3, 500-509, 1982

Balch, W. M., M. R. Abbott, R. W. Eppley, Remote Sensing of primary production-I. A comparison of empirical and semi-analytical algorithms, *Deep-Sea Research, 36*, 2, 281-295, 1989a

Balch, W. M., R. W. Eppley, M. R. Abbott, Remote Sensing of primary production-II. A semi-analytical algorithm based on pigments, temperature and light, *Deep-Sea Research, 36*, 8, 1201-1217, 1989b

Balch, W., R. Evans, J. Brown, G. Feldmann, C. McClain, W. Esaias, The Remote Sensing of Ocean Primary Productivity: Use of a New Data Compilation to Test Satellite Algorithms, *Journal of Geophysical Research, 97*, C2, 2279-2293, 1992

Balkanski Y., P. Monfray, M. Battle, M. Heimann, *The ocean primary production derived from satellite data: an evaluation with atmospheric oxygen*, 1998 (in press)

Banse K., Uptake of inorganic carbon and nitrate by marine plankton and the Redfield ratio, *Global Biogeochemical Cycles, 8*, 1, 81-84, 1994

Bates, R. G. and C. H. Culberson, Hydrogen Ions and the Thermodynamic State of Marine Systems, in: *The Fate of Fossil Fuel $CO_2$ in the Oceans*, N. R. Andersen, and A. Malahoff (editors), 45-61, Plenum Press, New York, 1977

Behrenfeld, M. J., and P. G. Falkowski, Photosynthetic rates derived from satellite-based chlorophyll concentrations, Limnol. Oceanogr., 42, 1-20, 1997

Berner, R. A., Burial of organic carbon and pyrite sulphur in the modern ocean: its geochemical and environmental significance, *American Journal of Science, 282*, 451-473,1982

Biggar, S. F., P. N. Slater, K. J. Thome, A. W. Holmes, R. A. Barnes, in: McClain, C. R., R. S. Fraser, J. T. McLean, M. Darzi, J.K. Firestone, F.S. Patt, B. D. Schieber, R.H. Woodward, E-n. Yeh, S. Mattoo, S. F. Biggar, P.N. Slater, K.J. Thome, A.W. Holmes, R. A. Barnes, and K.J. Voss, Case Studies for SeaWiFS Calibration and Validation, Part 2, *SeaWiFS Technical Report Series, Vol. 19*, Hooker Stanford B., Elaine R. Firestone, and James G. Acker (editors), NASA Technical Memorandum 104566, NASA, Goddard Space Flight Center, Greenbelt, Maryland, 1994

Bleck, R., C. Rooth, D. Hu, and L.T. Smith, Salinity-driven thermohaline transients in a wind and thermohaline-forced isopycnic coordinate model of the North Atlantic, *J. Phys. Oceanogr., 22*, 1486-1505, 1992

Bleck, R., H. P. Hanson, D. Hu, and R. B. Kraus, Mixed layer-thermohaline interaction in a three dimensional isopycnic coordinate model, *J. Phys. Oceanogr., 19*, 1417-1439, 1989

Boden, T. A., R. J. Sepanski, and F. W. Stoss (editors), *Trends '91: A Compendium of Data on Global Change*, Carbon Dioxide Information Analysis Center, Oak Ridge National Laboratory, Tennessee, 1991

Boyd P., A. Pomroy, S. Bury, G. Savidge, I., Joint, Micro-algal carbon and nitrogen uptake in post-coccolithophore bloom conditions in the Northeast Atlantic, July 1991, *Deep Sea Research I, 44*, 9-10, pp. 1497-1517, 1997

Brewer, P. G. and J. C. Goldman, Alkalinity changes generated by phytoplankton growth, *Limnol. Oceanogr., 21*, 108-117, 1976

Bricaud, A., A. Morel, and L. Prieur, Absorption by dissolved organic matter of the sea (Yellow substance) in the UV and visible domains, *Limnol. and Oceanogr., 26*, 43-53, 1981

Brock, J.C., C.R. McClain, M.E. Luther, and W. W. Hay, The phytoplankton bloom in the north-west Arabian Sea during the south-west monsoon, *J. Geophys. Res., 97*, C1, 733-750, 1991

Broecker, W. S. and T. Takahashi, The relationship between Isocline depth and *in situ* carbonate ion concentration, *Deep Sea Res., 25*, 65-95, 1978

Broecker, W. S., and T. H. Peng, *Tracers in the sea*, Lamont-Doherty Geological Observatory, Palisades, N. Y., 1982

Brown, C. W., and J.A. Yoder, Coccolithophorid blooms in the global ocean, *J. Geophys. Res., 99*, C4, 7467-7482, 1994

Brown, C. W., W. E. Esaias, A. M. Thompson, Predicting Phytoplankton Composition from Space-Using the ratio of Euphotic Depth to Mixed-Layer Depth: An Evaluation, *Remote Sens. Environ., 53*, pp. 172-176, 1995

Bukata, R. P., J. H. Jerome, K. Y. Kondratyev, D. V. Podzdnyakov, *Optical Properties and Remote Sensing of Inland and Coastal Waters*, 362 pp., CRC press, Boca Raton, 1995

Campbell J. W., Ocean Primary Productivity Algorithms, in: *Proceedings of the International Colloquium Photosynthesis and Remote Sensing*, 28-30 August 1995, Montpellier, France, G. Guyot (editors), 516 pp., Paris , Avignon, 1995a

Campbell J. W., S. R. Gaudreau, G. M. Weiss, The Challenge of Scaling Primary Productivity Models to the Global Ocean: A Statistical Approach, in: *Proceedings of the International Colloquium Photosynthesis and Remote Sensing*, 28-30 August 1995, Montpellier, France, G. Guyot (editors), 516 pp., Paris , Avignon, 1995b

Carder K. L., R. G. Steward, G. R. Harvey, P. B. Ortner, Marine humic and fulvic acids: Their effects on remote sensing of ocean chlorophyll, *Limnol. Oceanogr., 34*, 1, 68-81, 1989

Cho, B. C. and F. Azam, Major role of bacteria in biogeochemical fluxes in the ocean's interior, *Nature, 332*, 441-443, 1988

Chrisholm, S. W., and F.. M: Morel, What controls phytoplankton production in nutrient-rich areas of the open sea?, *Limnol. Oceanogr., 36*, 1507-1965, 1991

Cole, J. J., S. Findlay and M.L Pace, Bacterial production in fresh and saltwater ecosystems: a cross-system overview, *Marine Ecology Progress Series, 43*, 1-10, 1988

Cox, C. and W. Munk, 1955: Some Problems in Optical Oceanography, Scripps Institution of Oceanography, La Jolla, California, 63-77

Cox, C., and W. Munk, Measurement of the roughness of the sea surface from photographs of the sun's glitter, *J. Opt. Soc. Am., 44*, 838-850, 1954a

Cox, C., and W. Munk, Statistics of the sea surface derived from sun glitter, *J. Mar. Res., 13*, 198-227, 1954b

Darzi M., *SeaWiFS Science Algorithm Flow Chart*, Contractor Report, NASA, Goddard Space Flight Center, Greenbelt, Maryland, 1998a

Darzi M., W. Robinson, E.-n. Yeh, R. E. Eplee, J. K. Firestone, C. R. McClain, Quality Control of the SeaWiFS Archive Data Products, submitted to American Meteorological Society, 1998b

Dave, J.V., Development of programs for computing characteristics of ultraviolet radiation, Technical Report-Scalar Case, Program II, FSC-72-0011, IBM Federal Systems Division, Gaithersburg, Maryland, 38 pp., 1972

Dickey, T., J. Marra, T. Granata, C. Langdon, M. Hamilton, J. Wiggert, D. Siegel, and A. Bratkovich, Concurrent high-resolution bio-optical and physical time series observations in the Sargasso Sea during the spring of 1987, *J. Geophs. Res., 96*, C5, 8643-8663, 1991

Dickson, A. G., An exact definition of total alkalinity and a procedure for the estimation of alkalinity and total inorganic carbon from titration data, *Deep Sea Res., 28*, 609-623, 1981

Dickson, A. G., and F. J. Millero, A comparison of the equilibrium constants for the dissociation of carbonic acid in seawater media, *Deep-Sea Res., 34*, 1833-1743, 1987

Drange, H., A 3-Dimensional Isopycnic Coordinate Model of the Seasonal Cycling of Carbon and Nitrogen in the Atlantic Ocean, *Phys. Chem. Earth, 21*, 5-6, 503-509, 1996

Drange, H., *An Isopycnic Coordinate Carbon Cycle Model for the North Atlantic: and the Possibility of Disposing of Fossil Fuel $CO_2$ in the Ocean*, Ph.D. thesis, Nansen Environmental and Remote Sensing Center. and Dep. Of Math., University of Bergen, Bergen, Norway, 1994

Duchossois G., Europe's position concerning ocean colour activities, in: *Ocean Colour Workshop, Proceedings of an ESA Workshop held at Villefranche-sur-mer, France, 4-5 November 1987*, ESA SP-1083, European Space Agency, 1987

Dugdale R. C., A. Morel, A. Bricaud and F. P. Wilkerson, Modelling new production in upwelling centers: a case study of modelling new production from remote sensed temperature and colour, *Journal of Geophysical Research, 94*, C12, 18119-18132, 1989

Eckstein, B. A., and J.J. Simpson, Cloud Screening Coastal Zone Colour Scanner images using channel 5, *Int. J. Remote Sens., 12*, 2359-2377, 1991

Eppley, R. W. and B. J. Peterson, Particulate organic matter flux and planktonic new production in the deep ocean, *Nature, 282*, 677-680,1979

Eppley, R. W., New Production: History, methods, problems, in: *Productivity of the ocean: Present and Past*, edited by V. S. Smetacek, G. Wefer and W. H. Berger, 85-97, John Wiley, Chichester, 471 pp., 1989

Esbensen, S. and Y. Kushnir, Heat Budget of the Global Ocean: Estimates from Surface Marine Observations, Technical Report, Climate Research Institute, Oregon State University, Corvallis, OR, 27 pp., 1981

Evans, G. T., and V. C. Garçon (editors), *One-dimensional Models of Water Column Biogeochemistry*, JGOFS Report 23, JGOFS International Project Office, Bergen, 87 pp., 1997

Evans, G. T., M. J. R. Fasham, *Towards a Model of Ocean Biogeochemical Processes*, Nato ASI Series Vol. 10, Springer-Verlag, Berlin, Heidelberg, 350 pp., 1993

Evans, R. H., H. R. Gordon, Coastal zone colour scanner "system calibration": A retrospectice examination, *Journal of Geophysical Research, 99*, C4, 7293-7307, 1994

Evans, W. B., J. Brown, G. Feldman, C. McClain, W. Esaias, The Remote Sensing of Ocean Primary Productivity: Use of a New Data Compilation to Test Satellite Algorithms, *Journal of Geophysical Research, 97*, C2, 2279-2293, 1992

Falkowski, P. G., M. J. Behrenfeld, W. E. Esaias, W. Balch, J. W. Campbell, R. L. Iverson, D. A. Kiefer, A. Morel, J. A. Yoder, Satellite Primary Productivity Data and Algorithm Development: A Science Plan for Mission to Planet Earth, *SeaWiFS Technical Report Series, Vol. 42*, Hooker Stanford B., Elaine R. Firestone (editors), NASA Technical Memorandum 104566, NASA, Goddard Space Flight Center, Greenbelt, Maryland, 1998

Fasham, M. J. R., H. W. Ducklow, and S. M. McKelvie, A nitrogen-based model of phytoplankton dynamics in the oceanic mixed layer, *J. Mar. Res., 48*, 591-639, 1990

Fasham, M. J. R., Modelling the marine biota, in: *The Global Carbon Cycle*, M. Heimann (editor), 457-504 pp., Berlin, Springer-Verlag, 1993

Fasham, M. J., J. L. Sarmiento, R. D. Slater, H. W. Ducklow, and R Williams, Ecosystem Behaviour at Bermuda Station "S" and Ocean Weather Station "India": A general Circulation Model and Observational Analysis, *Global Biogeochemical Cycles, 7*, 2, 379-415, 1993

Fisher, P. F., Spatial Data Sources and Data Problems, in: *Geographical Information Systems, Principles and Applications*, D. J. Maguire, M. F. Goodchild, D. W. Rhind (editors), Longman Scientific & Technical, Harlow, 649 pp., 1991

Fofonoff, N. P., and R. C. Millard, Jr., Algorithms for computation of fundamental properties of sea-water, UNESCO Tech. Papers in Marine Science, 44, UNESCO, 53 pp., 1983

Fraser, R. S., The Effect of Oxygen Absorption on Band-7 Radiance, in: Mueller, J. L., R. S. Fraser, S. F. Biggar, K. J. Thome, P. N. Slater, A. W. Holmes, R. A. Barnes, C. T. Weir, D. A, Siegel, D. W. Menzies, A. F. Michaelis, and G. Podesta, 1995b: Case Studies for SeaWiFS Calibration and Validation, Part 3, *SeaWiFS Technical Report Series, Vol. 25*, Hooker Stanford B., Elaine R. Firestone, James G. Acker (editors), NASA Technical Memorandum 104566, NASA, Goddard Space Flight Center, Greenbelt, Maryland, 1995

Gargett, A. E., Vertical eddy diffusivity in the ocean interior, *J. Mar. Res., 42*, 359-393, 1984

Gaspar, P., Modelling the seasonal cycle of the upper ocean, *J. Phys. Oceanogr., 18*, 161-180, 1988

Gill, A. E., *Atmosphere-Ocean Dynamics*, Academic Press, San Diego, 662 pp. 1982

Goericke, R., and D. J. Repeta, Chlorophylls a and b and divinyl chlorophylls a and b in the open subtropical North Atlantic Ocean, *Mar. Ecol. Progr. Ser., 10*, 307-313, , 1993

Goldman, J. C. and P. G. Brewer, Effects of nitrogen source and growth rate on phytoplankton-mediated changes in alkalinity, *Limnol. Oceanogr., 25*, 352-357, 1980

Golub, G. H., and C. F. van Loan, *Matrix Computations*, North Oxford Academic, Oxford, 483 pp., , 1983

Gordon H. R., and A. Y. Morel, Remote assessment of ocean colour for interpretation of satellite visible imagery: review, *Lecture Notes on Coastal and Estuarine Studies, 4*, Springer-Verlag, 114 pp., 1983

Gordon, H. R, J.W. Brown, O.B. Brown, R.H. Evans, and W.W. Broenkow, Phytoplankton pigment concentrations in the Middle Atlantic Bight: Comparison of ship determinations and CZCS estimates, *Appl. Opt., 22*, 20-36, 1983

Gordon, H. R., and D. J. Castaño, Coastal Zone Colour Scanner atmospheric correction algorithm: multiple scattering effects, *Appl. Opt., 11*, 2111-2122, 1987

Gordon, H. R., and D.K. Clark, Remote sensing optical properties of a stratified ocean: an improved interpretation, *Applied Optics, 19*, 20, 3428-3430, 1980

Gordon, H. R., and K. Ding, Self Shading of in-water optical instruments, *Limnol. Oceanogr., 37*, 491-500, 1992

Gordon, H. R., and W. R. McCluney, Estimation of the Depth of Sunlight Penetration in the Sea for Remote Sensing, *Applied Optics, 14*, 2, 413-416, 1975

Gordon, H. R., J.W. Brown, and R.H. Evans, Exact Rayleigh scattering calculation for use with the Nimbus-7 Coastal Zone Colour Scanner, *Appl. Opt., 27*, 862-871, 1988b

Gordon, H. R., M. Wang, Retrieval of water-leaving radiance and aerosol optical thickness over the oceans with SeaWiFS: a preliminary algorithm, *Applied Optics, 33*, 3, 1994

Gordon, H. R., O. B. Brown, R. H. Evans, J. W. Brown, R. C. Smith, K. S. Baker, and D. K. Clark, A Semianalytical Radiance Model of Ocean Colour, *Journal of Geophysical Research, 93*, D9, 10909-10924, 1988c

Gordon, H. R., Ocean colour remote sensing systems: radiometric requirements, in: *Recent Advances in Sensors, Radiometry, and data Processing for Remote Sensing*, P.N. Slater (editor), SPIE, 924, pp. 151-167, 1988a

Gordon, H. R., Ship perturbation of irradiance measurements at sea, 1: Monte Carlo simulations, *Appl. Opt., 24*, 4172-4182, 1985

Griggs, M., Absorption coefficients of ozone in the ultraviolet and visible regions, *J. Chem. Phys., 49*, 857, 1968

Heinze, C., E. Maier-Reimer, and K. Winn, *Glacial $pCO_2$ reduction by the world ocean-experiments with the Hamburg Carbon Cycle Model*, Report 57, Max-Planck-Institut für Meteorologie, Hamburg, 1990

Hellerman, S., and M. Rosenstein, Normal monthly wind stress over the World Ocean with error estimates, *J. Phys. Oceanogr., 13*, 1093-1104, 1983

Holland, H. D., *The Chemistry of the Atmosphere and Oceans*, Wiley, New York, pp. 351, 1978

Holligan P.M., A. Morel, Remote Sensing of ocean colour for studies of biological productivity and biochemical cycles, in: *Ocean Colour Workshop, Proceedings of an ESA Workshop held at Villefranche-sur-mer, France, 4-5 November 1987*, ESA SP-1083, European Space Agency, 1987

Honjo, S., S. J. Manganini and J. J. Cole, Sedimentation of biogenic matter in the deep ocean, *Deep Sea Research, 29*, 609-625, 1982

Hooker S. B., C. R. McClain, J. K. Firestone, T. L. Westphal, E.-n. Yeh, Y. Ge, The SeaWiFS Bio-Optical Archive and Storage System (SeaBASS), Part 1, *SeaWiFS Technical Report Series, Vol.20*, Hooker Stanford B., Elaine R. Firestone (editors), NASA Technical Memorandum 104566, NASA, Goddard Space Flight Center, Greenbelt, Maryland, 1994

Hooker S. B., W. E. Esaias, G. C. Feldman, W. W. Gregg, C. R. McClain, An overview of the SeaWiFS and Ocean Colour, *SeaWiFS Technical Report Series, Vol.1*, Hooker Stanford B., Elaine R. Firestone (editors), NASA Technical Memorandum 104566, NASA, Goddard Space Flight Center, Greenbelt, Maryland, 1992

Hsiung, J., Mean Surface Energy Fluxes Over the Global Ocean, *J. Geophys. Res., 91*, C9, 10585-10606, 1986

Ingmanson, D. E., and W. J. Wallace, *Oceanography - An Introduction*, Wadsworth Publishing Company, Belmont, 459 pp., 1995

Inn, E.C.Y., and Y. Tanaka, Absorption coefficient of ozone in the ultraviolet and visible regions, *J. Opt. Soc. Amer., 43*, 870-873, 1953

Ishizaka, J., and E. E. Hofmann, Coupling of Ocean Colour Data to Physical-Biological Models, in: *Ocean Colour: Theory and Applications in a Decade of CZCS Experience*, V. Barale, P. M. Schlittenhardt (editors), Kluwer Academic Publishers, Dordrecht, 367 pp., 1993

Ishizaka, J., Data Assimilation For Biogeochemical Models, in: Geoffrey T. Evans, Michael J. R. Fasham (editors), *Towards a Model of Ocean Biogeochemical Processes*, NATO ASI Series I: Global Environmental Change, Vol. 10, Springer-Verlag, Berlin, Heidelberg, 350 pp. 1993

Jaeger, L. Monatskarten des Niederschlags fuer die ganze Erde, Technical Report 139, Berichte des Deutschen Wetterdienstes, Offenbach, Germany, 1976

Jerlov, N. G., *Marine Optics*, Elsevier Scientific Publishing Company, New York, pp. 231, 1976

Joint Global Ocean Flux Study, 1991: JGOFS Core Measurements Protocols. JGOFS Report No. 6, Scientific Committee on Oceanic Research, 40 pp.

Jursa A.S., *Handbook of Geophysics and the Space Environment*, Air Force Geophysics Laboratory, 18-11-18-24, 1985

Jäne, B., G. Heintz, and W. Dietrich, Measurement of the diffusion coefficient of sparingly gases in water with a modified Barrer method, *J. Geophys. Res.*, *92*, C10, 10767-10776, 1987

Kirk, J. T. O., *Light and Photosynthesis in Aquatic Ecosystems*, Cambridge University Press, Cambridge, 401 pp.,1986

Kneizys, F.X., E. P. Sheettle, W.O. Gallery, J.H. Chetwynd, L.W. Abreu, J.E.A. Selby, S.A. Clough, and R.W. Fenn, *Atmospheric transmittance / radiance: computer code LOWTRAN 6*, AFGL-TR-83-0187, Air Force Geophysics Lab, Hanscom AFB, Massachusetts, 200 pp., 1993

Kraus, E. B. and J. S. Turner, A one-dimensional model for the seasonal thermocline. II The general theory and its consequences, *Tellus*, *14*, 98-105, 1969

Levitus S., M. E. Conkright, J. L. Reid, R. G. Najjar, and A. Mantyla, Distribution of nitrate, phosphate and silicate in the world oceans, *Prog. Oceanog.*, *31*, 245-273, 1993

Levitus, S. Climatological Atlas of the World Ocean, Technical Report, NOAA Professional Paper 13, 173 pp., 1982

Libes, S. M., *An Introduction To Marine Biogeochemistry*, John Wiley & Sons, New York, 734 pp., 1992

Liebelt, P. B., *Introduction to Optimal Estimation*, 273 pp., Addison Wesley, New York, 1967

Liss, P. S., and P. G. Slater, Flux of Gases across the Air-Sea Interface, *Nature*, *247*, 181-184, 1974

Longhurst, A., S. Sathyendranath, T. Platt, and C. Caverhill, An estimate of global primary production in the ocean from satellite radiometer data, *J. Plankton Research*, *17*, 6, 1245-1271, 1995

Maier-Reimer, E. Geochemical cycles in an ocean General Circulation model. Preindustrial tracer distributions, *Global Biogeochem. Cycles*, *7*, 645-677, 1993

Maling, D. H., Coordinate Systems and Map Projections for GIS, in: *Geographical Information Systems, Principles and Applications*, D. J. Maguire, M. F. Goodchild, D. W. Rhind (editors), Longman Scientific & Technical, Harlow, 649 pp., 1991

Marshall, B. R., and R. C. Smith, Raman scattering and in-water optical properties, *Appl. Opt.*, *29*, 71-84, 1990

Martin, J. H. and R. M. Gordon, Northeast Pacific iron distribution in relation to phytoplankton productivity, *Deep Sea Research*, *35*, 2, 177-196, 1988

Martin, J. H., G. A. Knauer, D. M. Karl and W. W. Broenkow, VERTEX: Carbon cycling in the north-east Pacific, *Deep Sea Research*, *34*, 267-285,1987

Martin, J. H., R. M. Gordon, S. Fitzwater and W.W. Broenkow, VERTEX: Phytoplankton/iron studies in the Gulf of Alaska, *Deep Sea Research*, *36*, 5, pp. 649-680, 1989

McClain C. R., J. C. Comiso, R. S. Fraser, J. K. Firestone, B. D. Schieber, E.-n. Yeh, K. R. Arrigo, C. W. Sullivan, Case Studies for SeaWiFS Calibration and Validation, Part 1, *SeaWiFS Technical Report Series, Vol.13*, Hooker Stanford B., Elaine R. Firestone (editors), NASA Technical Memorandum 104566, NASA, Goddard Space Flight Center, Greenbelt, Maryland , 1994c

McClain C. R., K. Arrigo, W. E. Esaias, Michael Darzi, F. S. Patt, R. H. Evans, J. W. Brown, R. A. Barnes, L. Kumar, SeaWiFS Algorithms, Part 1, *SeaWiFS Technical Report Series, Vol.28*, Hooker Stanford B., Elaine R. Firestone, James G. Ackers (editors), NASA Technical Memorandum 104566, NASA, Goddard Space Flight Center, Greenbelt, Maryland, 1995

McClain, C. R., J. C. Comiso, R. S, Fraser, J. K. Firestone, B. D. Schieber, E.-n. Yeh, K. R. Arrigo, and C. W. Sullivan, Case Studies for SeaWiFS Calibration and Validation, Part 1, *SeaWiFS Technical Report Series, Vol. 13*, Hooker Stanford B., Elaine R. Firestone, and James G. Acker (editors), NASA Technical Memorandum 104566, NASA, Goddard Space Flight Center, Greenbelt, Maryland, 1994a

McClain, C. R., K. Arrigo, W. E. Esaias, M. Darzi, F. S. Patt, R. H. Evans, J. W. Brown, C. W. Brown, R. A. Barnes, and L. Kumar, SeaWiFS Algorithms, Part 1, *SeaWiFS Technical Report Series, Vol. 28*, Hooker Stanford B., Elaine R. Firestone, and James G. Acker (editors), NASA Technical Memorandum 104566, NASA, Goddard Space Flight Center, Greenbelt, Maryland, 1995

McClain, C. R., R. S. Fraser, J. T. McLean, M. Darzi, J.K. Firestone, F.S. Patt, B. D. Schieber, R.H. Woodward, E-n. Yeh, S. Mattoo, S. F. Biggar, P.N. Slater, K.J. Thome, A.W. Holmes, R. A. Barnes, and K.J. Voss, Case Studies for SeaWiFS Calibration and Validation, Part 2, *SeaWiFS Technical Report Series, Vol. 19*, Hooker Stanford B., Elaine R. Firestone, and James G. Acker (editors), NASA Technical Memorandum 104566, NASA, Goddard Space Flight Center, Greenbelt, Maryland, 1994b

Metzler, P. M., P. M. Glibert, S. A. Gaeta, J. M. Ludlam, New and regenerate production in the South Atlantic off Brazil, *Deep-Sea Research I*, *44*, 3, 363-384, 1997

Millero, F. J., and M. L. Sohn, *Chemical Oceanography*, CRC Press, Boca Raton, Florida, 531 pp., 1992

Millero, F. J., The thermodynamics of carbonate system in seawater, *Geoch. Cosm. Acta, 43*, 1651-1661, 1979

Mitchell, B.G., and D.A. Kiefer, Determination of absorption and fluorescene excitation spectra for phytoplankton, *Marine Phytoplankton and Productivity*, O. Holm-Hansen, L. Bolis, and R. Gilles (editors), Springer-Verlag, 157-169, 1984

Mitchell, B.G., and O. Holm-Hansen, Bio-optical properties of Antarctic peninsular waters: Differentiation from temperate ocean models, *Deep Sea Res., 38*, 1009-1028, 1991

Morel A., J.-F. Berthon, Surface pigments, algal biomass profiles, and potential production of the euphotic layer: Relationships reinvestigated in view of remote-sensing applications, *Limnol. Oceanogr., 34*, 8, 1545-1562, 1989

Morel A., Optical Modelling of the Upper Ocean in Relation to its Biogenious Matter Content (Case I Waters), *Journal of Geophysical Research*, 93, C9, 10749-10768, 1988

Morel, A., and L. Prieur, Analysis of variations in ocean colour, *Limnol. Oceanogr.*, 22, 709-722, 1977

Mueller J. L., R. W. Austin, Ocean Optics Protocols for SeaWiFS Validation, *SeaWiFS Technical Report Series, Vol. 5*, Hooker Stanford B., Elaine R. Firestone (editors), NASA Technical Memorandum 104566, NASA, Goddard Space Flight Center, Greenbelt, Maryland, 1992

Mueller J. L., R. W. Austin, Ocean Optics Protocols for SeaWiFS Validation, Revision 1, *SeaWiFS Technical Report Series*, Vol. 25, Hooker Stanford B., Elaine R. Firestone, James G. Acker (editors), NASA Technical Memorandum 104566, NASA, Goddard Space Flight Center, Greenbelt, Maryland, 1995a

Mueller, J. L., Nimbus-7 CZCS: electronic overshoot due to cloud reflectance, *Appl. Opt., 27*, 438-440, 1988

Mueller, J. L., R. E. Lange, Bio-optical provinces of the Northeast Pacific Ocean: A provisional analysis, *Limnol. Oceanogr., 34*, 8, 1572-1586, 1989

Mueller, J. L., R. S. Fraser, S. F. Biggar, K. J. Thome, P. N. Slater, A. W. Holmes, R. A. Barnes, C. T. Weir, D. A, Siegel, D. W. Menzies, A. F. Michaelis, and G. Podesta, 1995b: Case Studies for SeaWiFS Calibration and Validation, Part 3, *SeaWiFS Technical Report Series, Vol. 25*, Hooker Stanford B., Elaine R. Firestone, James G. Acker (editors), NASA Technical Memorandum 104566, NASA, Goddard Space Flight Center, Greenbelt, Maryland, 1995b

Neckel, H., and D. Labs, The solar radiation between 3300 and 12500 Å, *Sol. Phys., 90*, 205-258, 1984

Neuer S., V. Ratmeyer, R. Davenport, G. Fischer, G. Wefer, Deep water particle flux in the Canary Island region: seasonal trends in relation to long-term satellite derived pigment data and lateral sources, *Deep-Sea Research, 44*, 8, 1451-1466, 1997

New, A. L., and R. Bleck, An Isopycnic Model Simulation of the Atlantic Ocean. Part II: Interdecadal Variability of the Subtropical Gyre, *J. Phys. Oceanogr., 25*, 2700-2714, 1995b

New, A. L., R. Bleck, Y. Jia, R. Marsh, M. Huddleston, and S. Bernard, An Isopycnic Model Study of the North Atlantic. Part I: Model Experiment, *J. Phys. Oceanogr., 25*, 2667-2699, 1995a

Niiler, P. P., and E. B. Kraus, One-dimensional models of the upper ocean, in: *Modelling and Prediction of the Upper Layers of the Ocean*, Kraus, E. B. (editor), pp. 143-172, Oxford, Pergamon Press, 1977

Packard, T. T., M. Denis and P. Garfield, Deep-ocean metabolic CO2 production: calculations from ETS activity, *Deep Sea Res. 35*, 371-382, 1988

Parker, S. P., (editor), *Dictionary of scientific and technical Terms*, Mc-Graw-Hill Book Company, New York, St. Louis, San Francisco, 1984

Pedersen, A., Community metabolism on rocky-shore assemblages in a mesocosm: Fluctuations in production, respiration, chlorophyll a content and C:N ratios of grazed and non-grazed assemblages. Proceedings of the International Seaweed Symposium 12: 267-275, 1987

Peng, T.-H., T. Takahashi, W. S. Broecker, and J. Olafsson, Seasonal variability of carbon dioxide, nutrients and oxygen in the North Atlantic surface water: Observations and a model, *Tellus, 39B*, 439-458, 1987

Petzold, T.J., A method for obtaining analytical curve fits to underwater radiometric measurements, Tech. Memo. Oc Op/TJP-88-06t, Scripps Inst. of Oceanogr., 20 pp., 1988

Platt, T. S. Sathyendranath, O. Ulloa, W. G. Harrison, N. Hoepffner and J. Goes, Nutrient control of phytoplankton photosynthesis in the Western North Atlantic, *Nature, 356*, 229-231, 1992

Platt, T., S. Sathyendranath, Estimators of Primary Production for Interpretation of Remotely Sensed Data on Ocean Colour, *J. Geophys. Res., 98*, C8, 14561-14576, 1993

Prudnikow A. P., Y. A. Brychkov, O. I. Marichev, *Integrals and Series, Volume 1, Elementary Functions*, Gordon and Breach Science Publishers, Amsterdam, 1986

Prunet P., J.-F. Minster, V. Echevin, I. Dadou, Assimilation of surface data in a one-dimensional physical-biogeochemical model of the surface ocean 2. Adjusting a simple trophic model to

chlorophyll, temperature, nitrate and $pCO_2$ data, *Global Biogeochemical Cycles, 10*, 1, 139-158, 1996b

Prunet, P., J.-F. Minster, D. Ruiz-Pino, and I. Dadou, Assimilation of surface data in a one-dimensional physical-biogeochemical model of the surface ocean 1. Method and preliminary results, *Global Biogeochemical Cycles, 10*, 1, 111-138, 1996a

Quay, P., Carbon Sink and the Ocean ,in: R. G., Pirie (editor), *Oceanography, Contemporary Readings in Ocean Sciences*, Oxford University Press, New York, 425 pp., 1996

Redfield, A. C., , Ketchum, B.H., and Richardson, F. A., The influence of organisms on the composition of sea-water, in: *The sea*, edited by M. N. Hill, Vol. 2, 26-77, New York Interscience Publ., 1963

Reed, R. K., On Estimating Insolation over the Ocean, *J. Phys. Oceanogr., 7*, 482-485, 1977

Reilly, J. E., S. Maritorena, B. G. Mitchell, D. A. Siegel, K. L. Carder, S. A. Garver, M. Kahru, C. McClain, Ocean Colour Chlorophyll Algorithms for SeaWiFS, in press, 1998

Rosati, A. and K. Miyakoda, A General Circulation model for Upper Ocean Simulation, *J. Phys. Oceanogr., 18*, 1601-1626, 1988

Sambrotto, R. N., G. Savidge, C. Robinso, P. Boyd, T. Takahashi, D. M. Karl, C. Langdon, D. Chipman, J. Marra, and L. Codispoti, Elevated consumption of carbon relative to nitrogen in the surface ocean, *Nature, 363*, 248-250, 1993

Sarmiento, J L., J. C. Orr, and U. Siegenthaler, A Perturbation Simulation of $CO_2$ Uptake in an Ocean General Circulation Model, *J. Geophys. Res., 97*, C3, 3621-3645,1992

Sarmiento, J. L., R. D. Slater, M. J. R. Fasham, H. W. Ducklow, J. R. Toggweiler, and G. T. Evans, A Seasonal three-dimensional Ecosystem Model of Nitrogen Cycling in the North Atlantic Euphotic Zone, *Global Biogeochem. Cycles, 7*, 417-450, 1993

Sathyendranath S., and T. Platt, Underwater Light Field and Primary Production: Application to Remote Sensing, in: *Ocean Colour: Theory and Applications in a Decade of CZCS Experience*, edited by V. Barale, P. M. Schlittenhardt, Kluwer Academic Publishers, Dordrecht, 367 pp., 1993

Sathyendranath, S. and T. Platt, The spectral Irradiance Field at the Surface and in the Interior of the Ocean: A Model for Applications in Oceanography and Remote Sensing, *J. Geophys. Res., 93*, C8, 9270-9280, 1988

Schlesinger, W. P., *Biogeochemistry, An Analysis of Global Change*, Academic Press, San Diego, 443 pp., 1991

Shettle, E. P. and R. W. Fenn, *Models for the Aerosols of the lower atmosphere and the Effects of Humidity Variations on their Optical Properties*, Rep. AFGL-TR-79-0214, U.S. Air Force Geophysics Laboratory, Hanscom Air Force Base, Mass., 1979

Siegel, D.A., C.R. Booth, and T.D. Dickey, Effects of Sensor Characteristics on the Inferred Vertical Structure of the Diffuse Attenuation Coefficients Spectrum, in: *Ocean Optics VIII*, P.N. Slater (editor), SPIE, 637, 115-124, 1986

Siegenthaler, U. Carbon Dioxide: Its Natural Cycle and Anthropogenic Perturbation, in: *The Role of Air-Sea Exchange in Geochemical Cycling*, Buat-Ménard, P. (editor), 209-247, Dordrecht, Reidel, 1986

Simpson, J. J., The Coastal Zone Colour Scanner (CZCS) Algorithm. A critical Review of Residual Problems, in: *Ocean Colour: Theory and Applications in a Decade of CZCS Experience*, edited by V. Barale, P. M. Schlittenhardt, Kluwer Academic Publishers, Dordrecht, 367 pp., 1993

Singleton, P., and D. Sainsbury, Dictionary of Microbiology and Molecular Biology, John Wiley & Sons, Chichester, 1989

Slater, R. D., J. L. Sarmiento, M. J. R. Fasham, Some Parametric and Structural Simulations with a three-dimensional Ecosystem Model of Nitrogen Cycling in the North Atlantic Euphotic Zone, in: Geoffrey T. Evans, Michael J. R. Fasham (editors), *Towards a Model of Ocean Biogeochemical Processes*, NATO ASI Series I: Global Environmental Change, Vol. 10, Springer-Verlag, Berlin, Heidelberg, 350 pp. 1993

Smith, R. C., and K.S. Baker, Analysis of ocean optical data, in: *Ocean Optics VII*, M. Blizard (editor), SPIE, 478, 119-126, 1984

Smith, R. C., and K.S. Baker, Analysis of ocean optical data, *Ocean Optics VIII*, P.N. Slater (editor), SPIE, 637, 95-107, 1986

Smith, R. C., and K.S. Baker, Optical Properties of the clearest natural waters (200-800nm), *Appl. Opt., 20*, 177-184, 1981

Smith, R. C., K.J. Waters, and K.S. Baker, Optical variability and pigment biomass in the Sargasso Sea as determined using deep-sea optical mooring data, *J. Geophys. Res., 96*, 8665-8686, 1991

Smolarkiewicz , P. K., A Fully Multidimensional Positive Definite Advection Transport Algorithm with Small Implicit Diffusion, J. Comp. Phys., 54, 325-362, 1984

Smolarkiewicz, P. K., and T. L. Clark, The Multidimensional Positive Definite Advection Transport Algorithm: Further Development and Application, J. Comp. Phys., 67, 396-438, 1986

Smolarkiewicz., P. K., and W. W. Grabowski, The Multidimensional Positive Definite Advection Transport Algorithm: Nonoscillatory Option, J. Comp. Phys., 86, 355-375, 1990

Speer, K. G., A note on cross-isopycnal mixing in the North Atlantic ocean, *Deep-Sea Research I, 44*, 12, pp. 1981-1990, 1997

Strickland, J.D.H., and T.R. Parsons, *A Practical Handbook of Sea Water Analysis*, Fish. Res. Board. Canada, 310 pp., 1972

Stumm, W., and J.J. Morgan, *Aquatic Chemistry*, Wiley-Interscience, New York, 1981

Sugimura, Y. and Y Suzuki, A high-temperature catalytic oxidation method for the determination of non-volatile dissolved organic carbon in seawater by direct injection of a liquid sample, *Mar. Chem., 24*, 105-131, 1988

Suzuki, Y., Y. Sugiumura and T. Itoh, A catalytic oxidation method for the determination of total nitrogen dissolved in seawater, *Mar. Chem., 16*, 83-97, 1985

Söderström, J. and M. Rex, Carbon uptake: Chlorophyll a ratios in two Swedish Fjords, *Botanica marina 17*, 196-203, 1974

Takahashi, T., W. S. Broecker, and A. E. Bainbridge, The Alkalinity and Total Carbon Dioxide Concentration in the World Oceans, in: *Carbon Cycle Modelling, SCOPE 16*, B. Bolin (editor), 271-286, Chichester, John Wiley & Sons, 1981

Toggweiler, J. R. Carbon Overconsumption, *Nature, 363*, 210-211, 1993

Toggweiler, J. R., Is the downward dissolved matter (DOM) flux important in carbon transport?, in: *Productivity of the Ocean: Present and Past*, V. S. Smetacek, W. H. Berger and G. Wefer (editors), 65-83, John Wiley, New York, 1989

UNESCO, Thermodynamics of the carbon dioxide system in seawater, Technical Papers in Marine Science 51, UNESCO, Paris, 1987

Viollier, M., D. Tanré, and P.Y. Deschamps, An algorithm for remote sensing of water colour from space, *Bound.-Layer Metero., 18*, 247-267, 1980

Voss, K. J., 1994: Spectral reflectance of the moon, in: McClain, C. R., R. S. Fraser, J. T. McLean, M. Darzi, J.K. Firestone, F.S. Patt, B. D. Schieber, R.H. Woodward, E-n. Yeh, S. Mattoo, S. F. Biggar, P.N. Slater, K.J. Thome, A.W. Holmes, R. A. Barnes, and K.J. Voss, Case Studies for SeaWiFS Calibration and Validation, Part 2, *SeaWiFS Technical Report Series, Vol. 19*, Hooker Stanford B., Elaine R. Firestone, and James G. Acker (editors), NASA Technical Memorandum 104566, NASA, Goddard Space Flight Center, Greenbelt, Maryland, 1994b

Voss, K.J., and G. Zibordi, Radiometric and geometric calibration of aspectral electro-optic "fisheye" camera radiance distribution system, *J. of Atmos. And Oceanic Tech., 6*, 652-662, 1989

Walsh, J. J., G. T. Rowe, R. L. Iverson, C. P. McRoy, Biological export of the shelf carbon is a sink of the global $CO_2$ cycle, *Nature, 291*, 196-201,1981

Wanninkhof, R., Relationship Between Wind Speed and Gas Exchange Over the Ocean, *J. Geophys. Res., 97*, C5, 7373-7382, 1992

Wanninkhof, R., Relationship between wind speed and gas exchange over the ocean, *J. Geophys. Res., 97*, 7373-7382, 1992

Wheeler P. A., S. A. Kokkinakis, Ammonium recycling limits nitrate use in the oceanic subarctic Pacific, *Limnol. Oceanogr., 35*, 6, 1267-1278, 1990

Wolf, K. U., V. Strass, Seasonal and Meridional Variability of the Remotely Sensed Fraction of Euphotic Zone Chlorophyll Predicted by a Lagrangian Plankton Model, in: *Ocean Colour: Theory and Applications in a Decade of CZCS Experience*, V. Barale, P. M. Schlittenhardt (editors), Kluwer Academic Publishers, Dordrecht, 367 pp., 1993

Woodruff, S. D., R. J. Slutz, R. L. Jenne, and P. M. Steurer, A Comprehensive Ocean-Atmosphere Data Set, *Bull. Amer. Met. Soc., 68*, 1239-1250, 1987

Wyman, M., An *in vivo* method for the estimation of phycoerythrin concentrations in marine Cyanobacteria, *Limnnol. Oceanogr., 37*, 1300-1306, 1992

Yentsch, C. S. and D.W. Menzel, A method for the determination of phytoplankton, chlorophyll and phaeophytin by fluorescene, Deep-Sea Res., 10, 221-231, 1963

Yentsch, C. S., CZCS: Its Role in the Study of the Growth of Oceanic Phytoplankton, in: *Ocean Colour: Theory and Applications in a Decade of CZCS Experience*, edited by V. Barale, P. M. Schlittenhardt, Kluwer Academic Publishers, Dordrecht, pp. 367, 1993

Zibordi, G., and G. M. Ferrari, Instrument self-shading in underwater optical measurements: experimental data, *Applied Optics, 34*, 15, 2750-2754, 1995

# 9 Appendix

## 9.1 Computer Script

### 9.1.1 Imagine Script for the Comparison of Surface Chlorophyll Concentrations

```
# set cell size for the model
#
SET CELLSIZE MIN;
#
# set window for the model
#
SET WINDOW UNION;
#
# set area of interest for the model
#
SET AOI NONE;
#
# declarations
#
Float RASTER n1_M_4_phyto FILE OLD NEAREST NEIGHBOR AOI NONE
"/usr/data/troll1/Markus/imaginedata/M_4_phyto.img";
Float RASTER n5_S19980491998056 FILE OLD NEAREST NEIGHBOR AOI NONE
"/usr/data/troll1/Markus/imaginedata/S19980491998056.L3b_8D_chlor_a-Mean_300x300_4f.img";
Float RASTER n8_M_4_depth FILE OLD NEAREST NEIGHBOR AOI NONE
"/usr/data/troll1/Markus/imaginedata/M_4_depth.img";
Integer RASTER n14_R_4_prozthem FILE DELETE_IF_EXISTING USEALL THEMATIC BIN
DIRECT DEFAULT 8 BIT UNSIGNED INTEGER
"/usr/data/troll1/Markus/imaginedata/R_4_prozthem.img";
{
#
# function definitions
#
#define n10_memory Integer(CONDITIONAL {($n8_M_4_depth==-0.001 ||
$n5_S19980491998056==0.000 || $n8_M_4_depth==0.000) 1})
#define n4_memory Float($n1_M_4_phyto*14.01*7.5/50)
#define n6_memory Float(( $n4_memory / $n5_S19980491998056 )  *  100)
#define n12_memory Float(EITHER 0 IF ($n10_memory ==1) OR $n6_memory OTHERWISE)
n14_R_4_prozthem = CONDITIONAL {($n12_memory>0 && $n12_memory<=50) 1,
            ($n12_memory>50 && $n12_memory<=67) 2,
            ($n12_memory>67 && $n12_memory<=74) 3,
            ($n12_memory>74 && $n12_memory<=91) 4,
            ($n12_memory>91 && $n12_memory<110) 5,
            ($n12_memory>=110 && $n12_memory<135) 6,
            ($n12_memory>=135 && $n12_memory<150) 7,
            ($n12_memory>=150 && $n12_memory<200) 8,
            ($n12_memory>=200 && $n12_memory<1000) 9};
}
QUIT;
```

### 9.1.2 Imagine Script for the Comparison of Subsurface Chlorophyll Concentrations

```
# Satellite Pigment Concentration
#
# set cell size for the model
#
SET CELLSIZE MIN;
#
# set window for the model
#
SET WINDOW UNION;
#
# set area of interest for the model
#
SET AOI NONE;
#
# declarations
#
Float RASTER n1_M_4_phyto FILE OLD NEAREST NEIGHBOR AOI NONE
"/usr/data/troll1/Markus/imaginedata/M_4_phyto.img";
Float RASTER n5_temp;
Float RASTER n8_M_4_depth FILE OLD NEAREST NEIGHBOR AOI NONE
"/usr/data/troll1/Markus/imaginedata/M_4_depth.img";
Float RASTER n19_temp;
Float RASTER n21_temp;
Float RASTER n30_temp;
Float RASTER n37_temp;
Float RASTER n39_temp;
Float RASTER n44_temp;
Float RASTER n45_temp;
FLOAT SCALAR n54_Float;
FLOAT SCALAR n55_Float;
FLOAT SCALAR n56_Float;
FLOAT SCALAR n57_Float;
FLOAT SCALAR n74_Float;
Float RASTER n76_S19980491998056 FILE OLD NEAREST NEIGHBOR AOI NONE
"/usr/data/troll1/Markus/imaginedata/S19980491998056.L3b_8D_chlor_a-Mean_300x300_4f.img";
FLOAT SCALAR n77_Float;
FLOAT SCALAR n78_Float;
Integer RASTER n79_R_4_morelprozthem FILE DELETE_IF_EXISTING USEALL THEMATIC BIN
DIRECT DEFAULT 8 BIT UNSIGNED INTEGER
"/usr/data/troll1/Markus/imaginedata/R_4_morelprozthem.img";
{
#
# load scalar n54_Float
#
n54_Float = 0.327591;
#
# load scalar n55_Float
#
n55_Float = 0.25483;
#
# load scalar n56_Float
#
```

```
n56_Float = -0.284497;
#
# load scalar n57_Float
#
n57_Float = 1.42141;
#
# load scalar n74_Float
#
n74_Float = 0.76;
#
# load scalar n77_Float
#
n77_Float = -1.45315;
#
# load scalar n78_Float
#
n78_Float = 1.06141;
#
# function definitions
#
n5_temp = $n76_S19980491998056/$n74_Float;
#define n36_memory Float(0.768+0.087*LOG10 ( $n5_temp )-0.179*((LOG10 ( $n5_temp )) POWER 2)-
0.025*((LOG10 ( $n5_temp )) POWER 3))
n37_temp = 0.600-0.640*LOG10 ($n5_temp )+0.021*((LOG10 ( $n5_temp)) POWER 2)+0.115*((LOG10
( $n5_temp )) POWER 3)
;
#define n38_memory Float(0.299-0.289*LOG10 ( $n5_temp )+0.579*((LOG10 ($n5_temp)) POWER 2))
n39_temp = 0.710+0.159*LOG10 ( $n5_temp )+0.021*((LOG10 ( $n5_temp )) POWER 2)
;
#define n46_memory Float(($n37_temp POWER 2)/($n39_temp POWER 2))
n21_temp = EITHER 40.3 * ($n5_temp POWER 0.505) IF ($n5_temp>1.0) OR 38.0 * ( $n5_temp
POWER 0.432) OTHERWISE;
n19_temp = EITHER 568.2 * ($n21_temp POWER -0.746) IF ($n21_temp>10) OR 200.0 * ($n21_temp
POWER -0.293) OTHERWISE;
#define n72_memory Float(($n19_temp*2)-$n8_M_4_depth)
n45_temp = -(2*$n37_temp/($n19_temp*($n39_temp POWER 2)));
n44_temp = 1/(($n39_temp POWER 2)*($n19_temp POWER 2));
#define n58_memory Float($n45_temp/(2*SQRT($n44_temp)))
#define n50_memory Float(EITHER 1-
($n55_Float*(1/(1+$n54_Float*$n58_memory))+$n56_Float*((1/(1+$n54_Float*$n58_memory))POWER
2)+$n57_Float*((1/(1+$n54_Float*$n58_memory)) POWER
3)+$n77_Float*((1/(1+$n54_Float*$n58_memory)) POWER
4)+$n78_Float*((1/(1+$n54_Float*$n58_memory)) POWER 5))*EXP ( -($n58_memory POWER 2)) IF
($n58_memory>0) OR -(1-($n55_Float*(1/(1+$n54_Float*(-
$n58_memory)))+$n56_Float*((1/(1+$n54_Float*(-$n58_memory)))POWER
2)+$n57_Float*((1/(1+$n54_Float*(-$n58_memory))) POWER 3)+$n77_Float*((1/(1+$n54_Float*(-
$n58_memory))) POWER 4)+$n78_Float*((1/(1+$n54_Float*(-$n58_memory))) POWER 5))*EXP ( -((-
$n58_memory) POWER 2))) OTHERWISE)
n30_temp = EITHER $n8_M_4_depth IF ($n8_M_4_depth < (2 * $n19_temp)) OR (2 * $n19_temp)
OTHERWISE;
#define n59_memory Float($n30_temp*SQRT($n44_temp)+($n45_temp/(2*SQRT($n44_temp))))
#define n51_memory Float(EITHER 1-
($n55_Float*(1/(1+$n54_Float*$n59_memory))+$n56_Float*((1/(1+$n54_Float*$n59_memory)) POWER
2)+$n57_Float*((1/(1+$n54_Float*$n59_memory)) POWER
3)+$n77_Float*((1/(1+$n54_Float*$n59_memory)) POWER
```

```
4)+$n78_Float*((1/(1+$n54_Float*$n59_memory)) POWER 5))*EXP ( -($n59_memory POWER 2)) IF
($n59_memory>0) OR -(1-($n55_Float*(1/(1+$n54_Float*(-
$n59_memory)))+$n56_Float*((1/(1+$n54_Float*(-$n59_memory))) POWER
2)+$n57_Float*((1/(1+$n54_Float*(-$n59_memory))) POWER 3)+$n77_Float*((1/(1+$n54_Float*(-
$n59_memory))) POWER 4)+$n78_Float*((1/(1+$n54_Float*(-$n59_memory))) POWER 5))*EXP ( -((-
$n59_memory) POWER 2))) OTHERWISE)
#define n16_memory Float($n21_temp / $n19_temp)
#define n29_memory
Float($n16_memory*$n36_memory+(($n16_memory*$n38_memory)/(2*$n30_temp))*SQRT(PI/$n44_te
mp)*EXP ((($n45_temp POWER 2)-4*$n44_temp*$n46_memory)/(4*$n44_temp))*($n51_memory-
$n50_memory))
#define n10_memory Integer(CONDITIONAL {($n8_M_4_depth==-0.001 || $n5_temp==0.000 ||
$n8_M_4_depth==0.000) 1})
#define n4_memory Float($n1_M_4_phyto*14.01*7.5/50)
#define n6_memory Float(($n4_memory / ($n29_memory*$n74_Float)) * 100)
#define n12_memory Float(EITHER 0 IF ($n10_memory ==1) OR $n6_memory OTHERWISE)
#define n14_memory Integer(CONDITIONAL {($n12_memory>0 && $n12_memory<=50) 1,\
        ($n12_memory>50 && $n12_memory<=67) 2,\
        ($n12_memory>67 && $n12_memory<=74) 3,\
        ($n12_memory>74 && $n12_memory<=91) 4,\
        ($n12_memory>91 && $n12_memory<110) 5,\
        ($n12_memory>=110 && $n12_memory<135) 6,\
        ($n12_memory>=135 && $n12_memory<150) 7,\
        ($n12_memory>=150 && $n12_memory<200) 8,\
        ($n12_memory>=200 && $n12_memory<1000) 9})
n79_R_4_morelprozthem = EITHER 10 IF ( $n72_memory < 0  AND $n14_memory!=0 ) OR
$n14_memory OTHERWISE ;
}
QUIT;
```

## 9.2 The complete Data Set

### 9.2.1 Chlorophyll concentrations

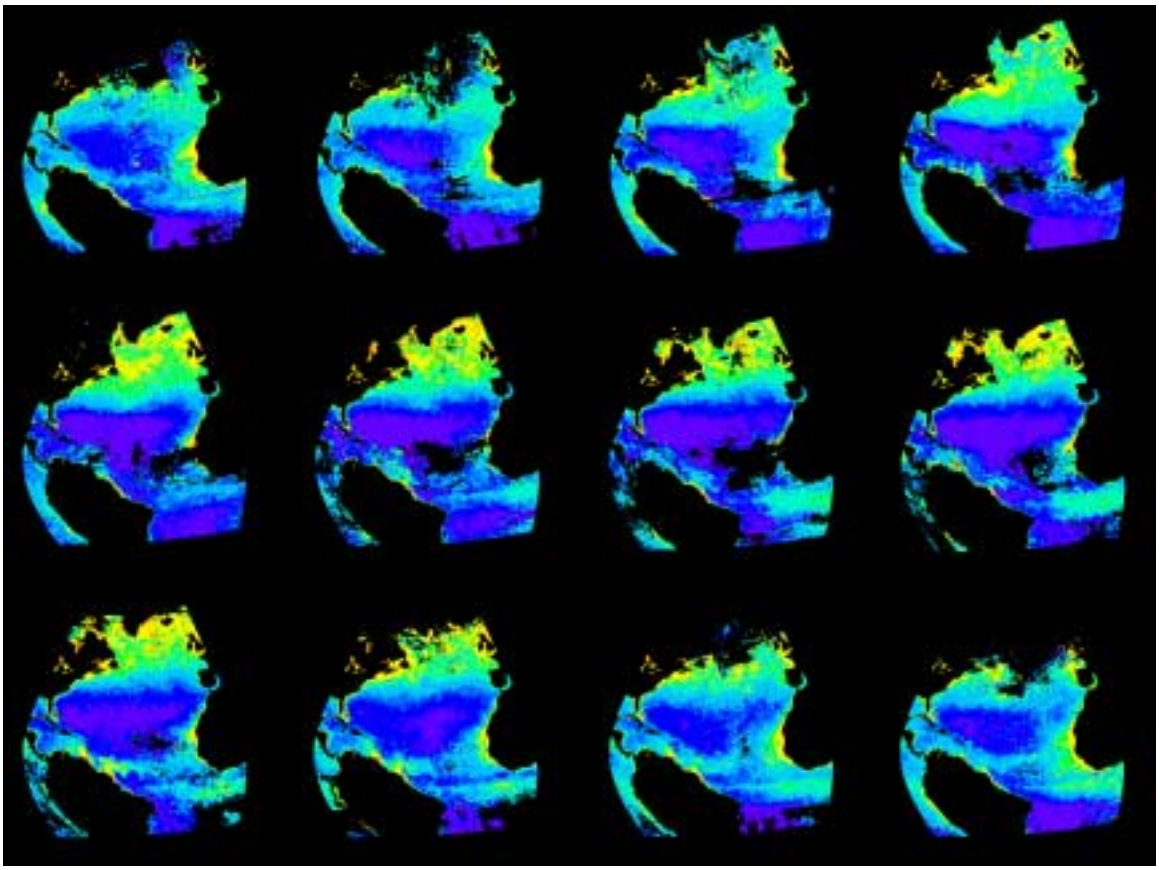

**Figure 18** Climatological CZCS chlorophyll concentration (Upper, left corner: January; lower, right corner: December)

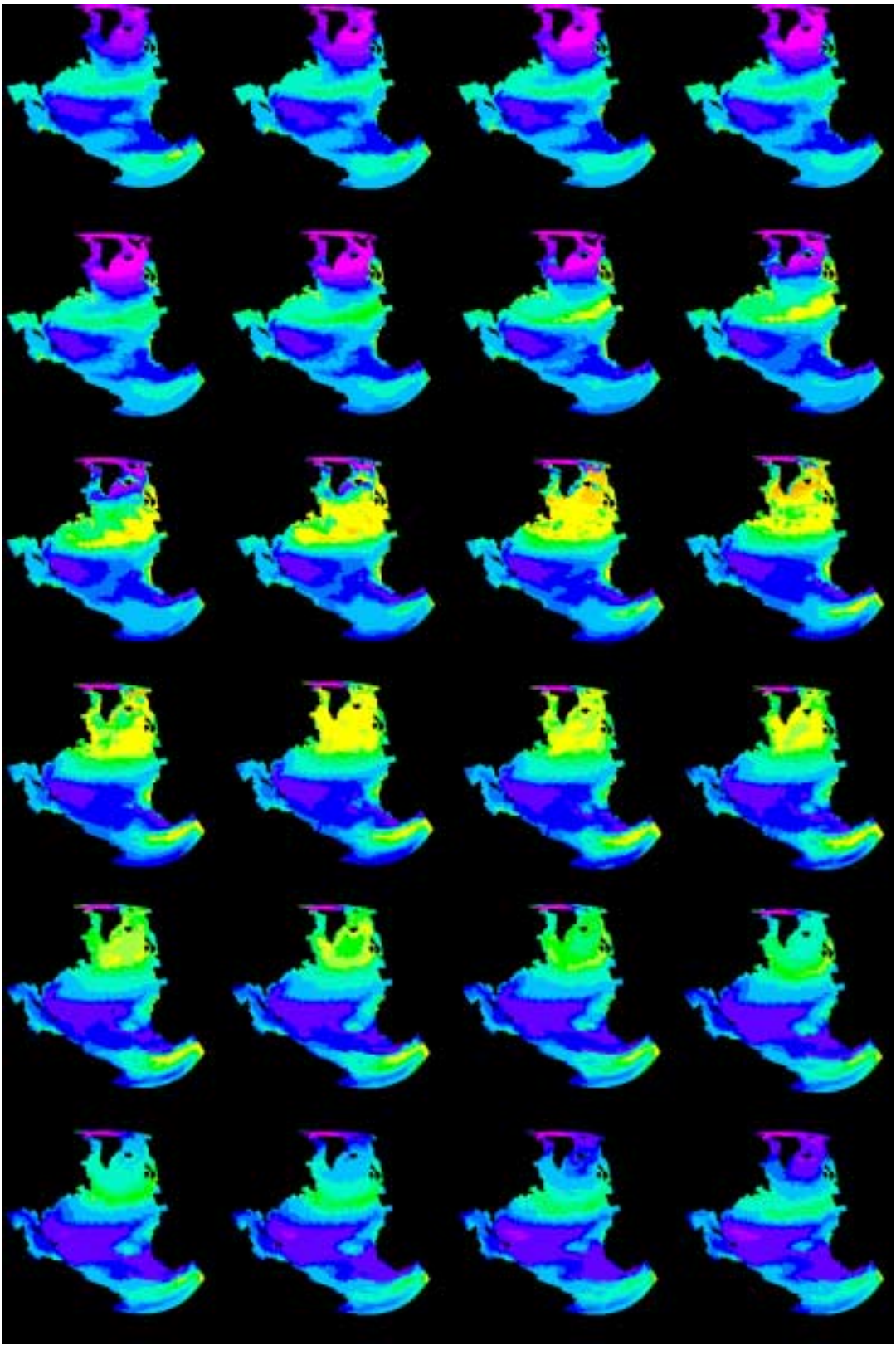

**Figure 19** Model chlorophyll concentration (Upper left corner: January, first 15 days, lower right corner: December, last 15 days)

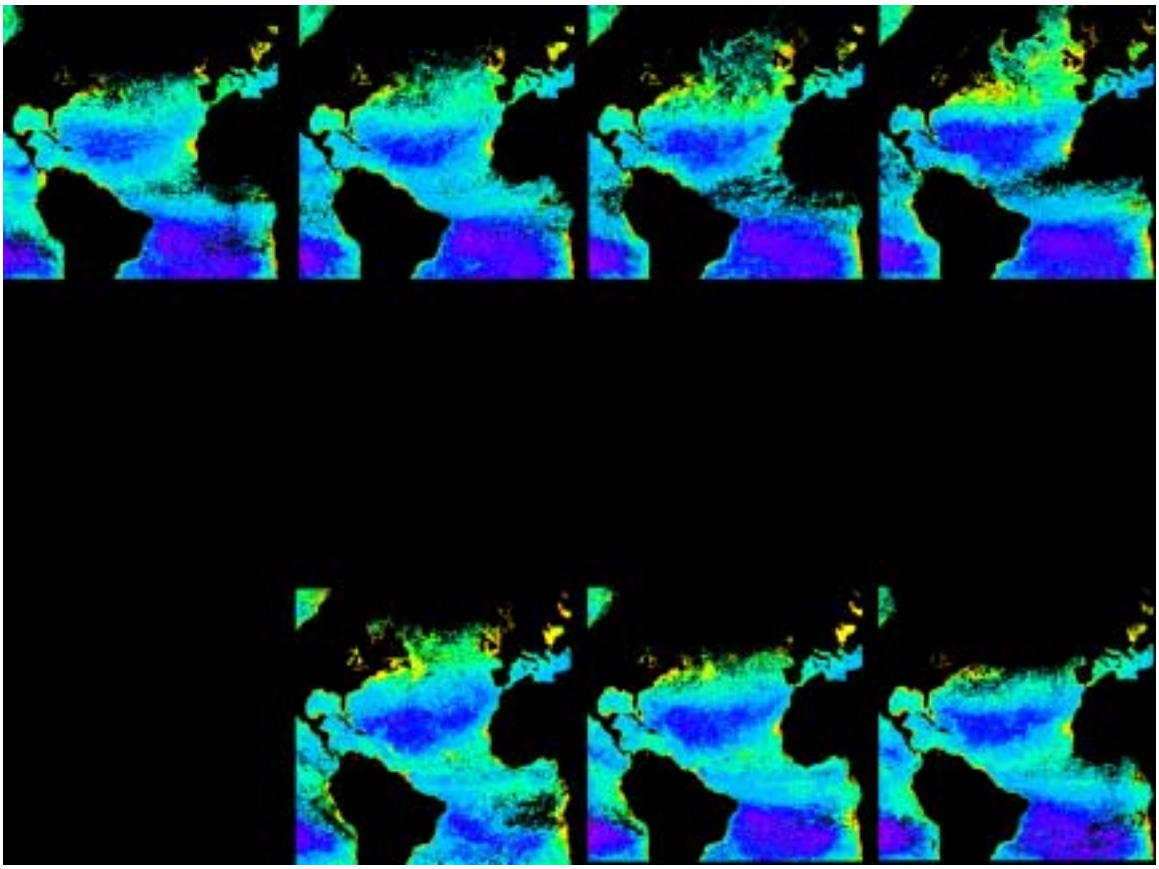

**Figure 20** Monthly SeaWiFS chlorophyll concentrations (Upper, four pictures: January 1998 - 1998; lower, three pictures: October 1997 - December 1997)

### 9.2.2 Quantitative comparisons

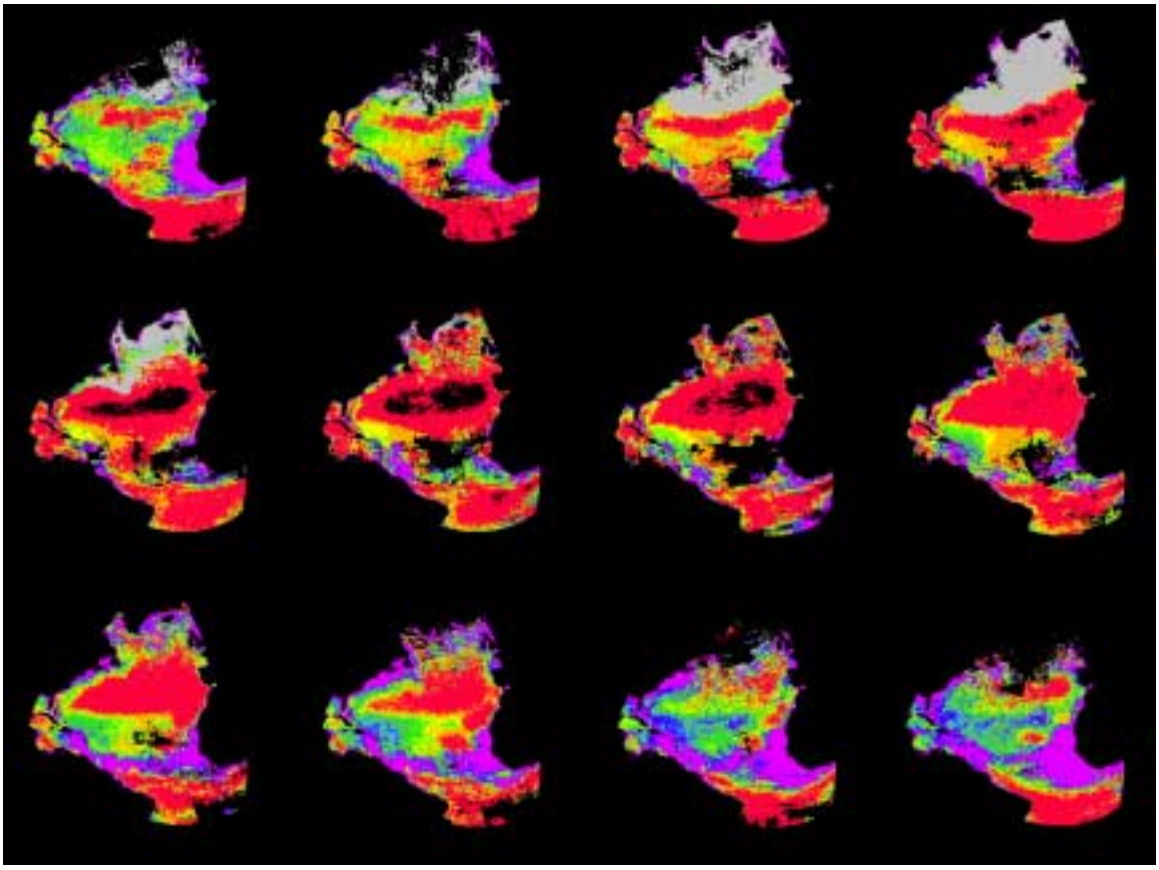

**Figure 21** Quantitative comparison between subsurface, climatological CZCS data (Upper, left corner: January; lower, right corner: December) and model chlorophyll

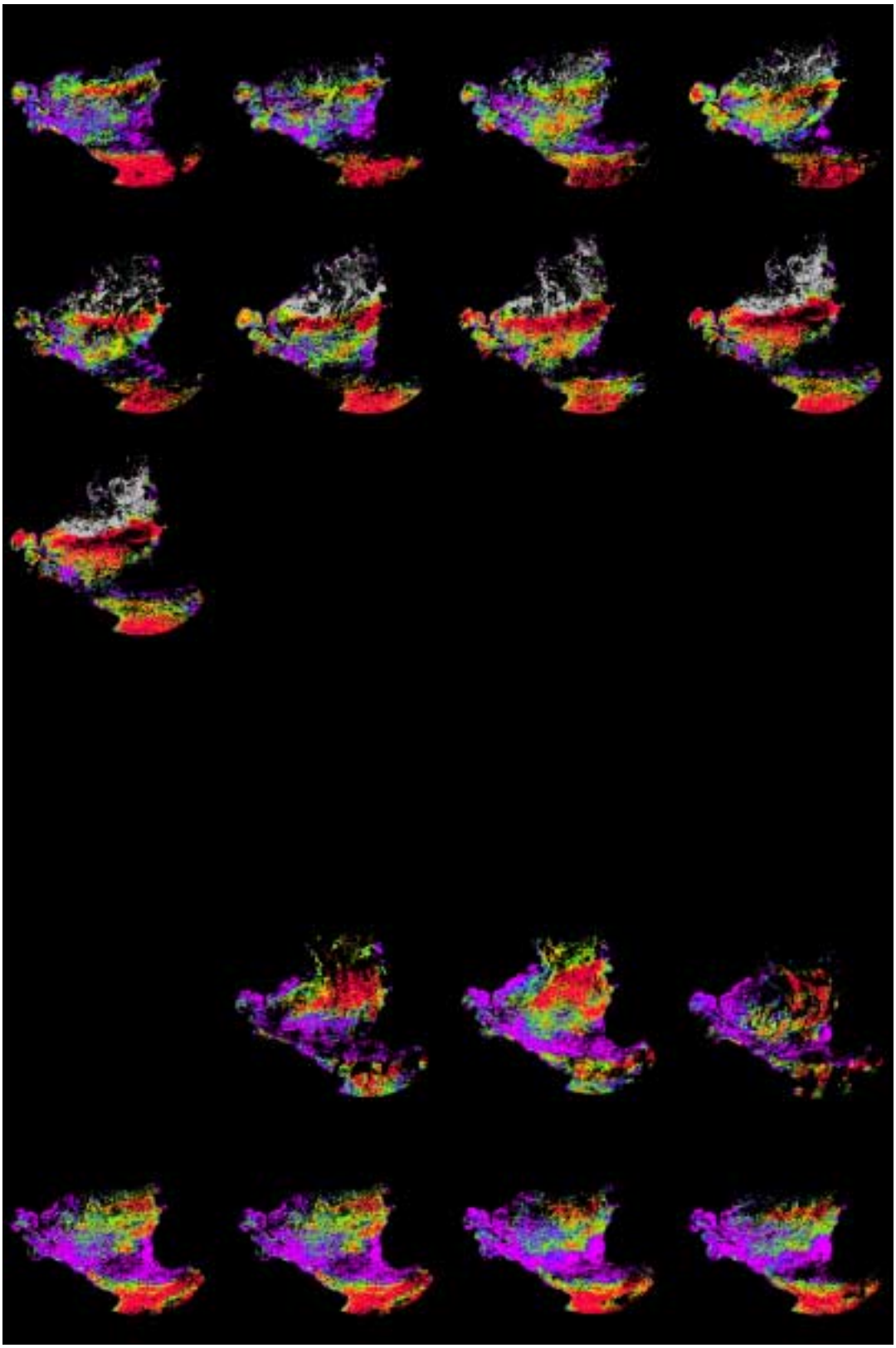

**Figure 22** Quantitative comparison between subsurface SeaWiFS (upper pictures 1998; lower pictures 1997) and model chlorophyll

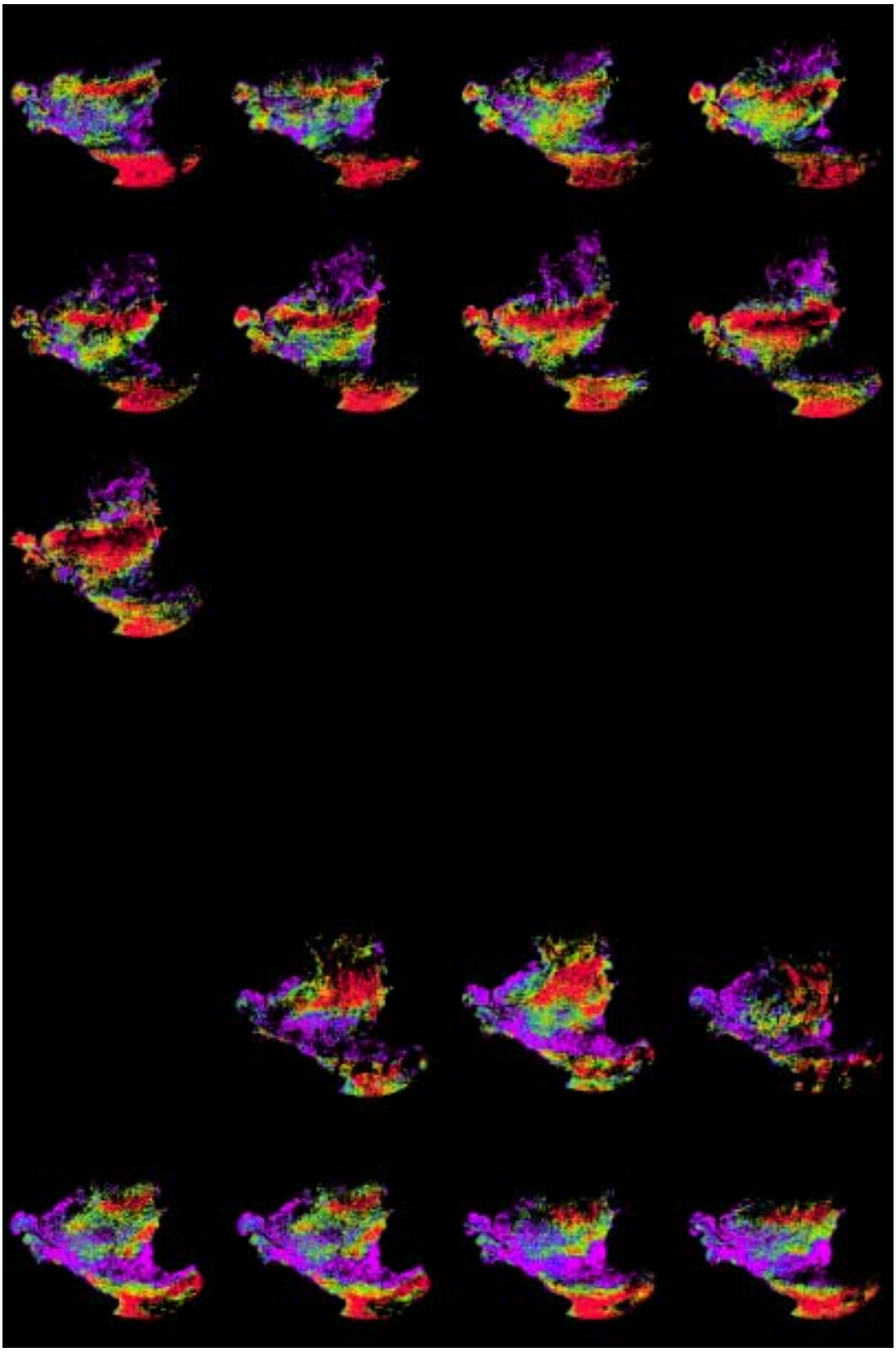

**Figure 23** Quantitative comparison between surface SeaWiFS (upper pictures 1998; lower pictures 1997) and model chlorophyll